SELF-DIFFUSION IN SILICON CARBIDE

by

Rathindra Nath GhoshTagore

B.Sc. (Hons.), University of Calcutta, India (1957)
M.Sc. (Tech.), University of Calcutta, India (1960)

Submitted in partial fulfillment of the requirements

for the degree of

DOCTOR OF SCIENCE

at the

Massachusetts Institute of Technology

(1965)

Signature of Author
Department of Metallurgy

Signature of Professor
in Charge of Research

Professor R. L. Coble

Signature of Chairman of
Departmental Committee on
Graduate Students

Professor P. L. DeBruyn

SELF-DIFFUSION IN SILICON CARBIDE

by

Rathindra Nath Ghoshtagore

SUBMITTED TO THE DEPARTMENT OF METALLURGY,
MARCH 1965, IN PARTIAL FULFILLMENT OF THE
REQUIREMENTS FOR THE DEGREE OF DOCTOR OF SCIENCE

ABSTRACT

Carbon diffusion coefficients have been determined in both hexagonal single crystal and dense polycrystalline silicon carbide using Carbon-14 as a tracer. Diffusion data in black crystals (containing about 600 ppm aluminum) along [0001] between 1853°C to 2060°C can be represented by the equation

$$D = 3.014 \times 10^{2} \exp\left[\frac{-141.5 \pm 16.6 \text{ Kcal}}{RT}\right]$$

whereas that for a light-green hexagonal crystal (containing about 100 ppm nitrogen) between 1977°C to 2088°C along the same direction can be represented by

$$D = 2 \times 10^{17} \exp\left[\frac{-302.4 \pm 48.6 \text{ Kcal}}{RT}\right]$$

The p-type (black) material is thus found to have a higher diffusion coefficient than the n-type (green) material within the temperature range of measurement conforming to the nature of carbon vacancies in SiC.

Carbon diffusion coefficients in dense black polycrystalline material between 1927°C to 2063°C can be represented by the equation

$$D = 2.36 \times 10^{2} \exp\left[\frac{-137.1 \pm 14.2 \text{ Kcal}}{RT}\right]$$

which, when compared with that in black single crystals, indicate a lattice diffusion process.

These data of carbon lattice diffusion coefficients in silicon carbide are in good agreement with the apparent diffusion coefficients obtained by creep measurements in polycrystalline silicon carbide (at and below 2000°C) using the Nabarro-Herring relationship. These studies indicate that carbon diffusion in silicon carbide is lattice vacancy controlled.

A method has also been developed for determining silicon diffusion coefficients in silicon compounds using a stable-tracer technique. Rough values of silicon diffusion coefficients at 1927°C and 2017°C show silicon about 1 to 1.5 orders of magnitude faster diffusing than carbon in silicon carbide at these temperatures.

Thesis Supervisor: R. L. Coble
Title: Associate Professor
of Ceramics

TABLE OF CONTENTS

V. Continued.

List of Illustrations

List of Tables

Acknowledgement

I express my deepest appreciation and utmost indebtedness to Professor Robert L. Coble for the invaluable education he has provided me with through his able guidance and merciless analysis during the course of this work.

Over years I have profited from many informal discussions with many members of the Ceramics Division. I want to thank them all. I specially want to mention Phillip L. Farnsworth and William H. Rhodes. During every day of painful experimental work we have shared our mutual problems. I express my special appreciation to McDonald Robinson for helping me solve the computation problem and to the M.I.T. Computation Centre for providing me with all the facilities.

I am particularly indebted to the Office of Naval Research for providing necessary funds for this investigation.

Several individuals have provided me with special materials for this investigation. Dr. J. Hornstra, of the Philips Laboratories, Eindhoven, Netherlands, helped me generously with several impurity-controlled and pure SiC crystals while Dr.Thomas Vasilos, of the AVCO Corporation, provided me with the polycrystalline SiC used in this work. I extend my sincere appreciation to them.

Miss Theresa M. Tardif deserves special acknowledgement for doing a wonderful job in typing this thesis, particularly for making some sense out of my handwriting. I want to thank all the members of the Ceramics Division for their friendly cooperation.

Finally, I express my deepest appreciation to my friend, Miss Lenore C. Spitzer, for all the encouragement and help she had provided me during most of my frustrating periods of study and research. As a foreigner,(in the truest sense of the term), I suppose no one knows that better than me.

I. INTRODUCTION

Diffusion is the transport, due to thermal motion, of atoms of an impurity or of a major constituent; it can occur in any material, whatever its state.(1) It may also be defined as the process which leads to an equalization of concentration within a single phase or, more broadly, the process wherein atoms or ions migrate through a crystal under the impetus of some thermodynamic force.(2) For a fuller understanding of such diffusion-controlled kinetic processes as sintering, grain growth, solid state reactions, ionic conductivity, oxidation and high temperature deformation, direct studies of diffusion rates and mechanisms as a function of various commonly encountered variables are considerably helpful. Analysis of kinetic processes have provided diffusivities inferred from models describing the particular kinetic process which can be compared with the directly measured diffusion coefficients for the purpose of evaluation of the proposed models.

Thermal energy keeps the atoms of a gas in random motion and constantly intermingles them. In the presence of concentration gradients, however, a directed diffusional flow arises and tends to even out any concentration gradient. A directed flow also appears when temperature gradients are present; this is the so-called thermal diffusion or Soret effect. In general, an organized diffusional flow is observed whenever a chemical potential gradient appears in a medium. The diffusional current J, due to a concentration gradient, is given by the differential equation

$$J = -D \text{ grad } C \tag{I.1}$$

where D is the diffusion coefficient, and C is the concentration of the diffusing species in suitable units. This equation (I.1) becomes, for the case of one-dimensional diffusion,

$$J_x = -D \frac{\delta C}{\delta x} \tag{I.2}$$

The negative sign in the above equation (known as Fick's first law) indicates that diffusion takes place in the direction of decreasing concentration. The parameter D has the dimensions L^2T^{-1} and is usually expressed in $cm^2 sec^{-1}$.

A second differential equation (known as Fick's second law) is often used in problems of solid state diffusion:

$$\frac{\delta C}{\delta t} = D \frac{\delta^2 C}{\delta x^2} \tag{I.3}$$

For a given diffusion coefficient, this equation describes the spatial distribution of the diffusing species as a function of time, t. The diffusion coefficient is the material parameter which characterizes the rate of diffusion. For solids, this coefficient usually increases steeply with temperature and can be described as an Arrhenius-type activated process:

$$D_T = D_o \text{ Exp } (-Q/RT) \tag{I.4}$$

where R is the universal gas constant, D_T is the diffusivity at the absolute temperature T, D_o is a constant frequently termed the frequency factor, and Q is the activation energy for diffusion. Their values are determined by the physiochemical properties of the medium in which diffusion is taking place and by those of the diffusing species. Occasionally, the diffusion coefficient is found to depend on the concentration of the diffusing particles.

The present understanding of diffusion in ionic systems has been mainly derived from the study of imperfections in crystals, particularly the alkali halides. The relationship among diffusion coefficient, electrical conductivity and transference number is given by the Nernst(3)-Einstein(4) equation:

$$\frac{D_i}{\sigma} = \frac{t_i kT}{n_i (Z_i e)^2} \qquad (I.5)$$

where D_i is the self-diffusion coefficient of the ith ion, σ is the total electrical conductivity, t_i its transference number, n_i the number of ions per unit volume, e the electronic charge, k the Boltzmann constant, and T the absolute temperature.

The early experimental work on ionic conductivity suggested the concept of intrinsic lattice disorder and the existence of equilibrium defects following the laws of thermodynamics. Frenkel(5) suggested that ions were capable of occupying interstitial lattice sites, leaving behind vacancies and migrating through a crystal by jumping to like neighboring sites until they recombined with vacancies left in the normal lattice by other migrating ions. This type of disorder (Frenkel defects) is found in silver halides(6) as well as other compounds. Schottky(7) developed another model for intrinsic lattice disorder (Schottky disorder) which postulates equivalent numbers of vacant anion and cation sites, or vacancy pairs for electronentrality requirements.

In addition to equilibrium imperfections, non-equilibrium lattice defects can be formed by the introduction of impurities. Depending on the sign and the valence of an impurity atom vacancies or interstitials can be introduced in both types of normal sites. For example, Ca^{2+} plus a vacancy can replace two Na^{+} ions and the crystal remains electrically neutral. The effect of the impurity introduced vacancy is to shift the equilibrium existing between positive and negative ion vacancies. The concentration product is constant, the alternate vacancy concentration is decreased. The presence of large amounts of impurities introduces imperfections in numbers greater than are normally present under equilibrium conditions. Consequently, an Arrehenius plot of the diffusion coefficient versus the reciprocal of temperature is divided into two distinct temperature regions. At low temperatures, the mobility of ions is via existing vacancies not thermally introduced and in such a temperature range the diffusion is referred to as extrinsic. At higher temperatures, the thermally introduced imperfections predominate and diffusion is referred to as intrinsic. In the extrinsic temperature range, gross imperfections, such as dislocations, affect diffusion phenomena and this region is also structure sensitive.

By extensive studies of conductivity, diffusion and transference numbers in alkali halides as a function of impurity type and level, prior heat treatment and deformation, a satisfactory interpretation of ionic and atomic mobility has been developed. Excellent reviews of the details of such studies have been given by Jost(2) and Lidiard.(8) Among other solids, those that have been intensively investigated over more than a decade for diffusional properties, are the refractory oxides(9); this field is still in its process of development.

In contrast, diffusion in covalent solids is only of recent interest; mainly spurred by the development of semiconductor technology. Exhaustive work in the diffusion of elements of the second, third, and fifth groups of the periodic table in silicon and germanium semiconductors has led to some appreciation of the variables and mechanisms operating in these materials.(1) Interest in III-V and II-VI compounds is very recent and the data available are not amenable to any sort of quantitative understanding. From this point of view, diffusion data on high-band gap refractory semiconductors constitute a major necessity for a general analysis of this phenomenon. The work undertaken here was to determine the diffusion coefficients of both species in SiC, selected because of its utility as a refractory and as a mid range choice of high band-gap covalently bonded semiconductor.

II. GENERAL THEORY AND LITERATURE REVIEW

A. SOLUTION OF THE DIFFUSION EQUATION

A large part of the diffusion literature is concerned with the solutions of the partial differential equations (I.2) and (I.3) for various conditions. They have been treated in detail by Jost(2), Crank(10), and others. In general, the solutions of equation (I.3) for constant D fall into two forms. When the diffusion distance is short relative to the dimensions of the initial inhomogeneity, C(x,t) can be most simply expressed in terms of error functions. When complete homogenization is approached, C(x,t) can be represented by the first few terms of an infinite trigonometric series or Bessel functions (for a cylinder). Our interest will be in the former type (non-steady-state solutions).

1. Diffusion from an infinitesimally thin layer into a semi-infinite body with a reflecting boundary (i.e., planes impermeable to matter).(1)

Let a quantity α of solute be plated as a thin film on one end of a long rod of solute-free material and the rod be then annealed for time t so that diffusion can occur. The concentration of solute along the bar will be given by the equation,

$$C(x,t) = \frac{\alpha}{\sqrt{\pi D t}} \exp\left(-\frac{x^2}{4Dt}\right) \qquad \text{(II.1)}$$

where x is the distance normal to the initial solute film. The value of the function $\exp(-x^2/4Dt)$ and, therefore, also the concentration $c(x,t)$

decreases with increasing distance from the source of diffusion and approaches zero asymptotically for $x \rightarrow +\infty$.

To show that equation (II.1) is the correct solution, two steps are necessary. First, differentiation shows that it is indeed a solution to equation (I.3). Second, the equation satisfies the boundary conditions of the problem since

$$x > 0 \quad \text{for } c \rightarrow 0 \quad \text{as } t \rightarrow 0$$

$$x = 0 \quad \text{for } c \rightarrow \infty \quad \text{as } t \rightarrow 0$$

yet the total quantity of solute is fixed because

$$\int_0^\infty c\ (x,t)\ dx = \alpha$$

Thus, if a thin layer of solute is applied to one end of a bar and allowed to diffuse, the resulting solute distribution is described by equation (II.1) with $x > 0$ and $x = 0$ at the solute-rich end. After an appropriate anneal, thin sections are removed parallel to the initial interface. There are sections of constant x, and after the solute concentration of each is measured, a plot of $\ell n(c)$ versus x^2 is made. From equation (II.1) it is seen that this is a straight line of slope $(4Dt)^{-1}$ so that if t is known, D can be calculated.

This procedure has been highly developed and is currently used for all the more accurate determinations of D for substitutional atoms. It is invariably used with a radioactive tracer as a solute since the concentration of a tracer can be determined with orders of magnitude greater sensitivity than is possible using chemical analysis. This means that D can be measured with such a small quantity of solute that the composition of the original sample is essentially unchanged. This technique is dealt in detail in the articles by Tomizuka(11) and Hoffman(12). In the case of self-diffusion of radioactive isotopes, the diffusion equation is written in terms of the concentration gradient of the radioactive species which, according to Zener(13), has a small dependence on the isotopic mass. The solute distribution under this boundary condition is schematically shown in Fig. 1a.

2. Diffusion in a semi-infinite body with a boundary acting as a perfect sink (capturing boundary) and with uniform initial distribution.(1)

In this case, we assume that the diffusing species is uniformly distributed throughout the isotropic body at time $t = 0$, i.e., $c(x,o) = \text{const.} = c_o$, but we impose the condition that the concentration at $x = 0$ is zero for all values of $t > 0$. We refer to boundaries which act as perfect sinks as capturing boundaries. This condition is represented by the equation

$$c(x,t) = C_o \operatorname{erf} \frac{x}{2\sqrt{Dt}} \qquad \text{(II.2)}$$

This is schematically shown in Fig. 1b.

In general, problems of this type are encountered in connection with the evaporation of solute from an initially saturated body or with the extraction of solute by surface getters of various kinds. An important example of the latter case is the diffusion couple made with a thin film deposited on one face (of a semi-infinite body) which is nearly completely depleted of one of its natural isotopes and then diffusion annealed. This depleted isotope then diffuses out of the bulk as a function of time following a

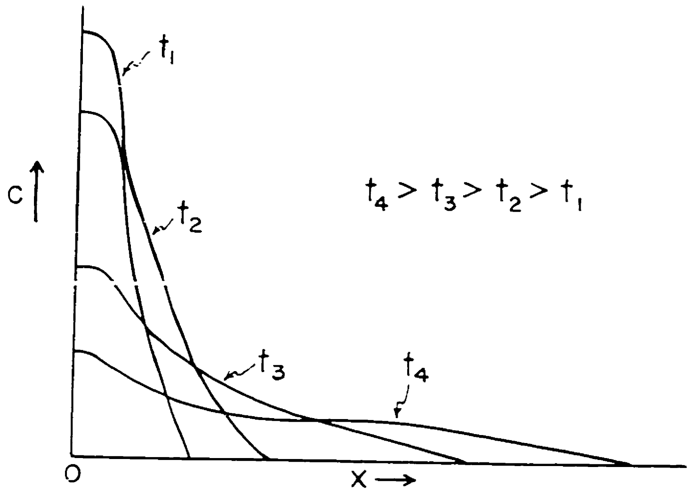

Fig. 1a CONCENTRATION PROFILE FOR DIFFUSION FROM A THIN-FILM INTO A SEMI-INFINITE BODY WITH A REFLECTING BOUNDARY

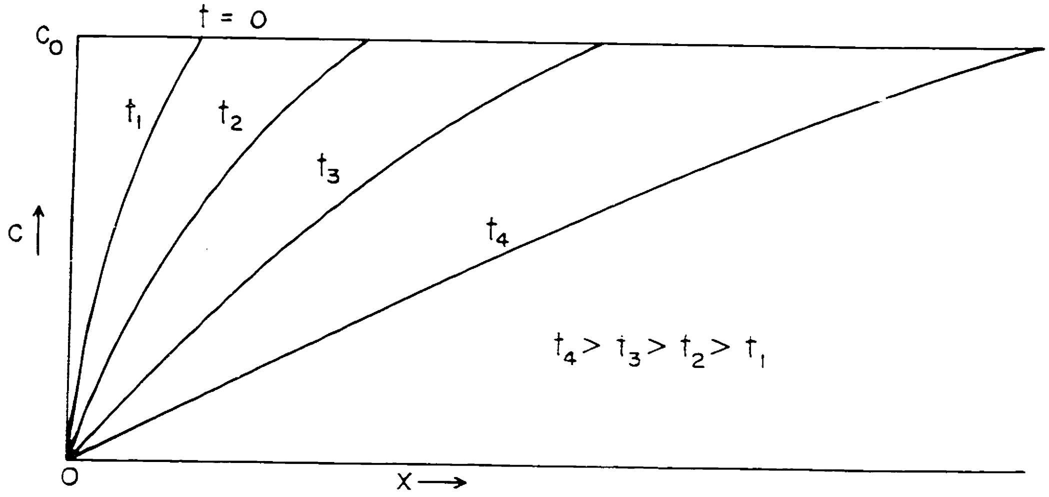

Fig. 1b CONCENTRATION PROFILE FOR DIFFUSION FROM SEMI-INFINITE BODY WITH A CAPTURING BOUNDARY WITH UNIFORM INITIAL DISTRIBUTION

pattern shown in Fig. 1b. After a suitable anneal the sample is sectioned. The concentration of this particular isotope in each of these sections can then be found (as a function of distance from the surface) either by mass spectrography or by activation analysis.

B. MECHANISMS OF SELF-DIFFUSION IN NON-OXIDE SEMICONDUCTORS

Self-diffusion in all solids have been identified to occur primarily by the following four mechanisms(14).

1. Interstitial mechanism
2. Vacancy mechanism
3. Interstitialcy and crowdion mechanism
4. Ring mechanism

Of these, the first two are of predominant importance. Because the self-diffusion mechanisms in metals and metal-oxides are quite well understood (1,12,14) only a short discussion of the mechanisms in non-oxide semiconductors is included here(1).

a. Elemental Semiconductors. The majority of the research work concerned with the transistor has been done on germanium and silicon. The novel diffusion effects which are peculiar to these materials occur because of the effect of one solute on the diffusion of another. The first of these "ternary" effects is due to the interaction between ionized acceptors and donors. A second effect appears if an impurity of valence other than 4 is diffused into very pure material. The solute ionizes at the high diffusion temperature, and the electrons, or holes, become the third component. Due to much higher mobility of electrons or holes than the ions, a local field is set up by the separation of charges by diffusion. The result is that the ions diffuse inward under the effect of a concentration gradient, plus, the electrostatic attraction of the electrons, or holes, which have diffused farther into the material.(15).

Among the elemental semiconductors, self-diffusion in germanium has been most extensively studied using the radioisotope germanium-71. The coefficient of self-diffusion of germanium was found to be very low; at least 50-100 times less than the diffusion coefficients of the slowest diffusing foreign atoms. The temperature variation of the most recent data can be represented by(16):

$$D_{Ge \rightarrow Ge} = 7.8 \exp \left(- \frac{68{,}500 \text{ Cal}}{RT} \right) \qquad \text{(II.3)}$$

The mechanism of self-diffusion in germanium is by no means established. A vacancy mechanism seems the most probable, with the germanium atoms moving into lattice vacancies. The self-diffusion coefficient would then be determined by two factors: the equilibrium concentration of vacancies and the rate at which the vacancies can exchange places with neighboring atoms. The latter quantity is the diffusion coefficient of vacancies, D_v . Now, if D_{Sd} is the experimentally observed self-diffusion coefficient,

$$D_{Sd} = D_v \frac{N_v}{N_L} \qquad \text{(II.4)}$$

where N_v and N_L are the concentrations of vacancies and of germanium atoms at lattice sites, respectively. Using the results of Mayburg and Rotondi(17) for the temperature variation of the concentration of vacancies in germanium,

$$N_v = 3 \times 10^{23} \exp\left(- \frac{46,300 \text{ Cal}}{RT}\right) \text{cm}^{-3} \qquad (II.5)$$

and equation (II.3), we obtain the following equation for the temperature variation of D_v:

$$D_v = 2.3 \exp\left(- \frac{22,200 \text{ Cal}}{RT}\right) \qquad (II.6)$$

Thus, the energy for the formation of vacancies is about 2 ev (46,300 Cal mole^{-1}), and the activation energy for the motion of vacancies through the crystal is about 1 ev (22,200 Cal mole^{-1}).

The effect of impurities on the self-diffusion of germanium was studied by Valenta and Ramasastry(18) who found a dependence of the activation energy for self-diffusion on the impurity type (donor or acceptor) and level and can be represented by a general equation of the form:

$$D = D_o \exp\left[- \frac{(Q-\Delta\mu)}{RT}\right] \qquad (II.7)$$

where $\Delta\mu$ is the change in the Fermi level from the intrinsic material caused by the presence of impurities. A theoretical justification of this type of behavior is given by Boltaks(1). At high temperatures, vacancies in germanium are electrically charged since they behave as acceptors with an energy level 0.2 ev above the valence band(19). On the other hand, the solubility of acceptors in germanium at a given temperature is increased by the presence of donors and decreased by the presence of other acceptors(20). It should, therefore, be possible to control the concentration of vacancies by doping germanium with donor or acceptor impurities. According to equation (II.7) the self-diffusion coefficient in an impurity semiconductor should be higher than in intrinsic material. The effect may be enhanced by an increase in the value of D_o following an increase in the entropy of the system(1).

Though no measurements have been made on the self-diffusion of silicon, Boltaks(1) has assumed an equation of the form:

$$D_{Si \rightarrow Si} = 10 \exp\left(- \frac{97,000 \text{ Cal}}{RT}\right) \qquad \text{(II.9)}$$

He has compared the behaviors in silicon and germanium based on the measured diffusivities of impurities in these elements. It has been found, in general, that acceptors diffuse more rapidly than donors in silicon; the opposite is true in germanium. It is to be remembered that the Coulomb interactions between ions and vacancies is negligible in silicon because most of the vacancies are neutral. Since the difference in ionic radii between acceptors and the solvent is much larger than that between donors and the solvent (silicon or germanium), the rate of diffusion of acceptors should be higher than that of donors. In silicon, where the effect is not masked by Coulomb interactions between ions and charged vacancies, this behavior is indeed observed. In germanium, however, Coulomb interactions increase the rate of diffusion, the effect being larger for donors ($\Delta H_c<0$) than for acceptors ($\Delta H_c>0$), where ΔH_c is the Coulomb interaction energy between charged vacancies and charged ions. In this case, the effect of Coulomb interactions exceeds the effect of the difference in ionic radii.

Cuddeback and Drickamer(21) have studied self-diffusion in rhombic sulfur between 309° and 374°K with radioactive sulfur-35. The strong anisotropy of self-diffusion in this material is striking. Their data can be represented by:

$$D_{I} = 8.32 \times 10^{-12} \exp\left(- \frac{3,080 \text{ Cal}}{RT}\right) \qquad \text{(II.10)}$$

$$D_{11} = 1.78 \times 10^{36} \exp\left(- \frac{78,000 \text{ Cal}}{RT}\right) \qquad \text{(II.11)}$$

where D_{11} and $D_{\perp}$ represent the self-diffusion coefficients parallel and perpendicular to the c-axis. The self-diffusion coefficients in monoclinic sulfur, measured by Hauffe(22) at various temperatures above 100°C are given by:

$$D_{S \rightarrow S} = 2.8 \times 10^{13} \exp\left(- \frac{46,800 \text{ Cal}}{RT}\right) \qquad (II.12)$$

Due to the presence of different allotropic modifications of selenium, the measured self-diffusion coefficients have been found to be structure-sensitive and depends on numerous factors outside the control of the experimenter. The results of Boltaks and Plachenov(23) for the self-diffusion in amorphous (am) and polycrystalline (cr) hexagonal selenium can be represented by:

$$D_{Se \rightarrow Se(cr)} = 7.6 \times 10^{-10} \exp\left(- \frac{3,200 \text{ Cal}}{RT}\right) + 1.4 \times 10^{-4} \exp\left(- \frac{11,800 \text{ Cal}}{RT}\right) \qquad (II.13)$$

$$D_{Se \rightarrow Se(am)} = 6.3 \times 10^{25} \exp\left(- \frac{53,000 \text{ Cal}}{RT}\right) \qquad (II.14)$$

According to the explanation furnished by these authors, the break in the curve for crystalline selenium is probably due to a change from a lattice diffusion mechanism to grain boundary diffusion. The higher D_0 value for the amorphous modification is consistent with the higher entropy of the amorphous form. The higher Q value with amorphous material indicates a different mechanism of diffusion; in the crystalline modification self-diffusion can occur by the motion of atoms along lattice vacancies, whereas in amorphous selenium atoms have to be transferred between disordered chains.

Nachtrieb and Handler's(24) data of self-diffusion in white polycrystalline phosphorus between 0° and 43.86°C can be described by:

$$D = 1.0 \times 10^{-3} \exp\left(-\frac{9,400 \text{ Cal}}{RT}\right) + 2.0 \times 10^{46} \left(-\frac{80,600 \text{ Cal}}{RT}\right) \qquad (II.15)$$

The break at around 30°C is explained on the same basis as that for crystalline selenium.(23)

Self-diffusion in graphite has been studied by Feldman et al(25) using polycrystalline material; their data have been accepted with considerable reservation(1). Dienes(26), however, has computed the activation energy for three possible self-diffusion mechanisms in graphite. The lowest activation energy (90.4 Kcal/mole) was found for assumed direct exchange between the atoms in the plane of a layer. Due to a unique layered structure of graphite a strong anisotropy of diffusion is expected in this material. Measurements on natural crystals of graphite by Kanter(27) give:

$$D = 40 f^2 \exp\left(\frac{-163 \pm 12 \text{ Kcal}}{RT}\right) \qquad (II.16)$$

where f is a geometry factor lying between 0.1 and 0.6. These data seem to indicate a vacancy mechanism of self-diffusion in graphite.

b. Compound Semiconductors. Interest in the self-diffusional properties in these groups is very recent with the result of very few available data and very poor understanding of the mechanism of self-diffusion in these materials.

Anderson and Richards(28) studied self-diffusion of lead in polycrystalline PbS between 733° and 1043°K using radioactive lead:

$$D_{Pb \rightarrow PbS} = 1.3 \exp\left(- \frac{42{,}000\ \text{Cal}}{RT}\right) \qquad \text{(II.17)}$$

and found a strong dependence of observed D values on the excess concentration of either lead or sulfur at various depths in the diffusion layer. This can be explained by assuming a vacancy mechanism of lead diffusion with excess sulfur generating additional cation vacancies and facilitating the transport of lead ions. No measurement for the diffusion of sulfur in PbS is available, however. It is to be remembered that heat treatment in an atmosphere of sulfur-vapor increases the p-type conductivity of PbS, whereas, heat-treatment in a vacuum increases the n-type conductivity.(29)

Similar conductivity type changes are observed in PbSe and PbTe, therefore, the p-n junction method can be used for the measurement of self-diffusion in them.(30) The data for single crystals can be represented by:

$$D_{Pb \rightarrow PbTe} = 2.9 \times 10^{-5} \exp\left(- \frac{13{,}830\ \text{Cal}}{RT}\right) \qquad \text{(II.18)}$$

and,

$$D_{Te \rightarrow PbTe} = 2.7 \times 10^{-6} \exp\left(- \frac{17{,}290\ \text{Cal}}{RT}\right) \qquad \text{(II.19)}$$

In PbTe, an anomalous behavior of lower activation energy for self-diffusion than for impurity diffusion (Sb, Sn) is observed. By comparing the self-diffusion coefficients with the results of electrical measurements on doped specimens, it is suggested(30) that the interstitial mechanism is operative here as in PbSe which can be represented by:

$$D_{Se \rightarrow PbSe} = 2.1 \times 10^{-5} \exp\left(- \frac{27,700 \text{ Cal}}{RT}\right) \qquad \text{(II.20)}$$

As in PbTe, impurity diffusion is energetically favored in PbSe. This is explained by the formation of stable complexes of the type SnTe, Sb_2Te_3, and Sb_2Se_3 with the donor atoms residing in cation vacancies.

Self-diffusion data of Zn in ZnS(31) crystals and their comparison with those of Zn in ZnO(32,33,34) have revealed some interesting facts:

Temp. (°C)	Exptl. Relation	System	Suggested Mechanism
<940	$D = 3.0 \times 10^{-4} \exp\left(- \frac{35,000 \text{ Cal}}{RT}\right)$	Zn-ZnS	----
940-1030	$D = 1.5 \times 10^{4} \exp\left(- \frac{75,000 \text{ Cal}}{RT}\right)$	Zn-ZnS	Interstitial
>1030	$D = 1.0 \times 10^{16} \exp\left(- \frac{150,000 \text{ Cal}}{RT}\right)$	Zn-ZnS	Vacancy
<940	$D = 3.0 \times 10^{-9} \exp\left(- \frac{20,000 \text{ Cal}}{RT}\right)$	Zn-ZnO	----
940-1025	$D = 5.0 \exp\left(- \frac{75,000 \text{ Cal}}{RT}\right)$	Zn-ZnO	Interstitial

Even though the same interstitial mechanism is operative between 940°-1025°C in both Zn-ZnS and Zn-ZnO systems, their D_0 values are different as are their absolute D values. No explanation has been furnished for these discrepancies.

Among other data available for polycrystalline intermetallic compound semiconductors, some are given below:(35,36,37,38,39)

$$D_{Sb\rightarrow ZnSb} = 30 \exp\left(-\frac{1.8\ \text{ev}}{kT}\right) + 4 \times 10^{-11} \exp\left(-\frac{0.2\ \text{ev}}{kT}\right) \tag{II.21}$$

$$D_{In\rightarrow InSb} = 1.8 \times 10^{-9} \exp\left(-\frac{0.28\ \text{ev}}{kT}\right) \tag{II.22}$$

$$D_{Sb\rightarrow InSb} = 1.4 \times 10^{-6} \exp\left(-\frac{0.75\ \text{ev}}{kT}\right) \tag{II.23}$$

$$D_{Sb\rightarrow GaSb} = 8.7 \times 10^{-3} \exp\left(-\frac{1.13\ \text{ev}}{kT}\right) \tag{II.24}$$

$$D_{Ga\rightarrow GaSb} = 3.2 \times 10^{3} \exp\left(-\frac{3.15\ \text{ev}}{kT}\right) \tag{II.25}$$

$$D_{Ga\rightarrow GaAs} = 1.1 \times 10^{7} \exp\left(-\frac{5.6\ \text{ev}}{kT}\right) \tag{II.26}$$

$$D_{As\rightarrow GaAs} = 3.6 \times 10^{21} \exp\left(-\frac{10.2\ \text{ev}}{kT}\right) \tag{II.27}$$

$$D_{In\rightarrow InP} = D_o \exp\left(-\frac{3.85\ \text{ev}}{kT}\right) \tag{II.28}$$

$$D_{P\rightarrow InP} = D_o \exp\left(-\frac{5.65\ \text{ev}}{kT}\right) \tag{II.29}$$

Efforts have been made to explain the mechanisms of these self-diffusion data with conventional interpretations but considerable controversy still exists.

III. OBJECTIVES OF THE PRESENT INVESTIGATION

The objectives of the present investigation may be divided into the following parts:

1. To develop suitable techniques for the direct measurement of diffusion coefficients of both species in both single and polycrystalline silicon carbide.
2. To determine the slower diffusing species between silicon and carbon in single crystal silicon carbide.
3. To measure diffusion coefficients of slower diffusing species as a function of temperature, impurity type and level, and crystal orientation.
4. From the measured diffusion coefficients of the slower diffusing species understand the mechanism of the process in this predominantly covalent refractory compound.

IV. MATERIALS AND PROCESSES

A. SILICON CARBIDE SAMPLES

a) Single Crystals. Single crystals of hexagonal silicon carbide were obtained from several sources: 1) Norton Company, Worcester, Massachusetts; 2) Carborundum Company, Niagara Falls, N. Y.; 3) Westinghouse Research Laboratory, Pittsburgh, Pennsylvania; and 4) Philips Research Laboratory, Eindhoven, Netherlands. They were primarily of three colors: dark blue to black, green to yellow-green, and light grey to almost transparent. Black and green crystals from Norton Company were the largest ones and could be used under the sensitivity of the method. Crystals from the Westinghouse Research Laboratory were smaller and more impure than the Norton green crystals. Philips Research Laboratory provided the best impurity content-and-type controlled crystals. Since they were too small and very thin, they were not actually used in the diffusion experiments but only used to compare the impurity type and content of the Norton crystals.

Typical SiC single crystals, from the Norton Company, (Crystolon "S") are shown in Fig. 2 . They were handpicked from large batches of electric-furnace produced abrasive quality SiC; SiC vapor escaping from hot furnace core deposit as single crystals in cooler parts of the furnace. They are up to 0.5 inch across by 0.1 inch thick. They are almost all of the 6H polytype. The large flat growth faces are the (0001) faces and the bounding growth faces are the $\{1\bar{1}0h\}$ faces, where h commonly varies from 0 to 5.(42)

Typical spectrochemical analyses for the commercial crystals are given(43) in Table I in Appendix E, whereas that of the crystals used are given in Table II in Appendix E. The major coloring agent to give dark blue to black appearance is aluminum (which also gives the p-type conductivity) and nitrogen produces yellow-green to green color (giving n-type conductivity at the same time).(44) The large amount of free SiO_2 observed in grey and black SiC is thought to be a surface oxidation product.(45,46)

b) Polycrystalline. Only one variety of polycrystalline material was used. This black sample was supplied by the courtesy of Dr. T. Vasilos of AVCO Corporation, Wilmington, Massachusetts. It has a uniform grain size and very little porosity, as shown in Fig. 3; its density is quoted in excess of 99 per cent of the theoretical density (3.210 gm/cm^3).(44) It is a self-bonded material which is produced by hot pressing at about 2600°C and it is of comparable purity to black SiC single crystals from which it is produced. It has an average grain size of 10^{-3} inch. This polycrystalline material came from the same piece from which Farnsworth(47) made samples for creep measurements.

FIG. 2 TYPICAL SiC SINGLE CRYSTALS

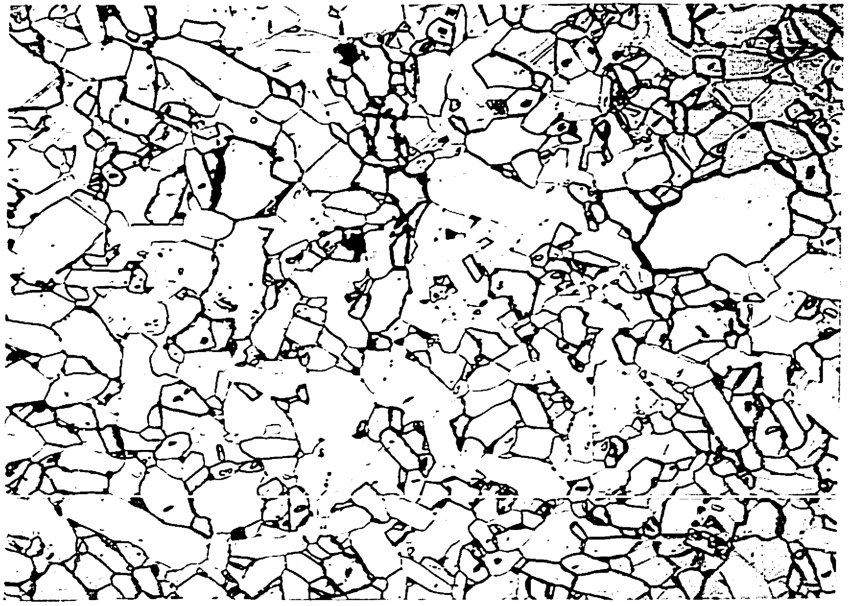

FIG. 3 MICROSTRUCTURE OF POLYCRYSTALLINE SiC. 250X.
ELECTROLYTIC ETCHING IN 20% KOH FOR 30 SECONDS.

B. EXPERIMENTAL PROCEDURE

a) Sample Preparation and Evaluation. Silicon carbide single crystals of sufficiently large size were selected with one plane side which were almost perfectly on the (0001) planes (basal). The samples were mounted with this plane down and carefully cut with a thin diamond wheel to a square or rectangular shape. These samples were then mounted with the basal (0001) plane side down on an accurately machined hard-steel cylinder of 0.50 inch diameter and 1-1/2 inch long which fitted closely inside a soft steel guard ring of 1.00 inch O.D. and 0.50 inch I.D. The ends of this sample holder (guard ring plus the cylinder) were machined exactly parallel to each other and perpendicular to their common vertical axis. The other sides of the samples were thus ground and polished to a fine finish with plane parallel sides. The mounting was then reversed to the polished side and the (0001) plane side finished. The crystals were then dismounted and the edges finished on a lapping wheel. To compare the accuracy of this sample preparation technique, a set of reference samples was made to specified order by the Van Keuren Company of Waltham, Massachusetts. This is given below:

Specifications for Silicon Carbide Wafers made by Van Keuren Company of Waltham, Massachusetts

1. Shape - square, 1/4 inch on each side.
2. Thickness - about 40 mils.
3. Finish - 2 micro inch on both faces.
4. Flatness - within one light wave band (11.6×10^{-6} inch) on both faces.
5. Parallelism - 20 millionths of an inch between two faces.

The samples were then evaluated for mechanical size with a micrometer reading up to 0.0001 inch. Each sample was then checked for orientation by Laue back-reflection pattern. A good amount of imperfections was introduced on the sample surface by this method of surface preparation, but they were found to anneal out very fast even at 1400°C. Some of the crystals were found to have some grown in porosity and were discarded. A few nearly transparent light green crystals were found to contain some grown-in crystallites deep inside the crystal which had the same orientation as the main crystal. This is shown in Fig. 1, in Appendix E. For all mounting purposes, colorless neutral solidified canada balsam was used on a hot plate. Polycrystalline samples were prepared in the same way.

<u>b) Deposition of Thin Film.</u> An intimate stoichiometric mixture of silicon-28 and carbon-14 isotopes was made in a "diamonite" (Al_2O_3) mortar with two to four drops of reagent-grade glycerol as the suspending medium. Complete search for a high density-high viscosity wetting suspending medium was made as shown in Table III in Appendix E. The best medium should not separate the isotope mixture into its constituents on standing and should not run down the sample sides at drying temperatures or below. The sample surfaces were cleaned with absolute alcohol and acetone. The isotopic paste was then brushed onto one surface of the sample with a very fine camel hair brush to a uniform layer. This was dried at about 64°C in air-oven for about 48 to 72 hours to remove glycerol as completely as possible. These samples were then carefully put inside covered green SiC crucibles (made by the Norton Company with 0.5 inch diameter × 0.5 inch

high × 1/16 inch wall) and sintered in 0.6 to 0.8 atmospheric pressure of pure argon for 8 hours at $1400^{o}C$ and 2 hours at $1600^{o}C$. The initial part of sintering just below the melting point of metallic silicon ($1420^{o}C$) supposedly made a uniform spreading of liquid silicon to engulf fine carbon-14 particles to form SiC before most of the silicon vaporized out. The latter part of sintering sintered this thin SiC film on to the single crystal. This schedule produced the most uniform thin film covering the entire surface, sufficiently strong to withstand subsequent treatments and having adequate C-14 activity for diffusion run. The thickness of the thin film produced this way was calculated to be about $1/4 \pm 1/4\ \mu$ (from weight gain) which gave an average ratio of diffusion penetration to film thickness of about 80 to 100:1; thus satisfying the boundary conditions. Incidentally, in deriving equation (II.1) it was assumed(2) that $d/2\sqrt{Dt} \ll 1$ where d is the thickness of the thin film. A comparison of the sample surface before and after thin film deposition is shown in Fig. 4a and 4b. Films deposited at higher temperatures or longer times or both produced uneven growth steps (up to 60 μ thick) and/or crystallites on the surface as shown in Fig. 5.

The samples thus sintered were weighed, counted for surface activity, and edges ground to remove traces of activity which might have developed by either surface diffusion or by vapor-phase transport of carbon-14 during sintering.

c) <u>Diffusion Annealing</u>. The samples thus prepared with a thin film were put into silicon carbide crucibles (to reduce sample decomposition

FIG. 4a A VIEW OF THE SURFACE OF SAMPLE S/N_B/10 BEFORE THIN-FILM DEPOSITION (500X)

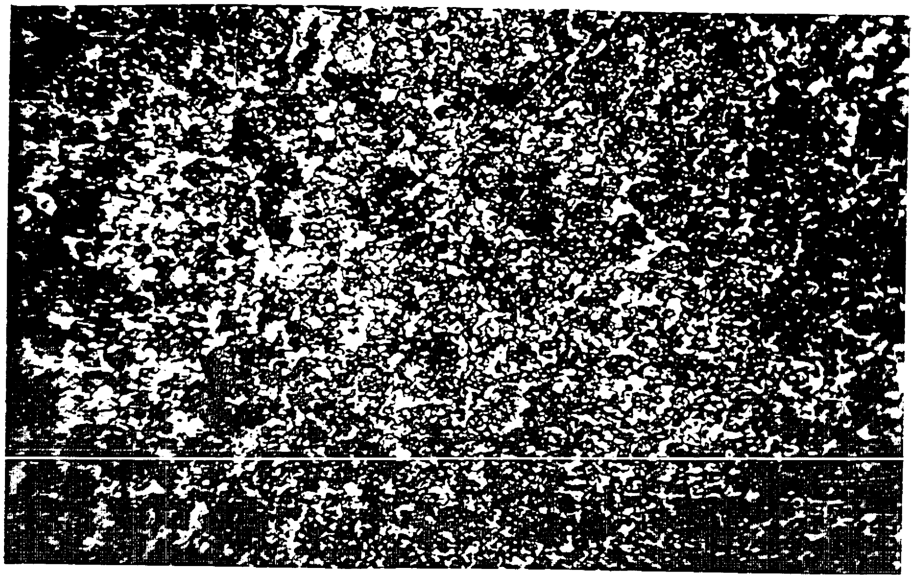

FIG. 4b A VIEW OF THE SURFACE OF SAMPLE S/N_B/10 WITH SINTERED THIN-FILM (500X)

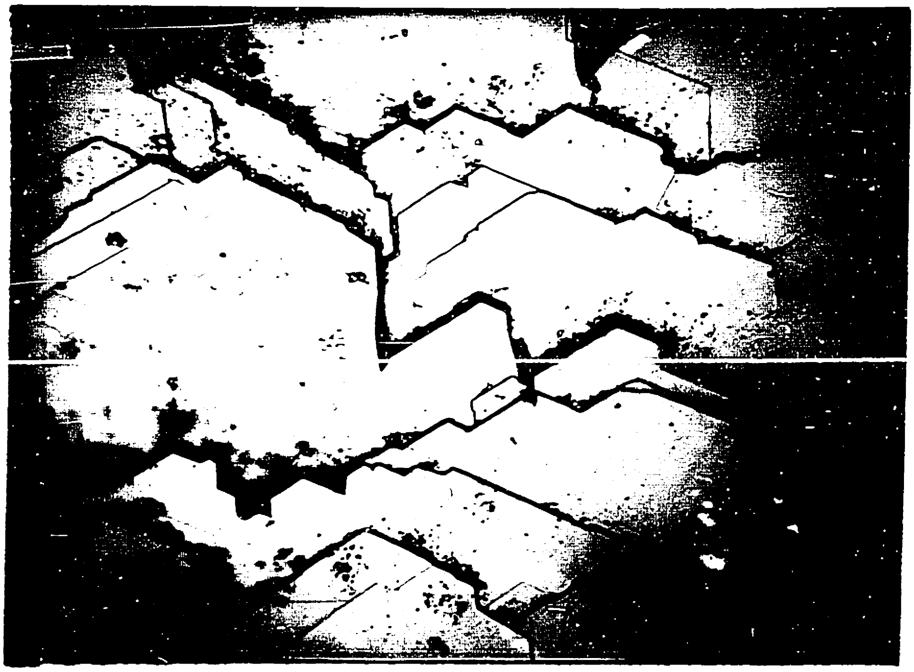

FIG. 5 GROWTH-STEPS ON A SAMPLE AFTER SINTERING THE THIN-FILM AT 1600°C FOR 22 HRS. (500X)

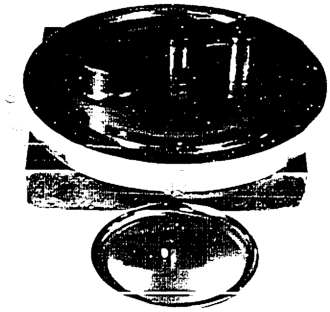

FIG. 6 PHOTOGRAPH OF HAND LAPPING DEVICE

loss) inside the induction-furnace. A detailed description of the furnace is given in the Appendix B. The furnace was then pumped down to 1.0×10^{-6} cm of mercury overnight and purged with pure argon four to five times. The furnace was then sealed with pure argon inside to a static atmospheric pressure of 55 to 60 cm of Hg. During heat up, the furnace was kept stationery for some time at about 850°C to purify its atmosphere from oxygen and nitrogen by -8 + 35 mesh spongy titanium "getters" put inside. After the furnace was slowly heated to about 1500°C it was very rapidly heated (in about 10 minutes) to the diffusion annealing temperature between 1850°C and 2100°C. The temperature was continuously recorded by Leeds and Northrup Optical pyrometer calibrated against a Siemens and Halske Laboratory Standard calibrated by the Bureau of Standards. The absorption of the vycor end window was found to require a correction of 36 ±2°C throughout the range of interest. The effective emissivity of about 0.99 between 1850°C to 2100°C required no correction of temperature for black-body conditions.

The sample was soaked for a predetermined time at the annealing temperature with a very accurate control of constancy of temperature. The total variation of ±5°C during the run was probably possible due to practically thermostatic watercooling (constant rate of flow of water) and was well within the limits of visual observation by an optical pyrometer.

After the anneal, the furnace was quenched at the rate of about 475°C/min. The samples were then weighed and counted for surface activity. Then the edges were ground to a depth of more than the anticipated penetration mounted with the diffusion side down and the backside ground and polished to attain parallelism of the two opposite faces. The samples were then weighed accurately to an accuracy of ± 0.01 mg and surface count recorded.

d) Sectioning and Counting. The procedure for removing layers from the samples perpendicular to the direction of diffusion for determining concentration profiles was critical and will be discussed in some detail. Most important in this process was grinding off sections parallel to the original surface. Due to some decomposition from the backside of the sample, the two surfaces were not parallel any more. What was required was a method of flattening this surface and making it parallel to the original surface using the thin-film coated surface as a reference plane.

Cylindrical hard-steel cylinders were prepared for mounting the sample with the active side up. This was a 0.50 inch diameter × 3/4 inch long hard steel cylinder tipped with 1/8 inch thick sintered pure boron carbide on both faces fitting tightly inside tabular 1.00 inch O.D. × 5/8 inch long hard steel guardring tipped with 1/8 inch thick sintered pure boron carbide on one face only. The two faces were parallel to each other and perpendicular to the cylinder axis conforming to the same type of specification as that for the samples made by the same Van Keuren Company of Waltham, Massachusetts, and given under sample preparation and evaluation part. Reference is made to Fig. 6 which shows the sample mounting assembly for sectioning with the lapping block.

Following the experience of sectioning by Paladino(48), a hand-lapping technique was selected. The lapping block selected for this purpose was a 99.999% pure aluminum disc of 4 inches in diameter and

1/2 inch thick with a 1/8 inch wide canal running around the disc-edge (1/4 inch away from the edge) and slowly sloping to a 1/8 inch diameter hole pressure fitted with a pure aluminum tubing protruding 1/4 inch from the bottom of the disc. The top surface of the lapping block was machined to 1 band flatness. The lapping block was supported on a carefully machined 3/4 inch thick hard steel plate. This design was made to collect the grindings as quantitatively as possible. The selection of materials for the lapping block and the sample mounting assembly was mainly made on the consideration of non-interference by the contaminations of the collected grindings upon irradiation in the reactor.

The sample mounting was done on a hot plate with Canada balsam. Molten balsam produced a viscous uniformly spread liquid onto which the sample was put and pressed by a 1/2 inch diameter flat steel cylinder weighing about 20 gms. This set up was then allowed to cool slowly to room temperature. The excess mounting material was removed from the sides of the mounted sample by wiping off with an acetone-soaked tissue paper. The sample was then placed on the lapping block and slowly lapped with 4-8 μ size virgin diamond powder. The parallelism of sectioning was periodically checked by both micrometer and reflected light. After each sectioning, the sample was dismounted, wiped clean, and weighed. The thickness of the removed section was calculated from this change in weight of the sample (to an accuracy of 0.01 mg) and the surface area of the sample which was determined by low-power photomicrography (about 16X). The entire sectioning procedure is illustrated in Fig. 7.

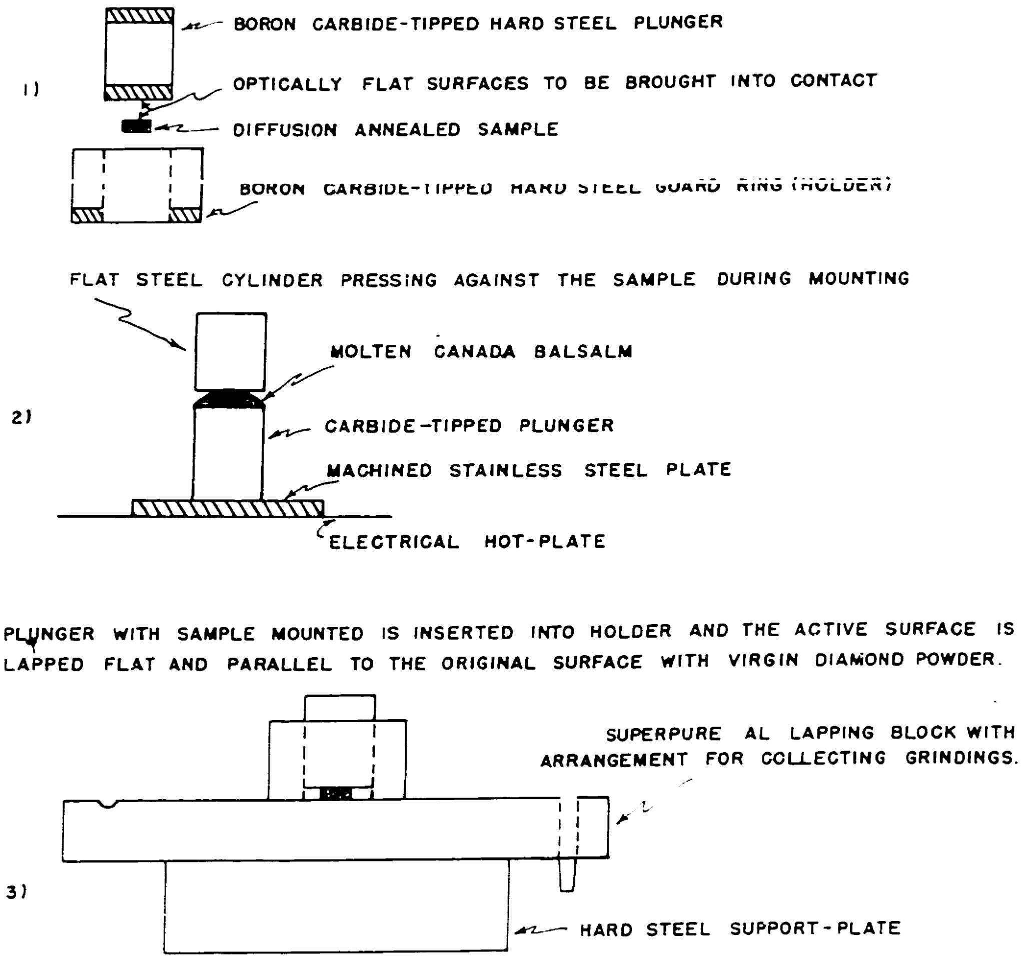

FIG. 7 HAND LAPPING PROCEDURE

The grindings were collected onto a 1/8 inch cupped stainless steel counting planchet of 2 inches in diameter by washing down the canal with absolute alcohol and rubber policeman. Any remaining activity was removed by a paper cleaner. The lapping block was cleaned of any activity in between two successive sectionings. A uniform loss of section material during this transfer was estimated to be about 5%.

The grindings were then freed of any alcohol over a hot plate and put into the windowless proportional counter and flushed with P-10 gas for about 2 minutes. Complete flushing of the detector chamber was taken when there was no change in count rate with flushing. The center wire anode was then subjected to 1.85 KV and the sample counted with a gas flow of about 15 bubbles/min. for an extended time or total count to reduce the statistical error of counting. This 1.85 KV is at about the center of the beta plateau for 0.155 MeV C-14 β^--radiations in this particular assembly. The determination of this plateau as also the positions of pulse-height discriminator and attenuator, were predetermined by calibration of the assembly against a standard C-14 sample supplied by the Nuclear Measurements Corporation. The calibration curve is shown in Fig. 8. Considerable reproducibility in the count rate was found and no difficulty due to either static charge build up on the sample or any other effect was observed.

After counting for C-14 activity, the sections were transferred to 1/2 inch diameter polyethylene vials and irradiated in the M.I.T. reactor for 1/2 hour at an average flux density of 2.0×10^{13} neutrons/cm^2 (neutron energy $\cong$ 0.4 ev). Blank samples were simultaneously irradiated with the

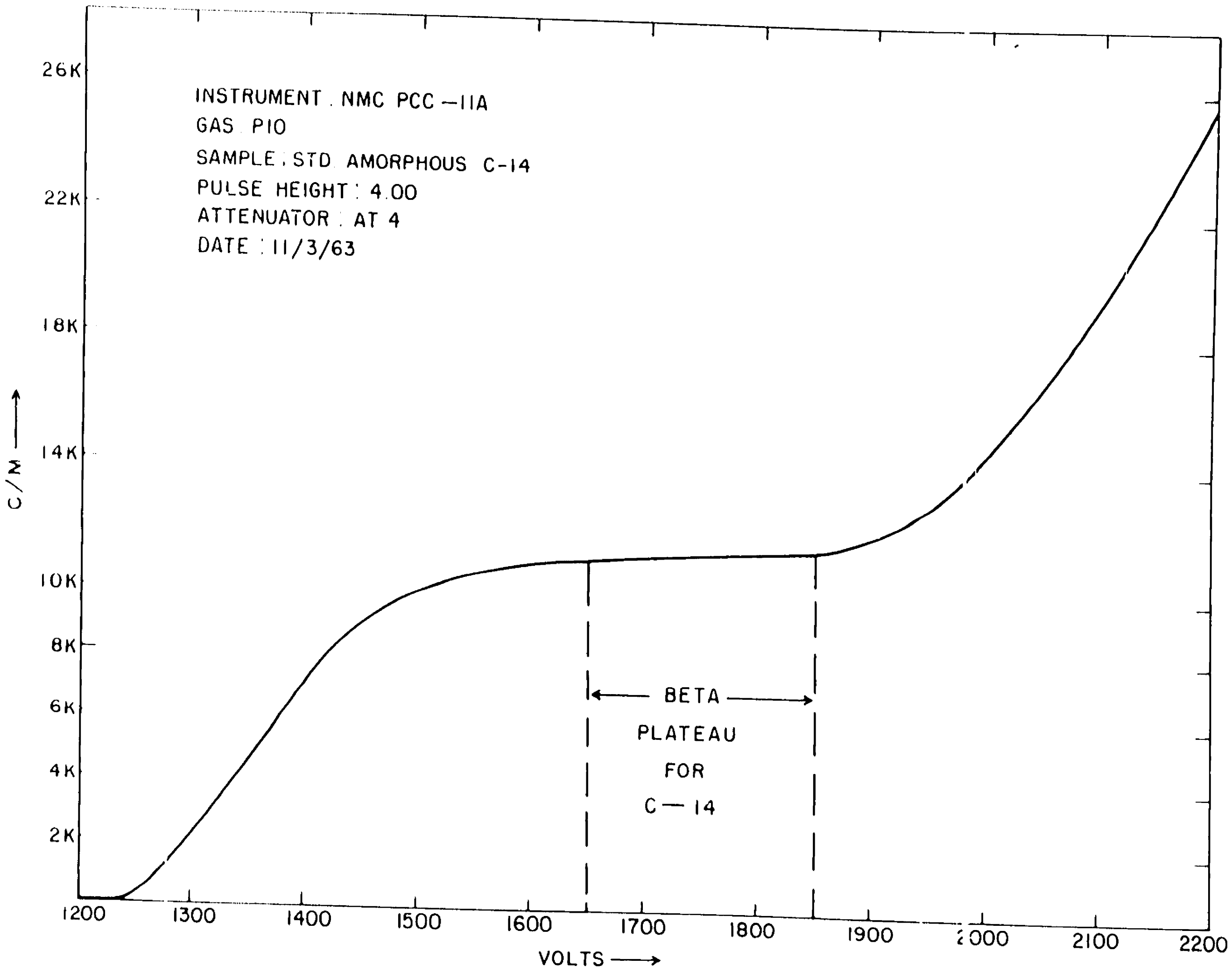

FIG 8 CALIBRATION CURVE FOR CARBON 14 β — PROPORTIONAL ASSEMBLY

sections which were prepared exactly the same way. On the completion of irradiation, the sample slices were transferred to new polyethylene vials and subjected to scintillation gamma spectroscopy for finding out the relative concentrations of silicon-31 in each section. After this step, the samples, which were still very hot, were disposed of properly.

V. RESULTS AND DISCUSSION

A. DIRECTLY MEASURED SILICON DIFFUSION COEFFICIENTS.

Among the samples subjected to thermal neutron-irradiation, only two produced any meaningful data. These samples were subjected to both scintillation γ-spectrometry and long time proportional counting to identify the impurity radionuclides produced by irradiation.

The possibility of the presence of any undesirable radioactive isotope in the irradiated product can be considered from the sources of contamination of the samples which are:

1. Aluminum lapping block.
2. Diamond powder.
3. Lubricants and solvents used during sectioning.
4. SiC sample.
5. Boron Carbide tipped sample mount.
6. Isotope mixture.

Of these, the analyses given in Appendix E shows the impurities in aluminum lapping block, SiC sample and isotope mixture. Of the solvents and lubricants used, absolute alcohol, ethanol and acetone were of A.R. grade and iso-octane was of spectrographic quality with 0.001% (as S) of sulfur compounds. Analysis for Norton Boron Carbide was not available but was claimed as hot-pressed high purity type. Very minute amounts of boron carbide hardly could contaminate the sample, however.

Proportional counting of the different sections (with blanks) over a period of 25 days identified the following β-emitting radioisotopes from their half-life determinations:

Radiation	Half-life Determined	Most probable radioisotope Half-life	Element
β^-	2.83 ± 0.32 days	2.70 days	Au-198
β^-	15.0 ± 1.2 days	14.5 days	P -32

The presence of both of these isotopes can be properly explained. According to Freeman(49) the gem-yellow coloration of natural diamond is due to minute amounts of gold in solid solution. He irradiated some natural diamond and identified Au-198 in the irradiation product formed by the reaction:

$$_{79}Au^{197} + {_o}n^1 \longrightarrow {_{79}}Au^{198} \tag{V.1}$$

Gold-197, with a thermal neutron capture cross-section of 97×10^{-24} cm^2 and a natural abundance of 100%, is one of the materials most easily activated in a reactor. Amplex 4-8 μ virgin diamond (natural) powder, used in exactly equal amounts for making each section of the diffused sample, is the carrier of this impurity. Its activity constituted a very large percentage of the total activity of each section during the first day of counting of the irradiated samples. Presence of Au-198 had also been identified by the irradiation of pure Amplex 4-8 μ diamond powder.

Regarding the presence of Phosphorus-32 in the irradiated product there could be two sources. First, it is a by-product of the irradiation of Silicon-30 by the following series of reactions(A 16):

$$\begin{gathered} {}_{14}\mathrm{Si}^{30} + {}_{0}n^{1} \rightarrow {}_{14}\mathrm{Si}^{31} \xrightarrow[\text{decay}]{\beta^-} {}_{15}\mathrm{P}^{31} \\ {}_{15}\mathrm{P}^{31} + {}_{0}n^{1} \rightarrow {}_{15}\mathrm{P}^{32} \xrightarrow[\text{decay}]{\beta^-} {}_{16}\mathrm{S}^{32} \end{gathered} \tag{V.2}$$

According to Koch(A 16) this is an accepted interference in the determination of Silicon-31. The activity of the sections, due to Phosphorus-32, was also found to be dependent on the time of irradiation with longer irradiation intervals (up to 10 hours) giving more activity due to Phosphorus-32. Secondly, considering the most widely accepted theory of the origin of diamond from petrified vegetations, a sizeable amount of phosphorus is expected in it. This natural phosphorus in diamond, as also in SiC (made from coke and sand), is 100% Phosphorus-31. Phosphorus-31, having a thermal neutron-absorption cross section of 0.2×10^{-24} cm^2, could be very easily converted to Phosphorus-32 under the irradiation conditions.

Typical representations of the proportional counting data are given in Figs. 9 and 10 which show the extremely large percentage of impurity activity. These data are only indicative, however, of the presence of Silicon-31 in all the sections in different amounts increasing in the expected direction.

To avoid the interference of all β^-- and γ-emitting impurity radionuclides, the samples were then subjected to multichannel analysis as described before. The analyzer was calibrated against standard γ-emitters, as shown in Table I.

This calibration curve is shown in Fig. 11. The samples are then counted in 400 channels for 10 minutes and the results plotted (from print out data) as shown in Fig. 12. The nine major peaks are identified as shown in Table II.

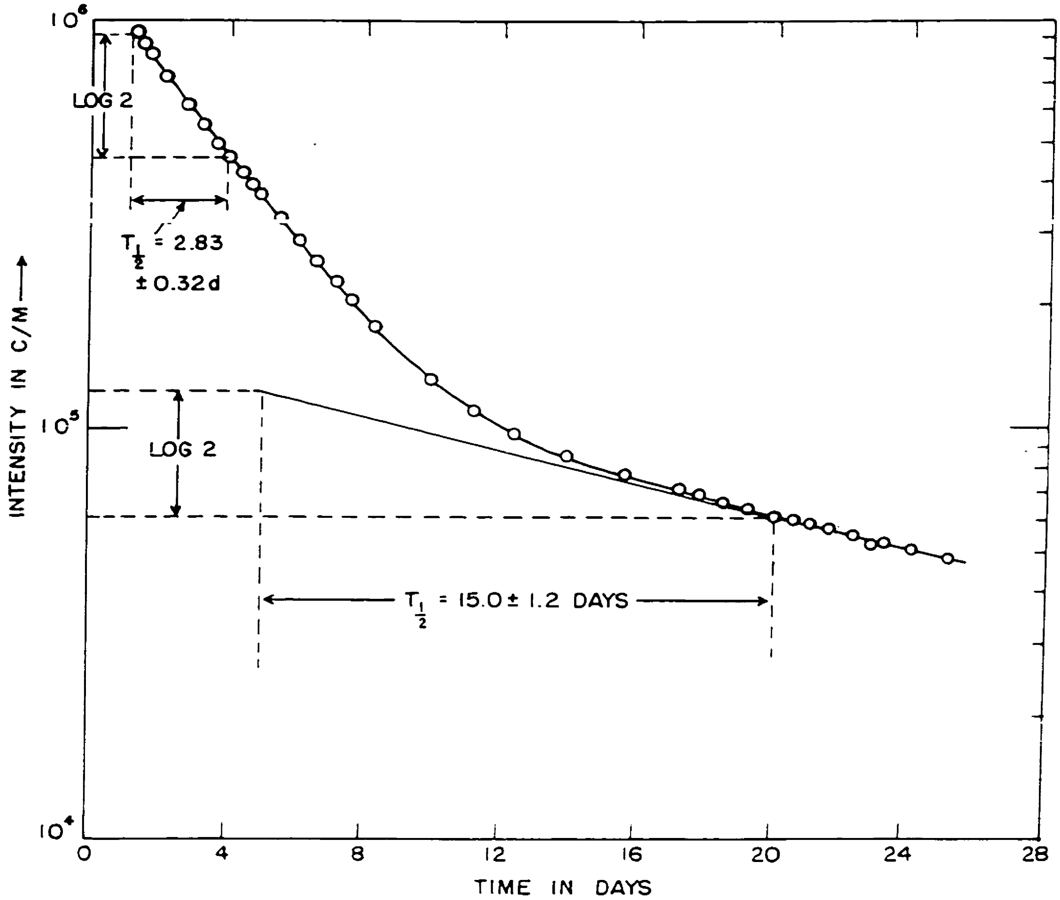

FIG. 9 PROPORTIONAL COUNT DATA FOR 3.00 ± 0.01 mg OF 4-8μ AMPLEX VIRGIN DIAMOND POWDER.

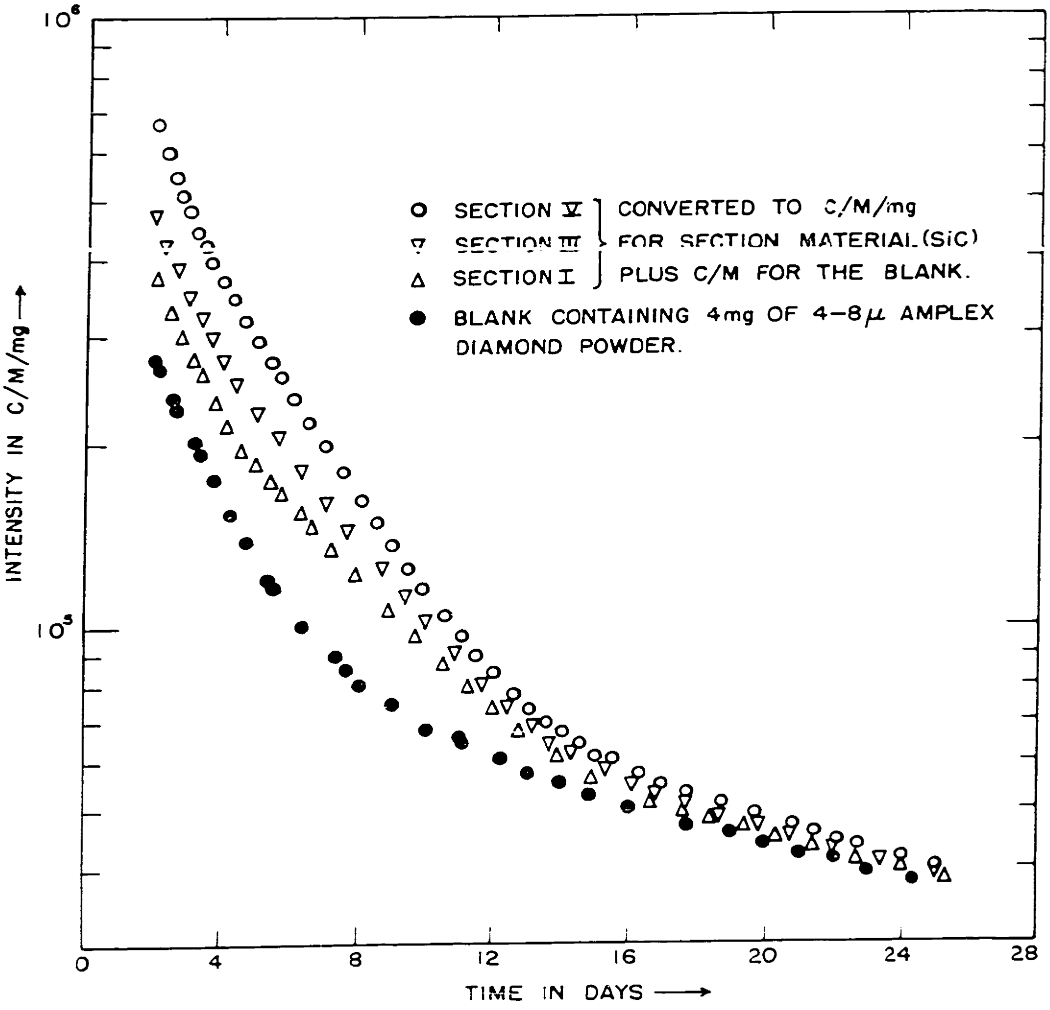

FIG. 10 TYPICAL PROPORTIONAL COUNT DATA FOR IRRADIATED SECTIONS. (SAMPLE $S/N_B/11$)

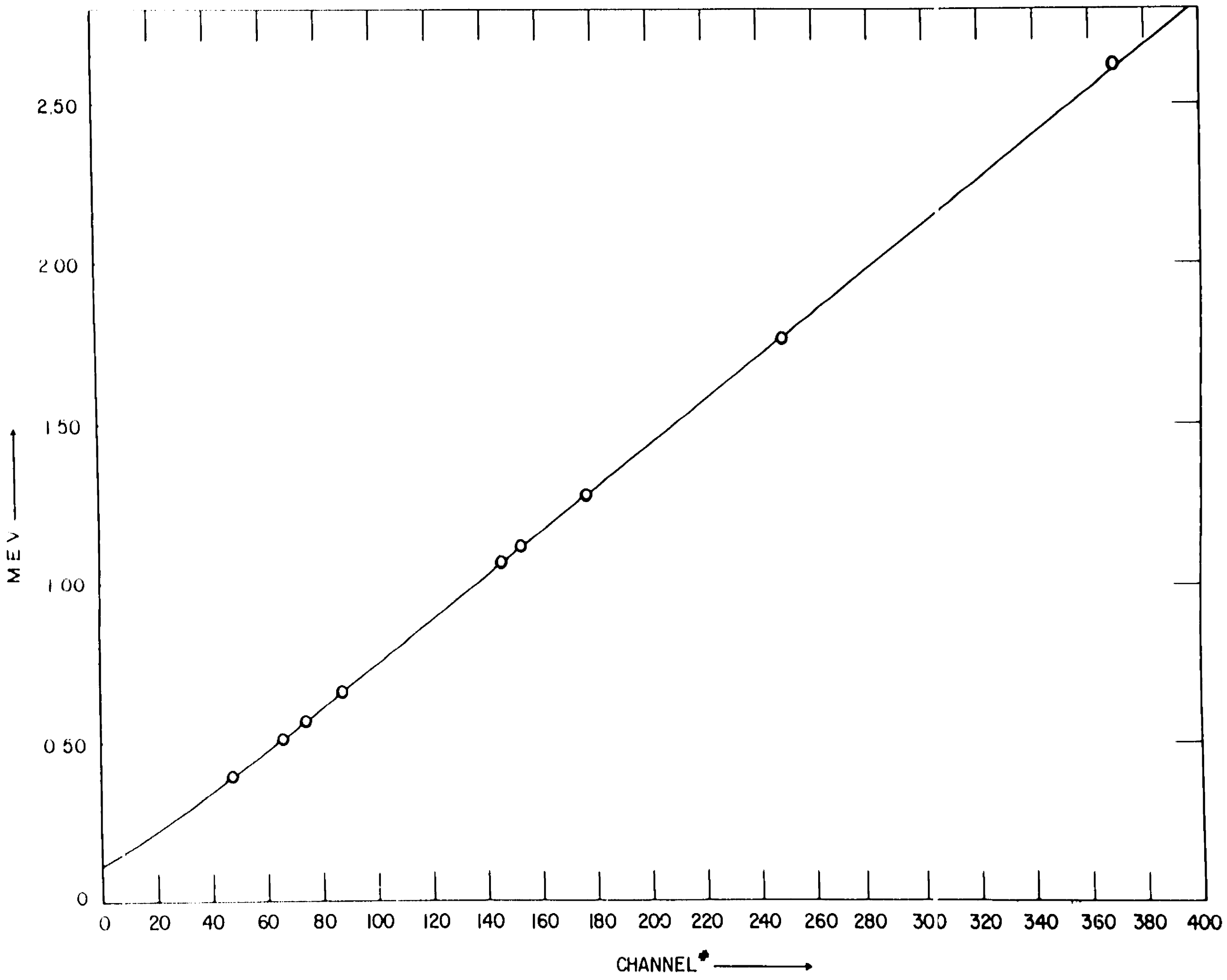

FIG 11. CALIBRATION CURVE FOR THE MULTICHANNEL ANALYZER

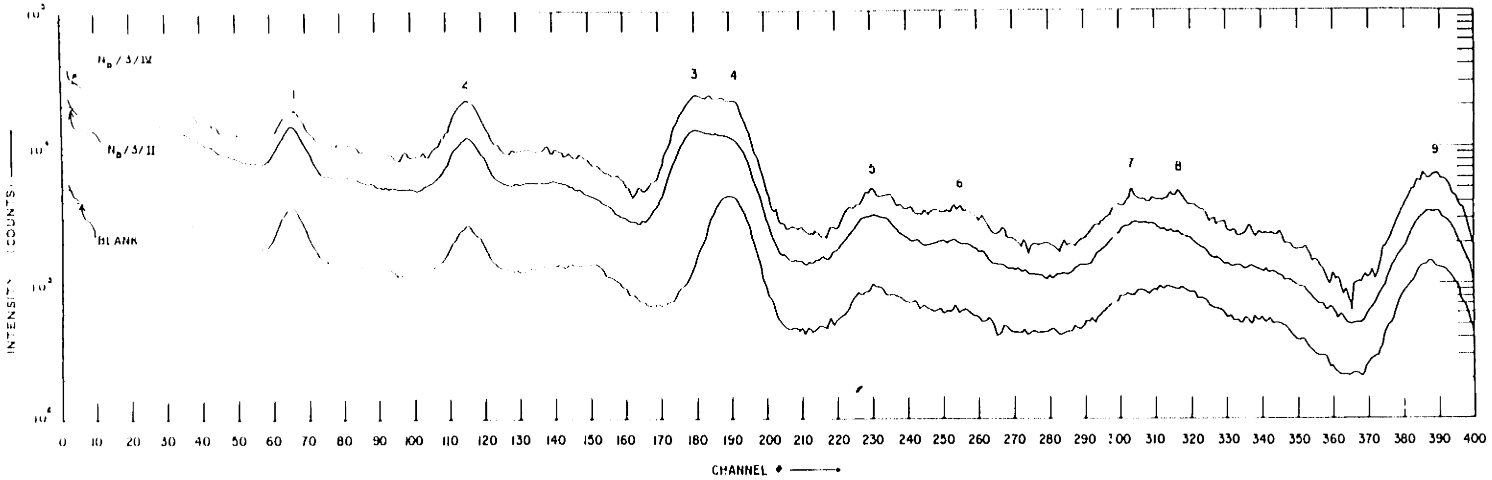

FIG 12 DATA FROM MULTICHANNEL ANALYSIS OF IRRADIATED SiC SECTIONS

TABLE I

Calibration of the Multichannel Analyzer

Isotope	Energy (MeV)	Channel No.
Bi-207	0.088	---
	0.570	74
	1.064	146
	1.771	248
Sn-113	0.393	47
Cs-137	0.662	87.5
Na-22	0.511	65.5
	1.274	177
Zn-65	1.114	153
ThC″ (Tl-208)	2.620	369

TABLE II

Identification of the Radioisotopes in Irradiated Sections

Peak No.	Channel No.	Corresponding Energy in MeV	Identity
1	66	0.511	From pair production (2.75 MeV γ of Na-24)
2	115.5	0.850	Mn-56
3	180	1.29	Si-31
4	190	1.37	Na-24
5	231	1.65	Cl-38
6	255	1.80	Mn-56
7	304	2.15	Mn-56, Cl-38
8	316	2.24	Na-24 (2.75 MeV γ first escape pulse)
9	388	2.75	Na-24

The uppermost curve in Fig. 12 represents Section IV, whereas, the middle curve represents Section III with the lowermost curve representing blank diamond powder. The absence of 1.26 MeV peak in channel no. 180 for the blank indicated the feasibility of Silicon-31 counting. All the sections were irradiated and analyzed along with a blank under the same conditions. The count rate of the blank in the channel corresponding to Silicon-31 1.26 MeV γ was subtracted from each section. Count rates of each section thus obtained were then used in equation (II.2) to determine D values from each section. Here C_o is taken corresponding to the count rate of a section well within the sample beyond the penetration depth. All these data were, however, corrected for the decay loss using the following equation:

$$C_t = \frac{C'_o}{2^{t/T_{\frac{1}{2}}}} \tag{V.3}$$

where C_t = the count rate at time t after the completion of irradiation.

C'_o = the decay corrected count rate.

t = time interval between the completion of irradiation and counting.

$T_{\frac{1}{2}}$ = half-life of the radioisotope.

All the time values are in the same unit. Since for all practical purposes after an interval of 10 × $T_{\frac{1}{2}}$, all the activity of an isotope had decayed, counting was done as quickly as possible after the samples were taken out of the reactor pneumatic tube. The data for the two samples are given in Tables III and IV.

As is seen from these data, there is considerable variation of D values from different sections. This is probably understandable from the fact that C_t and C'_o were obtained by the subtraction of two large numbers

TABLE III

CALCULATION OF DIFFUSION COEFFICIENTS FOR SILICON IN SILICON CARBIDE

Sample Number = $S/N_B/11$

Temperature of Diffusion = 2200° ±5K

Time of Diffusion = 1.0×10^{5} secs.

Section Number	Decay Corrected Specific Activity (C/M/Mg) C (Section-blanc)	C_o (Pure SiC-blanc)	C/C_o	$\frac{\bar{X}}{2\sqrt{Dt}}$	$\bar{X}$ (microns)	Diffusion Coefficients (cm^2/sec.)
I	12.7	423.1	0.030	0.027	2.11	1.5×10^{-10}
II	64.0	426.7	0.150	0.134	6.13	5.2×10^{-11}
III	123.3	425.3	0.290	0.263	10.11	3.7×10^{-11}
IV	115.9	424.4	0.273	0.247	15.10	9.3×10^{-11}
V	183.6	431.1	0.426	0.398	19.81	6.0×10^{-11}

TABLE IV

CALCULATION OF DIFFUSION COEFFICIENTS FOR SILICON IN SILICON CARBIDE

Sample Number = $S/N_B/6$
Time of Diffusion = 2.07×10^4 secs.
Temperature of Diffusion = $2290^\circ \pm 5K$

Section Number	Decay Corrected Specific Activity (C/M/Mg) C (Section-blanc)	C_o (Pure SiC-blanc)	C/C_o	$\frac{\bar{X}}{2\sqrt{Dt}}$	$\bar{X}$ (microns)	Diffusion Coefficients (cm^2/sec.)
I	62.0	4.22×10^2	0.147	0.131	3.36	7.9×10^{-10}
II	56.3	4.18×10^2	0.1347	0.120	5.78	2.8×10^{-10}
III	117.7	4.28×10^2	0.275	0.249	8.49	1.4×10^{-10}
IV	131.0	4.31×10^2	0.304	0.276	10.68	1.8×10^{-10}
V	195.8	4.26×10^2	0.463	0.437	13.78	1.2×10^{-10}
VI	199.0	4.07×10^2	0.489	0.465	16.95	1.6×10^{-10}

(one corresponding to the count rate of a section in channel no. 180 and the other corresponding to that for the blank in the same channel). To obtain a greater accuracy of these D values, extensive radiochemical separation of silicon in any section from the impurities (mainly sodium) will be necessary.

Since the accuracy of these data is only within a factor of two (at best) no attempt was made to obtain more D values as a function of the temperature of diffusion. They, however, confirmed the fact that silicon is by far the faster diffusing species in silicon carbide and is, thus, of very little importance in SiC formation. This is against the prediction of Tomonari(50) from a study of the kinetics of SiC formation. These data are shown in comparison with those of carbon in Fig. 21.

B. DIRECTLY MEASURED CARBON DIFFUSION COEFFICIENTS.

(a) Description of the Experimental Results: The concentration profiles obtained by sectioning black hexagonal samples are shown in Figs. 13-15 as logarithm of specific activity versus the square of the penetration distance at each section. The specific activity of each section was calculated from the count rate and the weight of the section. The count rate was determined with an accuracy of more than 1.0 C/M(B-5) with counting times varying from 30 minutes to 6 hours. The background rate was periodically checked and found almost constant. The net counting rate was obtained by subtracting the simulated background rate from that of the sections individually. Sectioning was generally discontinued when a section showed an activity only a few counts above background. The average penetration was calculated at the central point of any section by adding the total thicknesses of preceding sections. The average accuracy of determining the penetration of each section was 1.5×10^{-5} cm. Detailed sectioning and counting data are presented in the Appendices C and D.

The sample orientations (relative to the diffusion direction) and the dislocation densities are reported in Table V. The concentration profiles for a light-green crystal, a faint yellow-green crystal (both hexagonal) and polycrystalline material at different temperatures are shown in Figs. 16-20.

An important feature of all the concentration profiles is the presence of a high gradient near the surface (1-2μ) which has been observed in many other systems(51-55). Many attempts have been made to explain these effects of which the following may have bearing on this particular investigation:

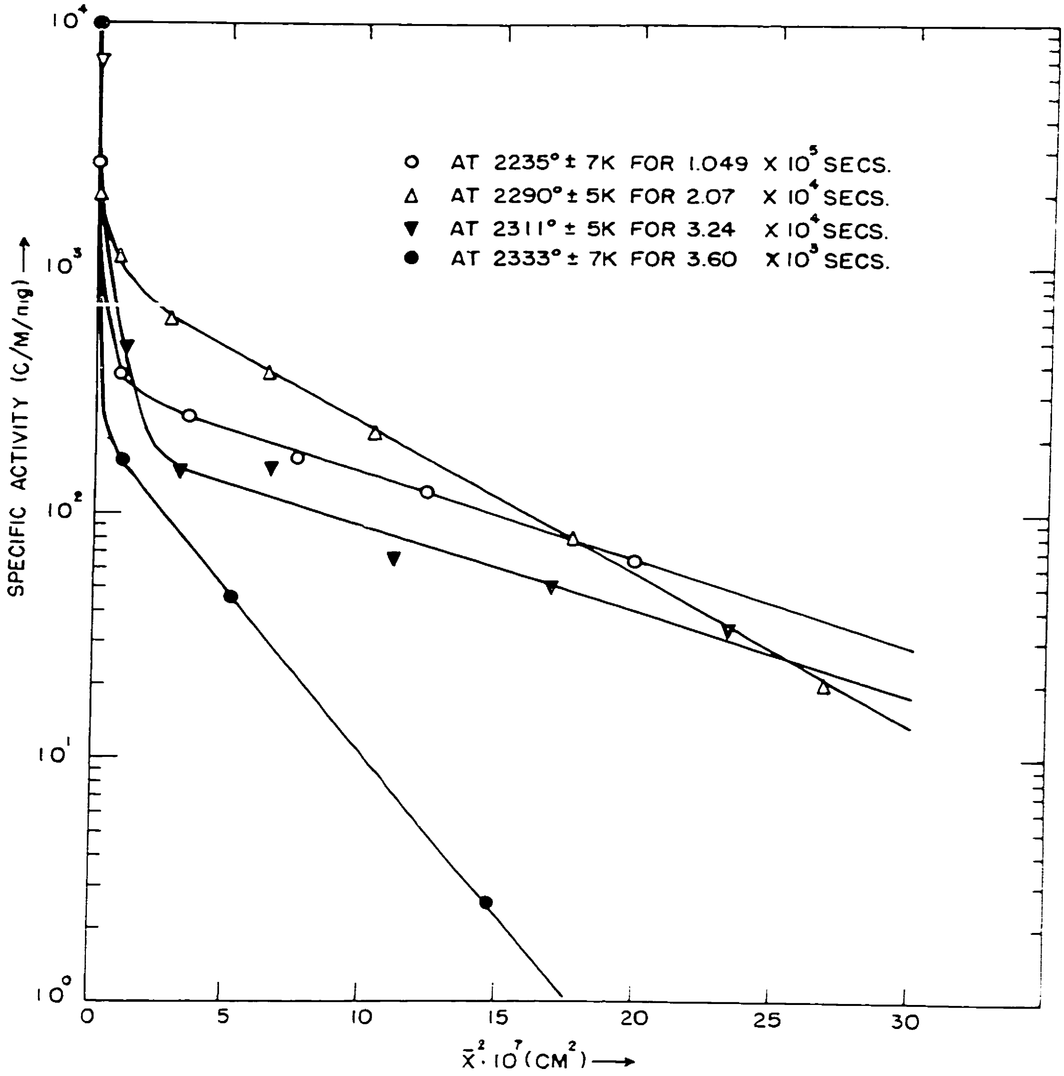

FIG. 13 CONCENTRATION PROFILES IN BLACK HEXAGONAL SILICON CARBIDE SINGLE CRYSTALS ALONG [0001] FOR DIFFUSION OF CARBON-14

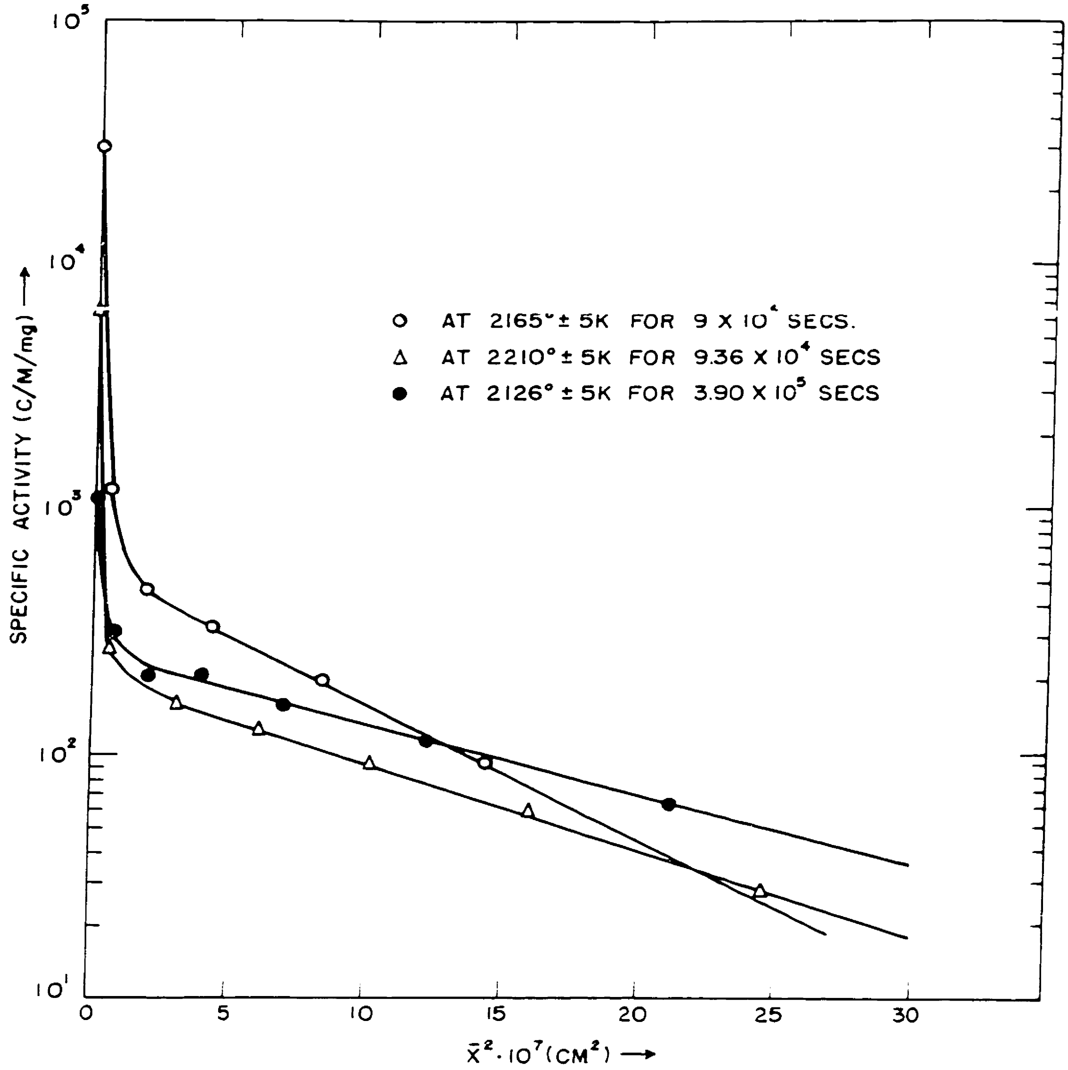

FIG. 14 CONCENTRATION PROFILES IN BLACK HEXAGONAL SILICON CARBIDE SINGLE CRYSTALS ALONG [0001] FOR DIFFUSION OF CARBON-14

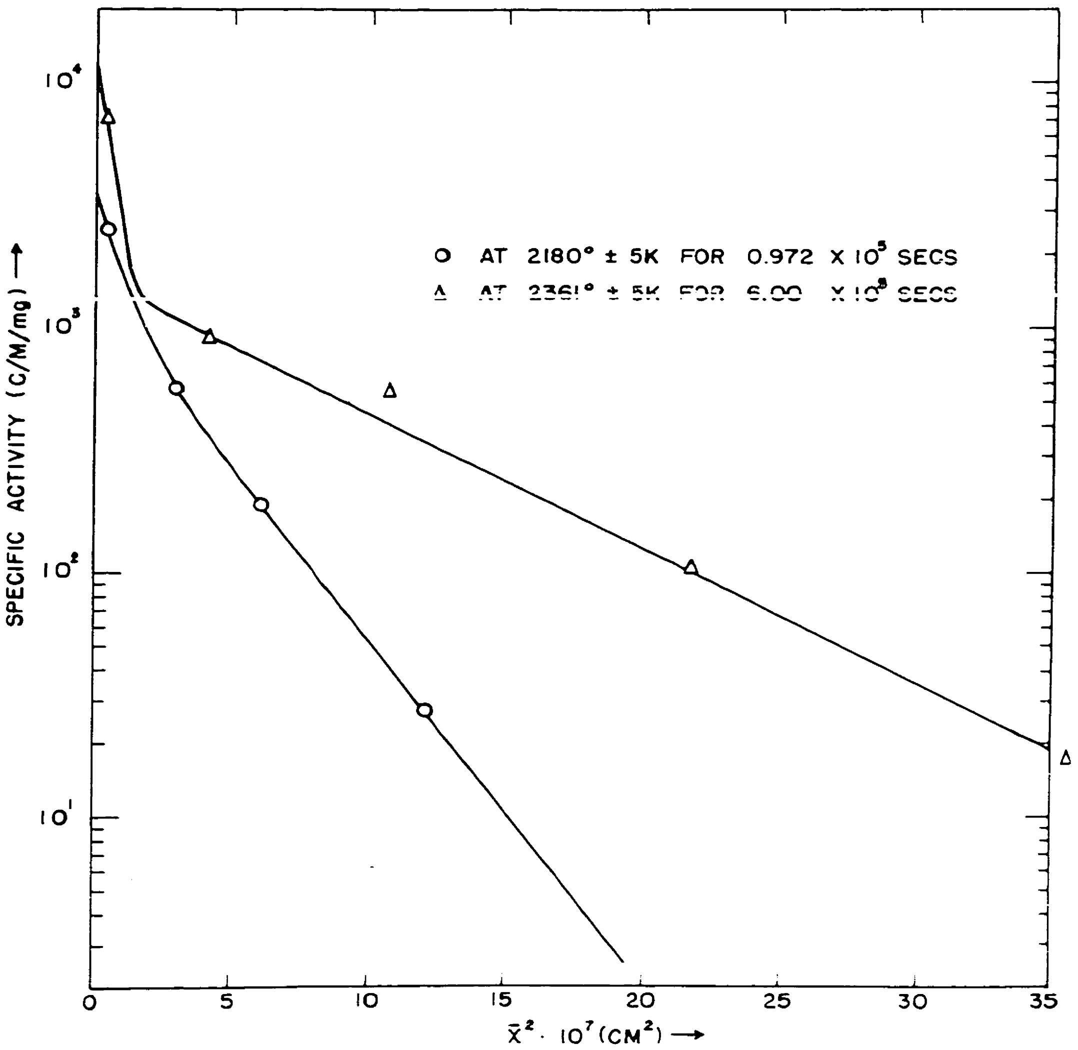

FIG. 15 CONCENTRATION PROFILES IN BLACK HEXAGONAL SILICON CARBIDE SINGLE CRYSTALS AT 22° TO [0001] FOR DIFFUSION OF CARBON-14

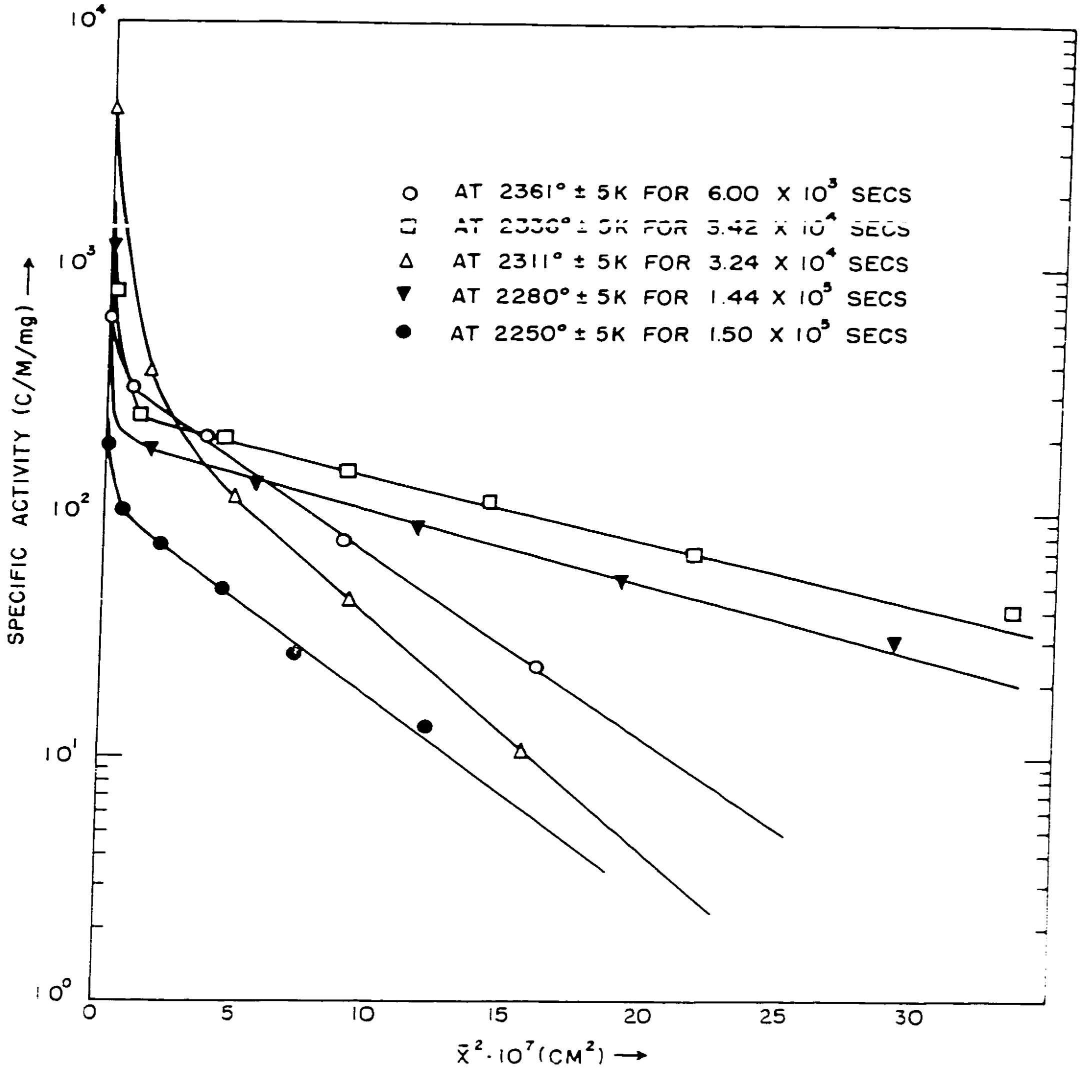

FIG. 16 CONCENTRATION PROFILES IN A LIGHT GREEN HEXAGONAL SILICON CARBIDE SINGLE CRYSTAL ALONG [0001] FOR DIFFUSION OF CARBON-14

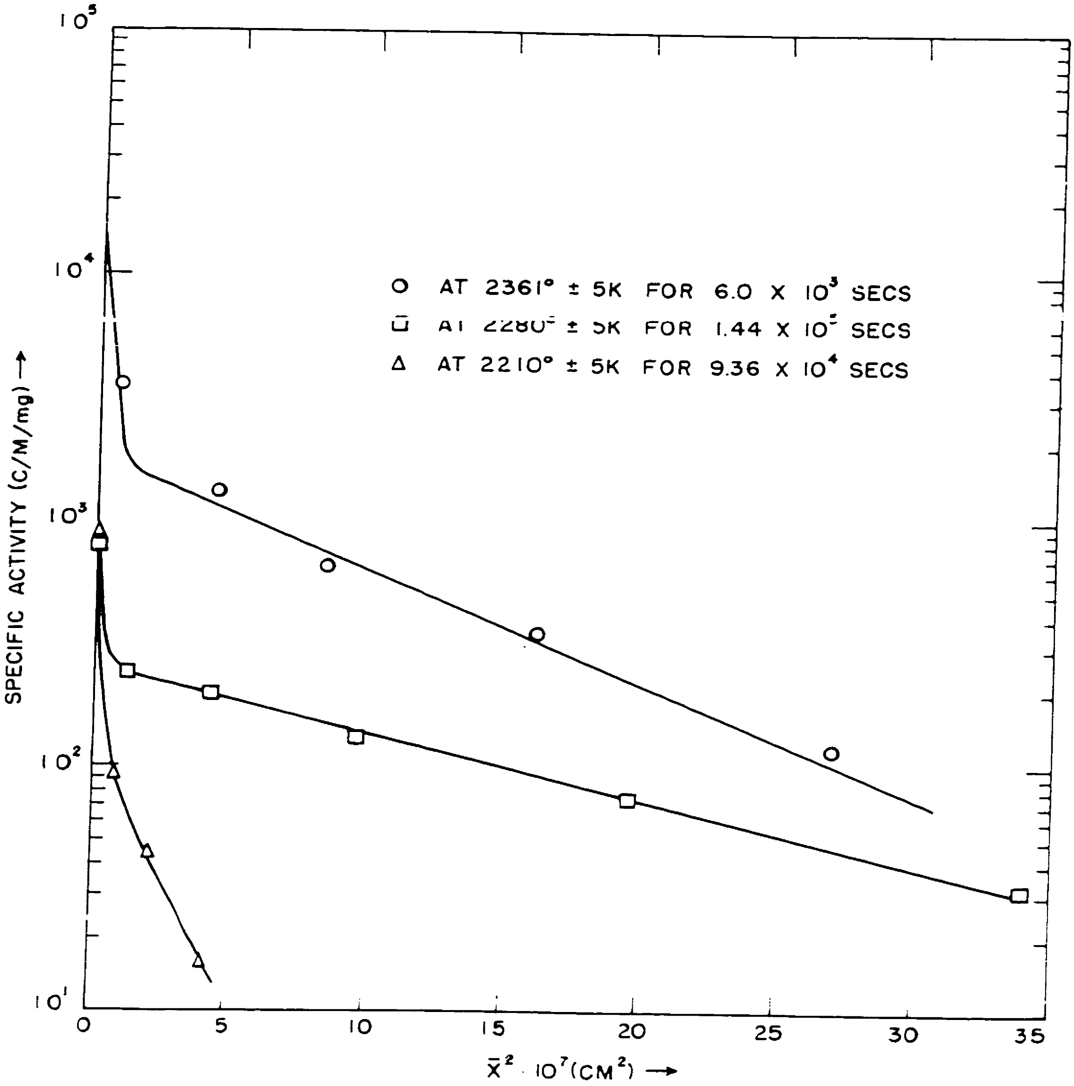

FIG. 17 CONCENTRATION PROFILES IN A FAINT YELLOW-GREEN HEXAGONAL SILICON CARBIDE SINGLE CRYSTAL ALONG [0001] FOR DIFFUSION OF CARBON-14

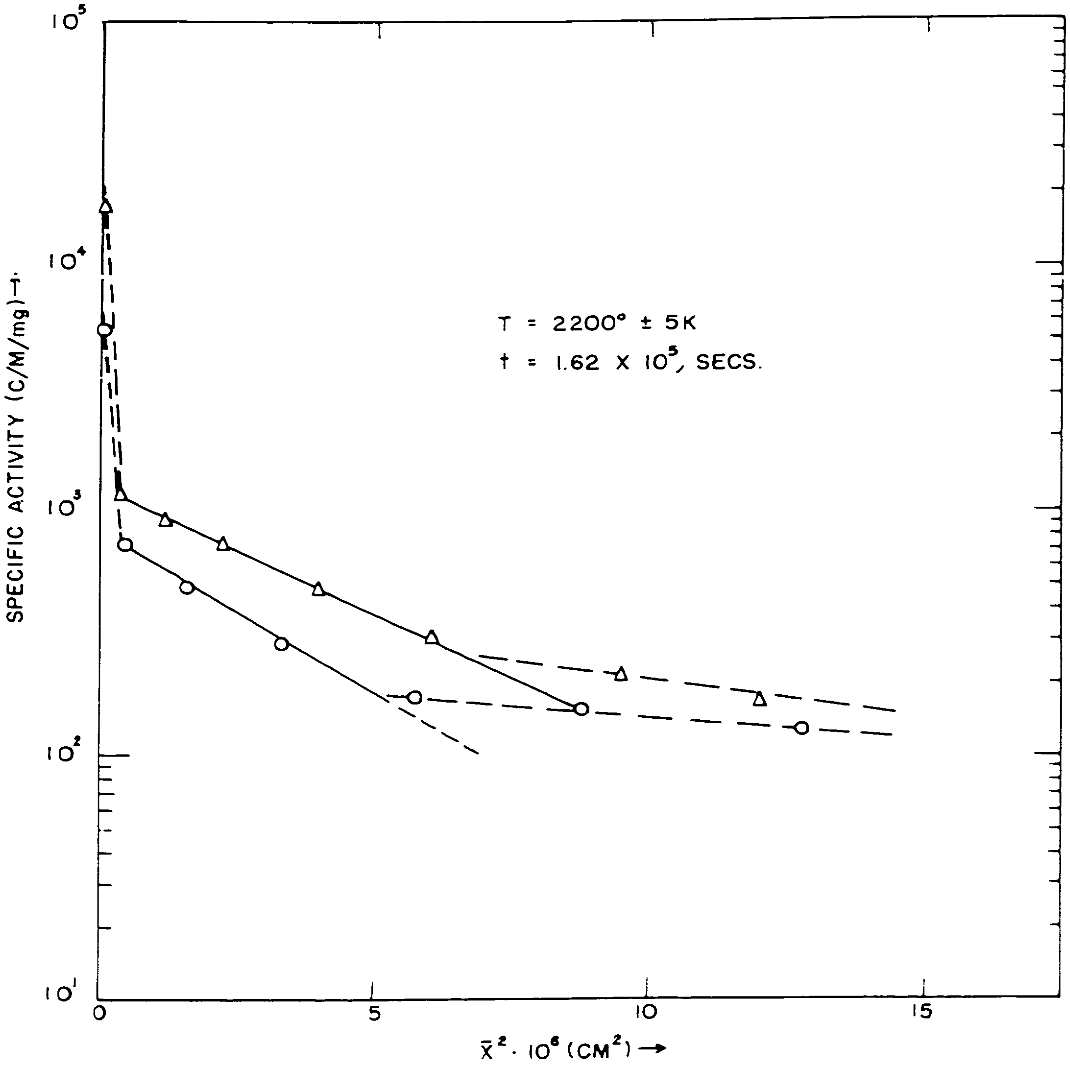

FIG. 18 CONCENTRATION PROFILES IN TWO POLYCRYSTALLINE SILICON CARBIDE SAMPLES

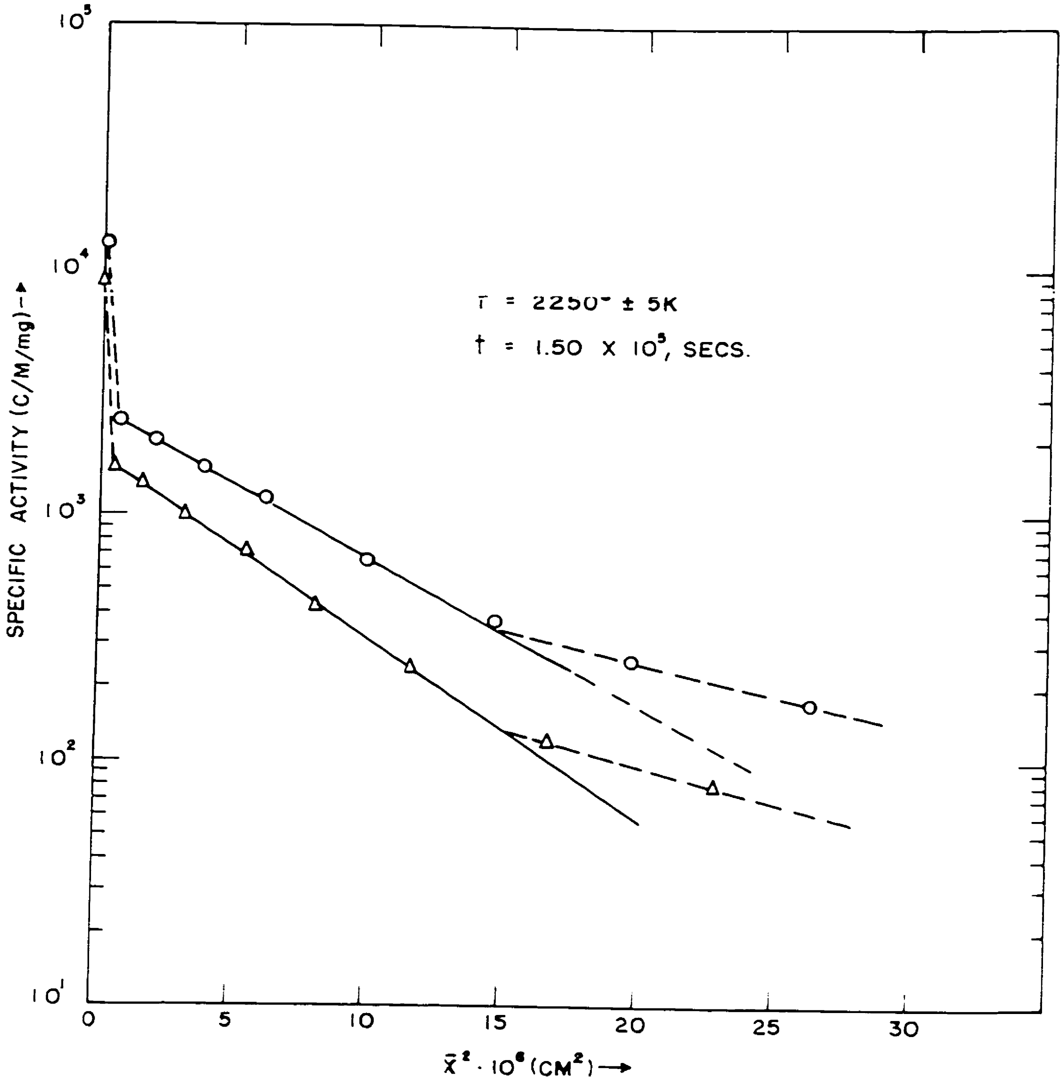

FIG. 19 CONCENTRATION PROFILES IN TWO POLYCRYSTALLINE SILICON CARBIDE SAMPLES.

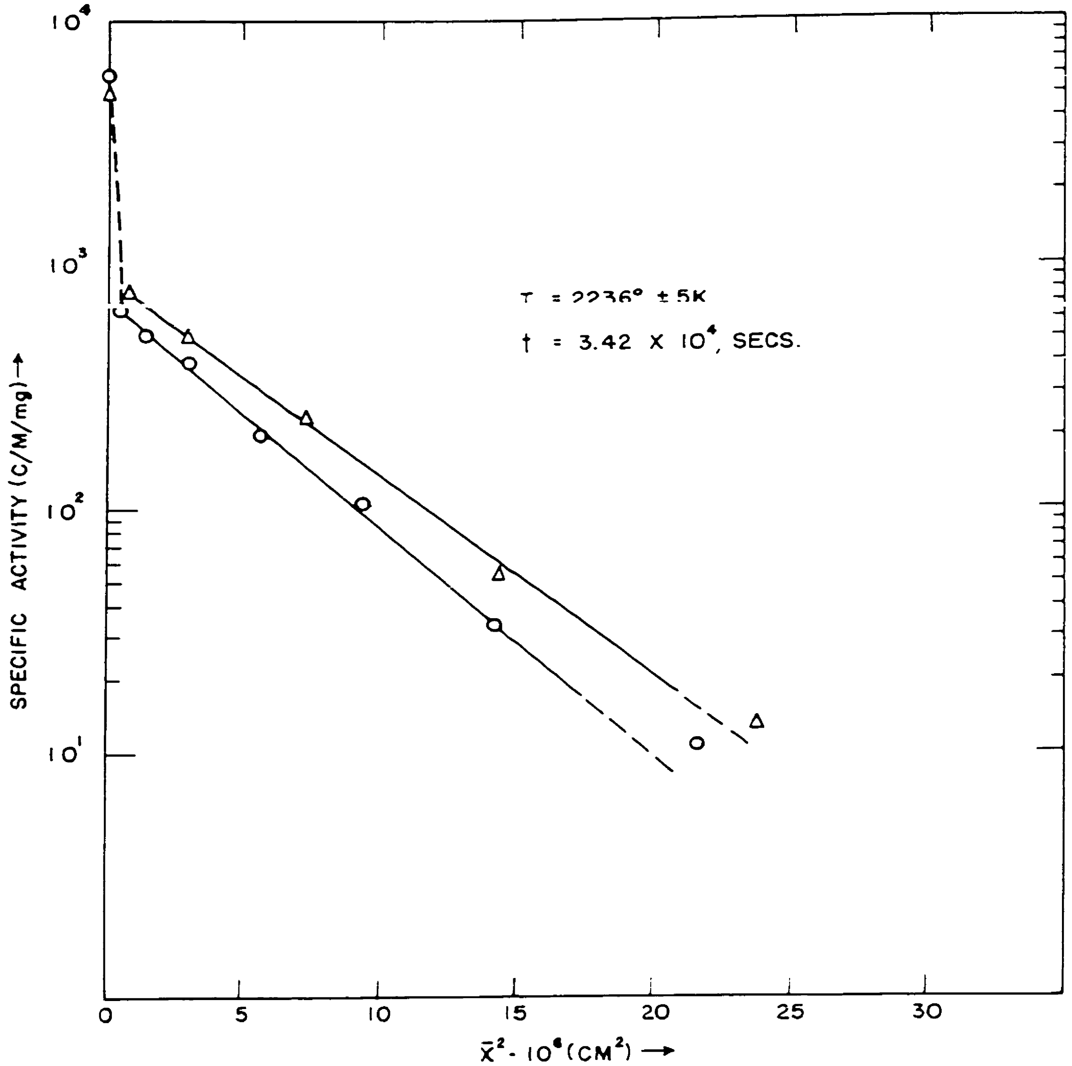

FIG. 20 CONCENTRATION PROFILES IN TWO POLYCRYSTALLINE SILICON CARBIDE SAMPLES.

TABLE V

CHARACTERIZATION OF SINGLE CRYSTAL SiC SAMPLES AS TO ORIENTATION AND DISLOCATION DENSITY

Sample	Orientation (off C-axis)	Dislocation Density (cm^{-2})	Avg. Separation of Dislocation Cores (microns)
S/N$_B$/3	0°	7.4×10^4	36.8
S/N$_B$/5	2.0°	1.0×10^3	316
S/N$_B$/7	0.5°	1.1×10^2	952
S/N$_B$/8	1.0°	4.1×10^3	156
S/N$_B$/10	2.5°	2.3×10^1	2,080
S/N$_B$/12	1.0°	1.1×10^3	301
S/N$_B$/14/A	1.0°	7.1×10^1	1,190
S/N$_B$/14/B	1.5°	----	--
S/N$_B$/11	22.5°	5.5×10^1	1,350
S/N$_B$/2/A	22.0°	9.2×10^2	330
S/N$_B$/2/B	22.0°	6.5×10^2	392
S/N$_G$/5/A	0°	2.1×10^2	690
S/N$_G$/5/B	0.5°	1.8×10^2	746
S/N$_G$/5/C	---	1.0×10^2	1,000
S/N$_G$/5/E	1.0°	8.0×10^1	1,120
S/N$_G$/5/F	0.5°	8.0×10^1	1,120
S/N$_C$/4/A	0.5°	3.8×10^1	1,620
S/N$_C$/4/B	1.0°	3.3×10^1	1,740
S/N$_C$/4/C	0.5°	2.9×10^1	1,860

(1) Eq. (II.1) has been derived from Fick's law for tracer diffusion on the assumption of unit exchange coefficient between the surface and the matrix atoms. Any deviation to a lower value of this exchange coefficient should result in a steep drop near the surface in the concentration profile. This would be possible for an impurity diffusion study by a tracer and also for self-diffusion from a poorly formed thin film.

(2) The existence of a steep drop near the surface in the concentration profile indicates the presence of a resistance layer. In the case of silicon carbide, a thin layer of oxide film on the surface, which is known to form even at room temperature(44), might provide this resistance.

(3) For the polycrystalline material, a grain boundary high-diffusivity path may be an important contributing factor to this effect as has been explained by Shewmon(14) in the case of Wajda's(55) data of zinc-tracer penetration in polycrystalline zinc.

(4) According to Ballufi and Ruoff(56-58) vacancy supersaturation either inside a grain in polycrystalline material or within a single crystal may be responsible for a steep drop of the concentration profile near the surface. Since tracer diffusivity is proportional to the vacancy concentration (assuming a vacancy mechanism operative) they have suggested that an accumulation of tracer at the surface (within a few microns depth) occurs under such circumstances leading to a non-Gaussian tracer concentration distribution. This hypothesis, however, postulates no formal limit of the lifetime of the supersaturation (after an initial fast drop at a given temperature). For silver-110 diffusion in silver(58) they

calculated a ratio for the resultant surface tracer concentration to that extrapolated from the interior of the crystal. The calculated value is about an order of magnitude higher. Supersaturated vacancy concentration may be conceived to exist in crystals due to quenching at the completion of growth.

Melngailis and O'Hara(59) showed that up to 3/4 φ_o vacancies (where ϕ_o = equilibrium vacancy concentration at the melting point) can be trapped inside silicon and germanium by only radiation quenching with less than 10^4 dislocations/cm^2 of the sample. Quenching-in of vacancies in platinum was studied by Bacchella et al(61) and in gold and platinum by Lazarev et al(60).

Ballufi and Ruoff(58) have also shown that, in the case of self diffusion in silver, roughening of the isoconcentration contours of the tracer (before the start of the diffusion anneal) may produce a final surface tracer concentration in excess by a factor of 2-3.

(5) In explaining this effect, it should be remembered, however, that the main cause of this effect has been traced to dislocations(51) in most systems. The single crystals used in this study had surprisingly low dislocation densities. The average distance between the dislocation cores is more than an order of magnitude higher than the penetration (shown in Table V). Therefore, in this study, dislocations cannot be the cause of the sharp drop of concentration near the surface.

Diffusion coefficients (D_ℓ) calculated from the deep section of the concentration profiles using Eq. (II.1) are given in Tables VI and VII and are plotted in Fig. 21. The functions are:

1. For black hexagonal single crystals along [0001]:

$$D_\ell = 3.014 \times 10^2 \exp\left[\frac{-141.5 \pm 16.6 \text{ Kcal}}{RT}\right] \text{cm}^2/\text{sec} \qquad (V.4)$$

2. For black dense polycrystalline material:

$$D_\ell = 2.36 \times 10^2 \exp\left[\frac{-137.1 \pm 14.2 \text{ Kcal}}{RT}\right] \text{cm}^2/\text{sec} \qquad (V.5)$$

3. For the light-green hexagonal single crystal along [0001]:

$$D_\ell = 2 \times 10^{17} \exp\left[\frac{-302.4 \pm 48.6 \text{ Kcal}}{RT}\right] \text{cm}^2/\text{sec} \qquad (V.6)$$

Due to the insufficiency of the data no effort was made to obtain a relation either for the faint yellow-green hexagonal crystal or for the black hexagonal sample where the direction of diffusion is 22° to [0001].

(b) Violation of Boundary Conditions: Two of the boundary conditions imposed by the solution (II.1) were found to vary during the diffusion runs. They are: (a) Decomposition of the sample and consequent movement of the original surface and, (b) Large decrease of surface concentration of tracer. In the following analysis, the effect of the violation of the boundary conditions on calculated D_ℓ values will be evaluated.

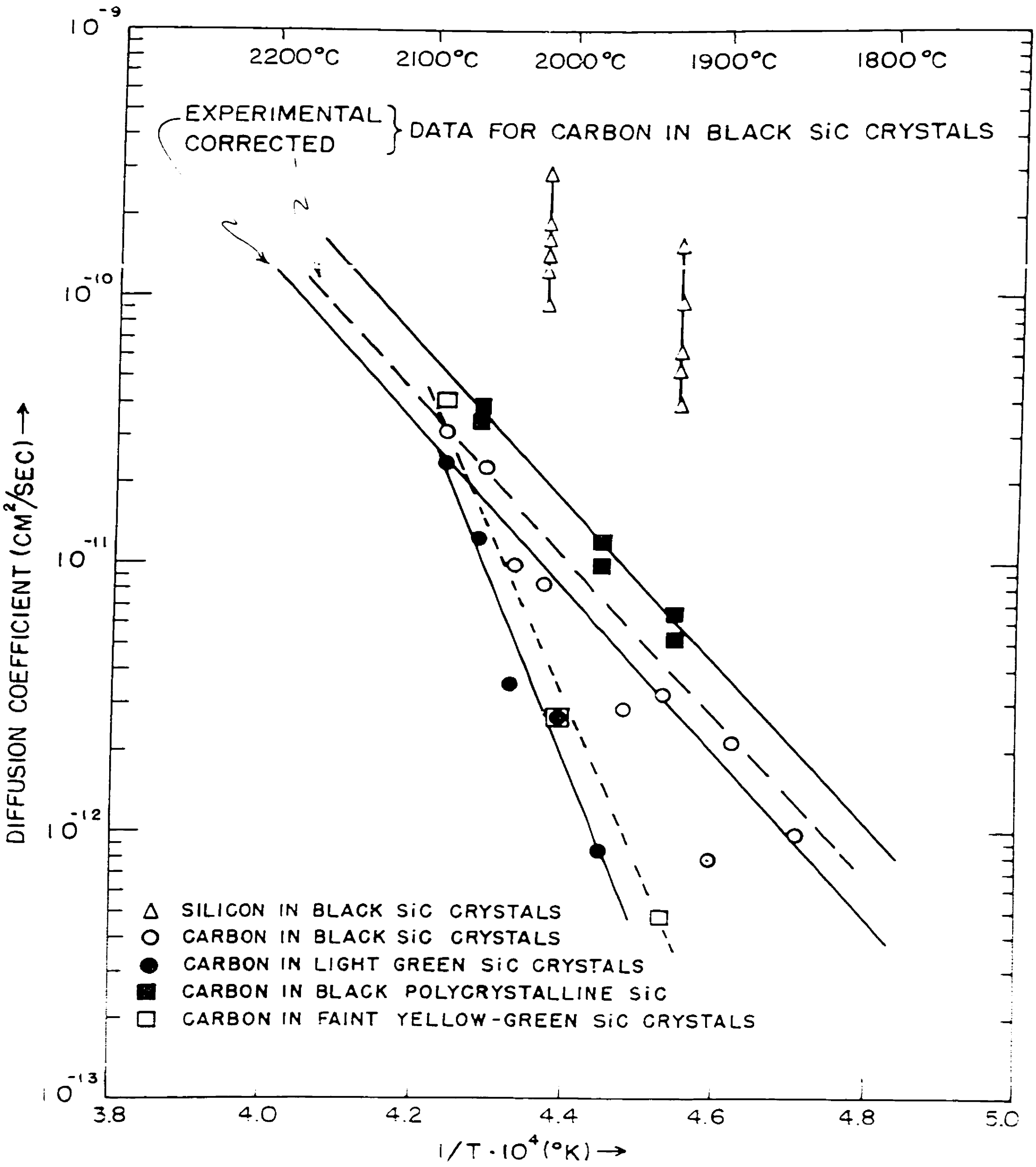

FIG. 21 DIFFUSION COEFFICIENTS FOR SILICON AND CARBON IN SILICON CARBIDE AS A FUNCTION OF TEMPERATURE.

TABLE VI

DATA FOR THE ARRHENIUS PLOT OF SINGLE CRYSTAL SILICON CARBIDE

1. Black SiC along [0001]:

Sample	Temperature(°C.)	$1/T \times 10^4$(°K)	D(cm^2/sec)
$S/N_B/10$	1853 ± 5	4.703 ± 0.011	9.83×10^{-13}
$S/N_B/14/B$	1892 ± 5	4.619 ± 0.011	2.17×10^{-12}
$S/N_B/7$	1937 ± 5	4.525 ± 0.010	3.25×10^{-12}
$S/N_B/8$	1962 ± 7	4.474 ± 0.014	2.88×10^{-12}
$S/N_B/5$	2017 ± 5	4.367 ± 0.010	8.40×10^{-12}
$S/N_B/14/A$	2038 ± 5	4.327 ± 0.009	9.82×10^{-12}
$S/N_B/12$	2060 ± 7	4.286 ± 0.013	2.29×10^{-11}

2. Black SiC at 22° to [0001]:

$S/N_B/2/A$	1907 ± 5	4.587 ± 0.011	7.94×10^{-13}
$S/N_B/2/B$	2088 ± 5	4.235 ± 0.013	3.07×10^{-11}

3. Light Green SiC along [0001]:

$S/N_G/5/C$	1977 ± 5	4.444 ± 0.010	8.36×10^{-13}
$S/N_G/5/F$	2007 ± 5	4.389 ± 0.013	2.58×10^{-12}
$S/N_G/5/A$	2028 ± 5	4.327 ± 0.009	3.50×10^{-12}
$S/N_G/5/E$	2063 ± 5	4.280 ± 0.013	1.24×10^{-11}
$S/N_G/5/B$	2088 ± 5	4.235 ± 0.013	2.35×10^{-11}

4. Faint Yellow-green SiC along [0001]:

S/N /4/A	1937 ± 5	4.525 ± 0.011	4.61×10^{-13}
S/N /4/C	2007 ± 5	4.389 ± 0.013	$2.64 \times 10^{=12}$
S/N /4/B	2088 ± 5	4.235 ± 0.013	4.05×10^{-11}

TABLE VII

DATA FOR THE ARRHENIUS PLOT OF POLYCRYSTALLINE DENSE SILICON CARBIDE

Sample Number	Temperature(°C)	$1/T \times 10^4$ (°K)	D(cm^2/sec)
P/A_B/1/B	1927° ± 5	4.545 ± 0.010	6.60×10^{-12}
P/A_B/2/B	1927° ± 5	4.545 ± 0.010	5.23×10^{-12}
P/A_B/1/A	1977° ± 5	4.444 ± 0.010	1.20×10^{-11}
P/A_B/2/A	1977° ± 5	4.444 ± 0.010	9.81×10^{-12}
P/A_B/1/C	2063° ± 5	4.281 ± 0.010	3.81×10^{-11}
P/A_B/2/C	2063° ± 5	4.281 ± 0.010	3.38×10^{-11}

TABLE VIII

VAPOR PRESSURE OF C(g) IN EQUILIBRIUM WITH C(graphite) AT 1700°-2200°K

Temperature	Vapor Pressure in Atm.
1700°K	$10^{-13.78}$
1800°K	$10^{-13.29}$
1900°K	$10^{-12.81}$
2000°K	$10^{-12.33}$
2200°K	$10^{-11.37}$

TABLE IX

DATA FOR THE DECOMPOSITION PLOT OF SINGLE CRYSTALS

Sample Number	Temperature (°C)	$1/T \times 10^4$ (°K)	Rate (Mg/cm^2/sec)
S/N_B/2/A	1907 ± 5	4.587 ± 0.011	2.05×10^{-5}
S/N_B/7	1937 ± 5	4.525 ± 0.011	2.80×10^{-5}
S/N_C/4/A	1937 ± 5	4.525 ± 0.011	3.10×10^{-5}
S/N_B/3	1943 ± 5	4.513 ± 0.011	3.10×10^{-5}
S/N_B/8	1962 ± 5	4.474 ± 0.014	3.30×10^{-5}
S/N_G/5/A	2038 ± 5	4.327 ± 0.009	8.80×10^{-5}
S/N_B/14/A	2038 ± 5	4.327 ± 0.009	9.65×10^{-5}

The predominant decomposition reaction for silicon carbide is(89):

$$SiC(hex) \rightleftharpoons C(graphite) + Si(g) \qquad (V.7)$$

Other vapors in the system: Si_2C_3, Si_2C_2, Si_3C, SiC, Si_2, Si_2C, and SiC_2 (as shown in Fig. 22) have vapor pressure so small (compared to that of Si(g)) that they may be neglected. This silicon loss from the thin films is considered to be primarily responsible for the poor reproducibility of the silicon diffusion coefficients determined.

Only about 30-40% of the total tracer activity was retained by the sample. This loss has presumably taken place by the evaporation of different vapors of carbon and silicon carbide and by isotope exchange with the carbon-containing atmosphere.

Carbon contains three vapor species at high temperatures: C(g), $C_2(g)$, and $C_3(g)$ of which C(g) is predominant. From the thermodynamic data of C(graphite) and C(g)(62), the vapor pressure of C(g) in the region of interest is given in Table VIII which, when compared with Fig. 22, shows that the vapor pressure of C(g) is lower by 6-7 orders of magnitude than that of Si(g). Thus, the loss of tracer is predominantly by the evaporation of different silicon carbon species. A certain amount of tracer evaporation loss is an inherent disadvantage of thin-film technique with radioactive tracers(1). Feldman et al(25) reported a loss of more than 50% of tracer by evaporation in their study of diffusion of C-14 in graphite.

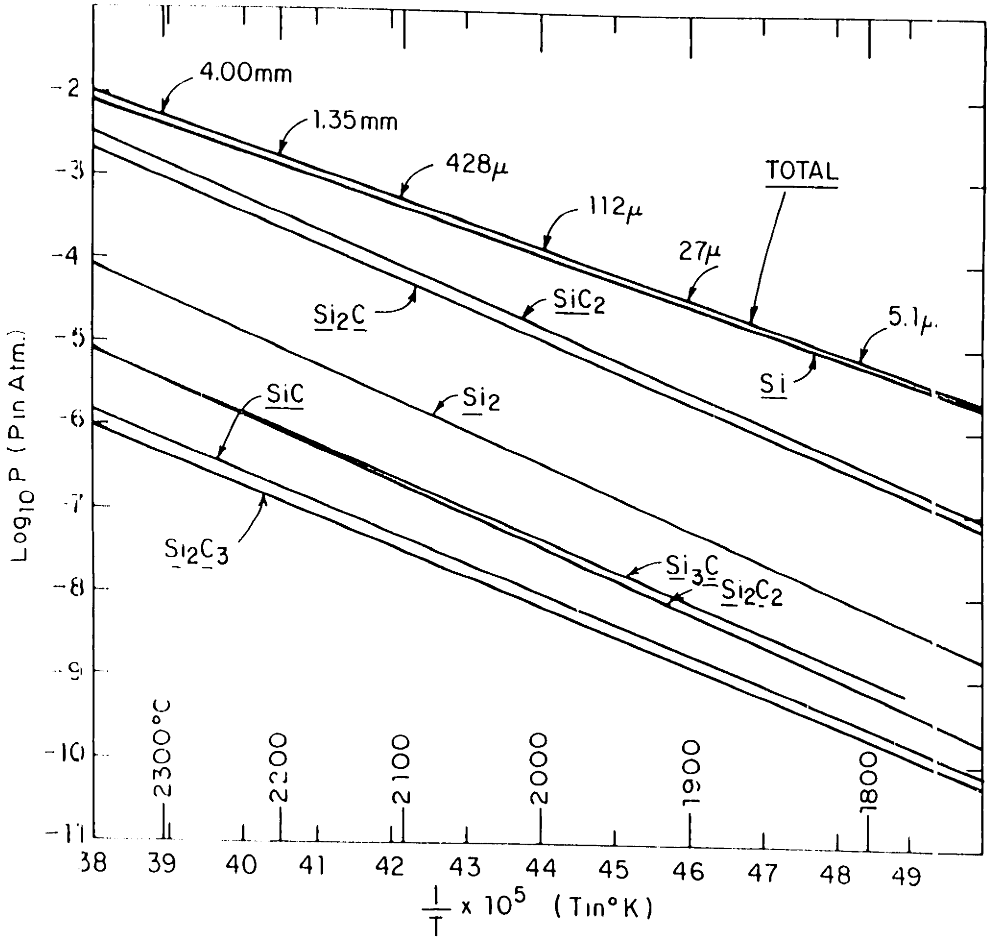

FIG. 22 EQUILIBRIUM GASEOUS SPECIES PARTIAL PRESSURES VERSUS TEMPERATURE IN SILICON CARBIDE + GRAPHITE SYSTEM.

The decomposition rate for single crystals was calculated from the surface area, weight loss and annealing duration. Some data (Table IX) are plotted as a function of temperature in Fig. 23. (Samples where an effort was made to decrease the decomposition rate by putting SiC crystals all around the samples$^{(63)}$ were omitted). The decomposition rate is:

$$k = 2.96 \times 10^{6} \exp \left(\frac{-111.4 \pm 16.5 \text{ Kcal}}{RT}\right) \text{ mg/cm}^2\text{/sec} \qquad (V.8)$$

The activation energy (111.4 ±16.5 Kcal/mole) compares favorably with the heat of formation of hexagonal silicon carbide by the reverse reaction of Eq. (V.7) (123 ±3 Kcal/mole at 2000°K$^{(89)}$). Also, the activation energy for evaporation of silicon is 104 Kcal/mole$^{(64)}$. So, all these activation energies (111.4, 123 and 104 Kcal/mole) probably describe the same process mechanistically.

The principle of the modified Lely technique$^{(63)}$, in which SiC crystals were placed all around the samples, is to maintain a vapor pressure of silicon over solid silicon carbide sufficient to arrest the decomposition reaction.

From the observed Si(g) vapor pressure dependence of the decomposition rate of SiC, the rate controlling step in the decomposition of hexagonal silicon carbide is concluded to be the escape of silicon (gas) from the solid surface. It is also noteworthy that the diffusion data of carbon-14 in polycrystalline graphite$^{(25)}$ is about three orders of magnitude higher than in silicon carbide (1800°-2100°C). Thus, the layer of decomposition-produced spongy graphite is assumed to contain no concentration gradient of tracer. Complete decomposition data is presented in Table E IV of Appendix E.

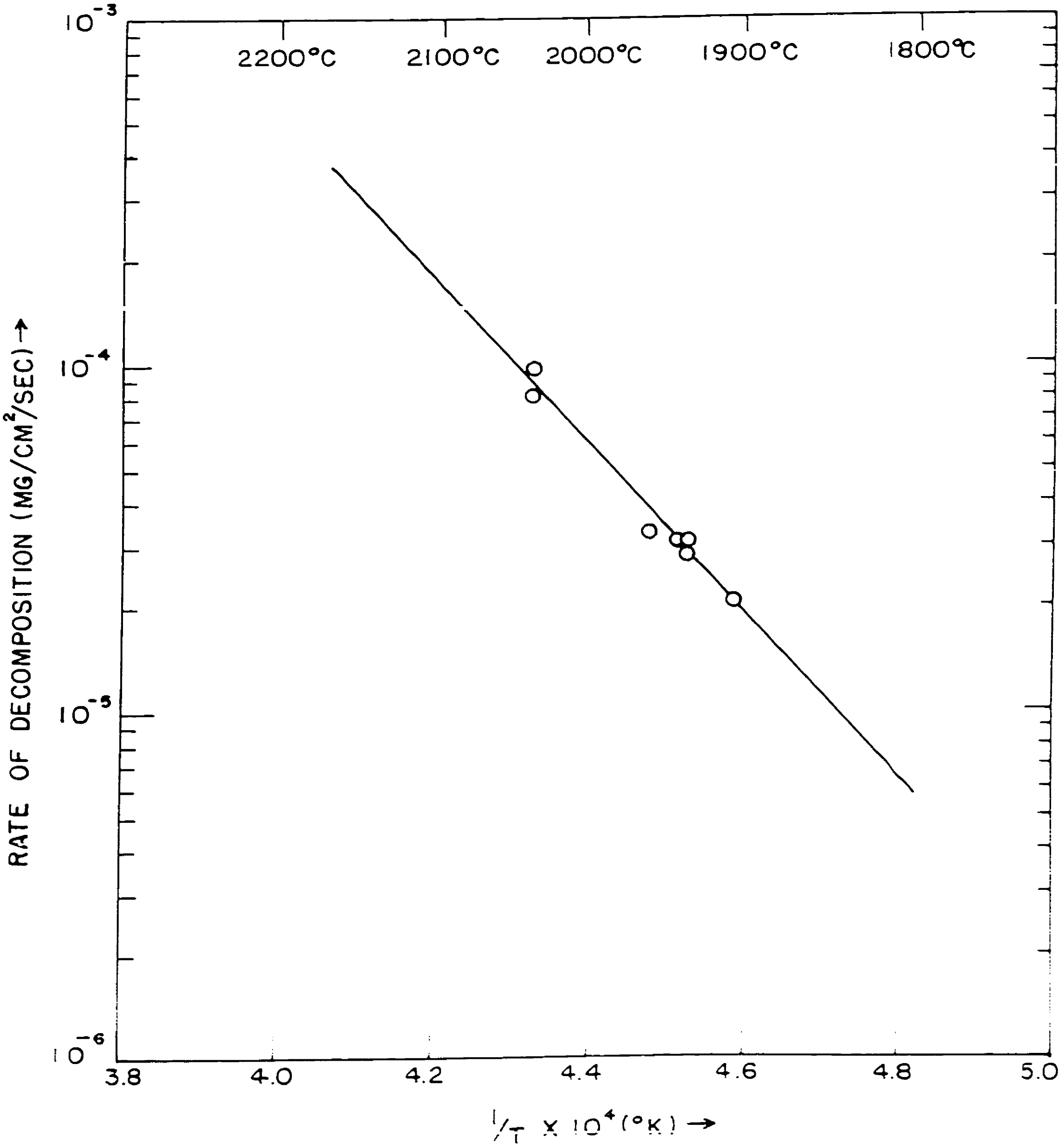

FIG. 23 ARRHENIUS PLOT FOR THE DECOMPOSITION OF SINGLE CRYSTALS OF SILICON CARBIDE.

(c) Computation of the Effects of Varying Boundary Conditions: The effect of surface decomposition on the concentration gradient of carbon-14 has been calculated and is shown schematically in Fig. 24. The exponential ℓnC vs. $\bar{X}$ relationship described by the curve ACD is that for an ideal case, i.e., no (evaporated) tracer loss and no surface decomposition (no movement of the initial interface). The surface concentration decreases with $1/\sqrt{t}$ as predicted by Eq. (II.1). The insert in Fig. 24 describes three ways the surface concentration can change with time. This result only affects the bump (near the surface) of the resultant profiles, as shown by the calculated curves BED, BE'D or BE"D; it does not have any effect on the constant slope part of the ℓnC vs. X^2 curves where the resultant profiles meet the ideal profile. The aforementioned ideas were verified by a numerical analysis of the second order differential equation (diffusion equation) under a given set (fixed by experimental data) of varying boundary conditions as described below.

Fick's second law states that:

$$\frac{\delta c}{\delta t} = D \frac{\delta^2 c}{\delta x^2} \qquad (I.3)$$

where c, x, t, and D have usual meanings.

Substituting the following difference equation for above:

$$\frac{c(x,t+\Delta t)-c\ \ (x,t)}{\Delta t} = \frac{\Delta c}{\Delta t} = D\left[\frac{c(x+\Delta t,t)-2c\ \ (x,t)+c(x-\Delta x,t)}{(\Delta x)^2}\right]$$

or

$$c(x,t+\Delta t) = D\left[\frac{\Delta t}{(\Delta x)^2}\{c(x+\Delta x,t)\}\right] + \left[1-2D\frac{\Delta t}{(\Delta x)^2}\right]c(x,t) + D\left[\frac{\Delta t}{(\Delta x)^2}\{c(x-\Delta x,t)\}\right]$$

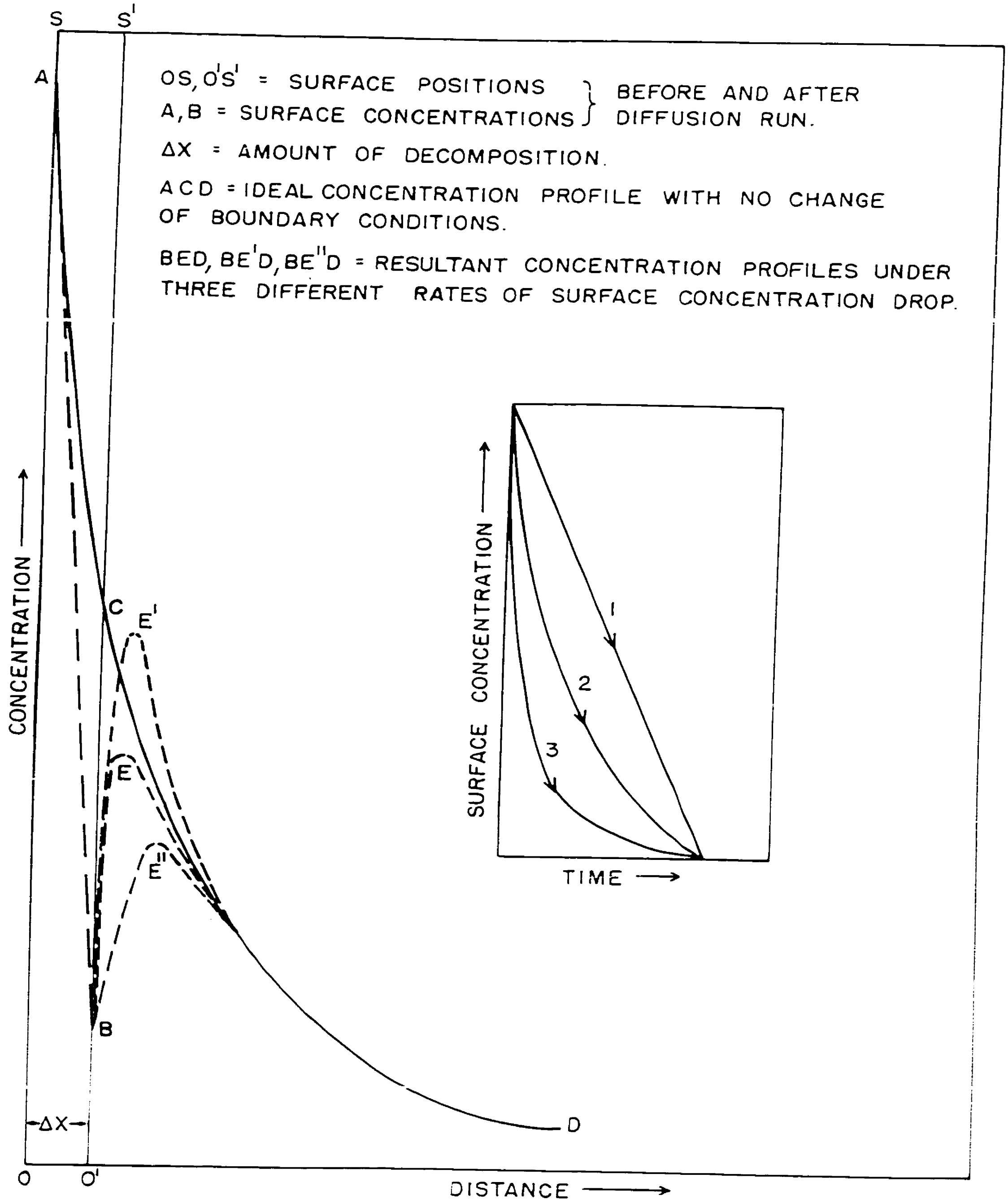

FIG. 24 SCHEMATIC REPRESENTATION OF THE EFFECTS OF DECOMPOSITION AND EVAPORATION ON A CONCENTRATION PROFILE FOR TRACER DIFFUSION AFTER ANNEALING FOR TIME t AT TEMPERATURE T.

It is convenient to choose Δx and Δt such that

$$(\Delta x)^2 = 2D\,\Delta t \qquad (V.9)$$

So that

$$c(x,t+\Delta t) = 1/2\left[c(x+\Delta x,t) + c(x-\Delta x,t)\right] \qquad (V.10)$$

i.e., at time $t + \Delta t$, the concentration at x is equal to the average of the concentrations at $x-\Delta x$ and $x + \Delta x$ at time t. A grid with x and t as coordinates can now be conceived with Δx and Δt as units (following the above condition) to produce a numerical solution of the diffusion equation under varying c and x as observed in each case. An assumption is to be made, however, that the surface concentration changes linearly following an equation of the form

$$CS(t) = CO - RCS \times TTOT \qquad (V.11)$$

where, CS(t) = surface concentration at any time t.

CO = original surface concentration before diffusion anneal.

RCS = rate of change of surface concentration calculated from initial and final values assuming linear decrease with increasing time.

TTOT = total duration of diffusion anneal.

The concentration profiles for each sample thus obtained using the experimental data for the original and final surface concentrations, total shift of boundary by decomposition, total duration of diffusion anneal and the apparent diffusion coefficient for a total distance of 30-40 microns at increments of 0.2 micron show all the types of behavior visualized in Fig. 25. Concentration profiles of ℓnC vs. $\bar{X}^2$ show non-conformity to the solution given in Eq. (II.1) near the surface but are linear at large distances from the surface where theoretically the real profile approximates the ideal.

These computed profiles were obtained by first using the experimentally obtained D value to obtain a profile for each sample. The constant slope part of this profile produced a lower D value in all cases. The D values to be used to obtain a profile numerically were then increased stepwise until the D value calculated from the constant slope part of the computed profile is within 1.0 - 1.5% of the experimental value. The corrected D values thus obtained are given in Table X for the black crystals. They are described by an equation of the form:

$$D = 2.19 \times 10^2 \exp \left(\frac{-138.6 \pm 18.0 \text{ Kcal}}{RT}\right) \text{cm}^2/\text{sec} \qquad \text{(V.12)}$$

which is essentially identical with Eq. (V .4) within the limits of experimental error. The computer programs used are given in Appendix E. All profiles were obtained using an initial (CO) and final (CF) surface tracer concentrations (calculated). The data for CO and CF for black single crystals are also given in Appendix E.

Four corrected profiles obtained by this method are shown in Fig. 25 with an ideal profile for the sample indicated. The reasons that the calculated ideal profile did not exactly coincide with the corrected experimental profile in absolute numbers are probably due to the facts:

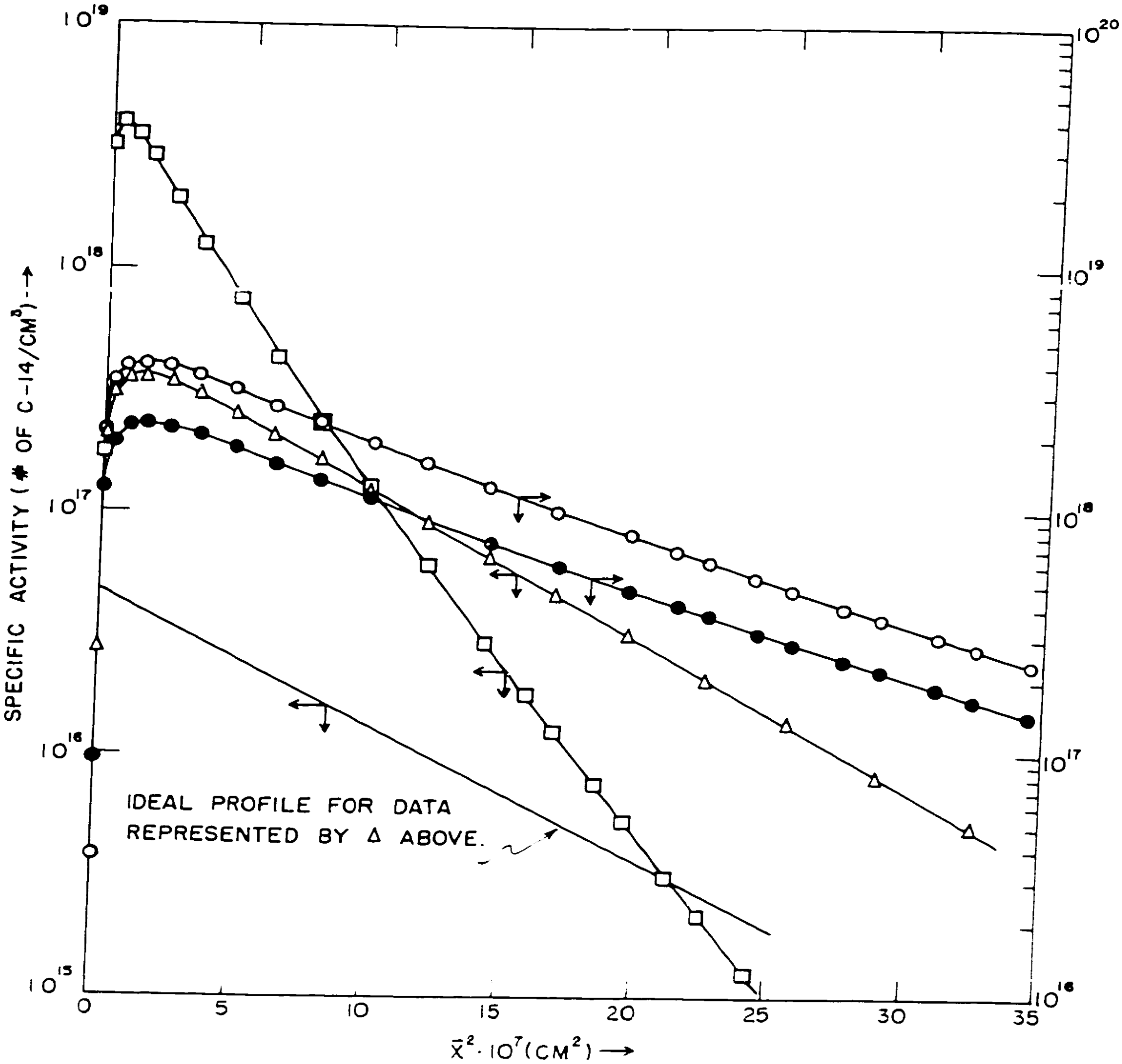

FIG. 25 CONCENTRATION PROFILES OF FIG. 13 CORRECTED FOR DECOMPOSITION AND TRACER LOSS FROM THE SURFACE

TABLE X

CORRECTED DATA FOR THE ARRHENIUS PLOT OF SINGLE CRYSTAL SILICON CARBIDE

1. Black SiC along [0001]:

Sample	Temp. (°C)	1/T × 10^4 (°K)	$D_{App.}$ (Cm^2/Sec)	$D_{Corr.}$ (Cm^2/sec)
S/N_B/10	1853 ± 5	4.703 ± 0.011	9.83×10^{-13}	1.20×10^{-12}
S/N_B/14/B	1892 ± 5	4.619 ± 0.011	2.17×10^{-12}	2.45×10^{-12}
S/N_B/7	1937 ± 5	4.525 ± 0.010	3.25×10^{-12}	5.20×10^{-12}
S/N_B/8	1962 ± 7	4.474 ± 0.014	2.88×10^{-12}	5.15×10^{-12}
S/N_B/5	2017 ± 5	4.367 ± 0.010	8.40×10^{-12}	9.40×10^{-12}
S/N_B/14/A	2038 ± 5	4.327 ± 0.009	9.82×10^{-12}	1.63×10^{-11}
S/N_B/12	2060 ± 7	4.286 ± 0.013	2.29×10^{-11}	2.85×10^{-11}

2. Black SiC at 22° to [0001]:

S/N_B/2/A	1907 ± 5	4.587 ± 0.011	7.94×10^{-13}	1.16×10^{-12}
S/N_B/2/B	2088 ± 5	4.235 ± 0.013	3.07×10^{-11}	3.45×10^{-11}

i) that the corrected experimental profiles were obtained with CF (final surface concentration) calculated from the activity of the first section which is not representative of the rest of the experimental profile (as seen earlier) and thus the corrected values have an elevated position compared to the experimental profile, and

ii) that the ideal profile was calculated with respect to a value of original surface concentration calculated from the original surface count rate and is thus probably lower than the real original surface concentration (due to C-14 β-absorption by the thickness of the thin-film).

All assumptions for the time-dependence of the drop of the surface concentration produced the same constant slope part (from which the corrected D values were calculated). The exact behavior, therefore, has no influence on the corrected D values reported in Table X. Use of different relations for this drop, however, facilitated the identification of the constant slope part.

So, the apparent values of D_ℓ obtained by ignoring any decomposition will represent the actual diffusion coefficients quite realistically. Another correction which was neglected in the data presented is that due to thermal expansion of the sample at the annealing temperature.

C. DIFFUSION COEFFICIENTS CALCULATED FROM CREEP DATA.

Recently, Farnsworth(47) observed viscous deformation of polycrystalline silicon carbide. Assuming a lattice-diffusional model the apparent diffusion coefficients are given by:

1. Black, dense SiC:

$$D_{\text{Apparent}} = 1.27 \times 10^{-4} \exp\left[\frac{-73 \pm 15 \text{ Kcal}}{RT}\right] \text{cm}^2/\text{sec} \qquad (\text{V.13})$$

2. Green, porous SiC:

$$D_{\text{Apparent}} = 6.0 \times 10^{-2} \exp\left[\frac{-104 \pm 20 \text{ Kcal}}{RT}\right] \text{cm}^2/\text{sec} \qquad (\text{V.14})$$

These data are compared with the directly measured diffusion coefficients in both black single and polycrystalline silicon carbide obtained in the present investigation in Fig. 26. Aluminum diffusion coefficients in silicon carbide(65) are also presented in the same.

So far as the parameters Q and D_o are concerned, there is apparently no agreement. But Farnsworth's calculated D values are approximately within the range of error of the present investigation. His data at and below 2000°C are in surprisingly good agreement with the data obtained in polycrystalline samples in the present investigation.

The following considerations are presented to explain the difference between the D_ℓ values obtained in single crystals and the D values obtained from creep data and in polycrystalline material.

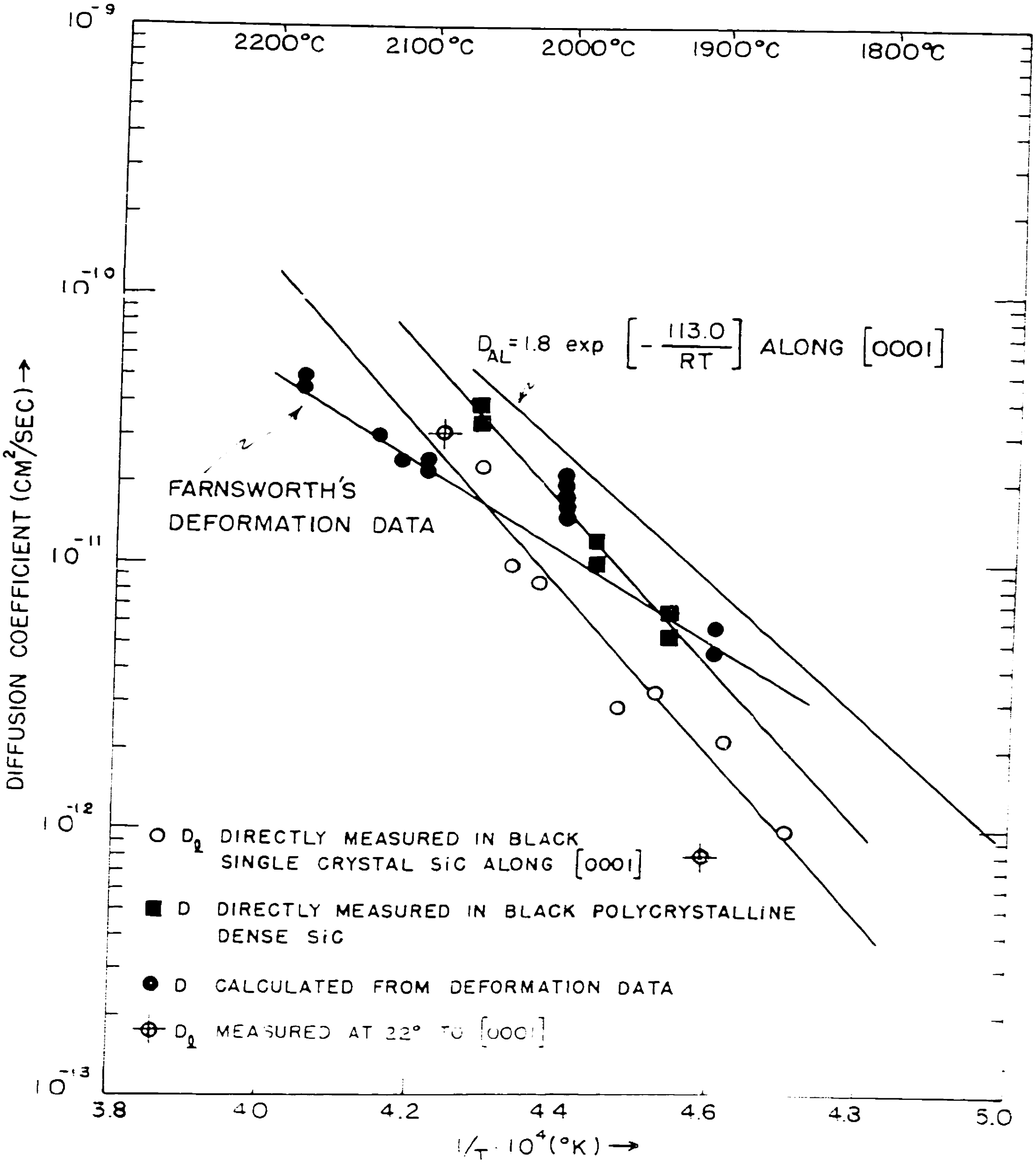

FIG. 26 COMPARISON OF CARBON DIFFUSION COEFFICIENTS IN SiC ALONG WITH THE D_{AL} DATA IN SiC BLACK SINGLE CRYSTALS

a) Grain boundary diffusion, which is a few orders of magnitude higher at these temperatures (indicated from the long tails of the concentration profiles in polycrystalline material as shown in Figs. 18-20) has an appreciable contribution to both the apparent measured D values for tracer diffusion in polycrystalline material and the apparent D values calculated from creep data.

b) Surface diffusion along the uniformly distributed pores might also have decreased the slopes of the ℓnC vs. $\bar{X}^2$ plots. Since surface diffusion is in general several orders of magnitude higher than both lattice and grain-boundary diffusion even a fraction of a per cent of porosity would be important.

D. DISCUSSION IN THE LIGHT OF RELATED DATA.

(a) Some Important Properties of Group III, IV, V Elements and SiC.

In the following Tables and Figures, a few monotonously varying properties of the Group IV semiconductors are compiled in comparison with the same properties for the Group III acceptors and Group V donors (which are usually present in these semiconductors). These are pertinent to further discussions.

TABLE XI(66)

Tetrahedral Radii in Å

B = 0.88	C = 0.77	N = 0.70
Al = 1.26	Si = 1.17	P = 1.10
Ga = 1.26	Ge = 1.22	As = 1.18
In = 1.44	Sn = 1.40	Sb = 1.36
Tl = 1.47	Pb = 1.46	Bi = 1.46

TABLE XII(67)

Heats of Atomization (Kcal/mole) from their Standard States at 25°C

B $\simeq$ 100	C $\cong$ 138(?)	N $\cong$ 86(?)
Al = 75	Si = 89	P = 75
Ga = 65	Ge = 89	As = 60(?)
In = (58)	Sn = 70	Sb = 61
Tl = 43	Pb = 46	Bi = 50(?)

TABLE XIII(68)

Ionization Potentials in Electron-Volts

Element	1st	2nd	3rd	4th	5th
B	8.26	25.00	37.75	258.1	338.5
Al	5.96	18.74	28.31	119.37	153.4
Ga	5.97	20.43	30.6	63.8	---
In	5.76	18.79	27.9	57.8	---
Tl	6.07	20.32	29.7	50.5	---
C	11.22	24.27	47.65	64.22	390.1
Si	8.12	16.27	33.35	44.93	165.6
Ge	8.09	15.86	34.07	45.5	93.0
Sn	7.30	14.5	30.5	39.4	80.7
Pb	7.38	14.96	(31.9)	42.11	69.4
N	14.48	29.47	47.40	77.0	97.4
P	10.9	19.56	30.01	51.11	64.70
As	10.5	20.1	28.0	49.9	62.5
Sb	8.5	(18)	24.7	44.0	55.5
Bi	8.0	16.6	25.42	45.1	55.7

TABLE XIV

Some Properties of Group IV Semiconductors

Element	X-ray Density (100)	Bond Gap(eV)	Melting (68) Point(°C)	Boiling (68) Point(°C)	Bond Strength (66) (Kcal/mole)	Hardness (68)		Crystal Structure (100)
						Mohr	Knoop	
C	2.266 (graphite)	5.6 (diamond)	3550	4200	83.1 (graphite)	10.0 (diamond)	7000 (diamond)	Cubic (diamond)
	3.516 (diamord)					0.5-1 (graphite)		Hexagonal Rhombohedral (graphite)
SiC	3.208 (hexagonal)	3.86	2600 (dissociates)	---	69.3	9-10	2500	Hexagonal (alpha)
	3.210 (cubic)	1.9 (beta)						Diamond-cubic (beta)
Si	2.3293	1.1	1420	2600	42.2	7.0	820	Diamond-cubic
Ge	5.3248	0.80	958	2700	37.6	---	---	Diamond-cubic
Sn	5.770 (gray tin)	0.08 (gray tin)	232	2260	--	1.5-1.8	30	Diamond-cubic (gray tin)
	7.285 (white tin)							Tetragonal (white tin)

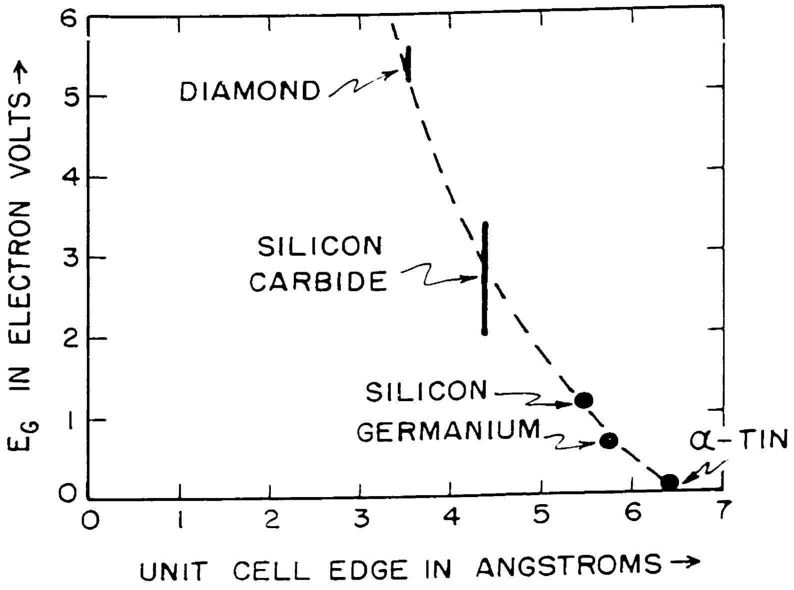

FIG. 27 VALUES OF BAND GAP ENERGY (E_G) PLOTTED AGAINST THE SIZE OF THE DIAMOND-TYPE UNIT CELL FOR THE GROUP IV ELEMENTS AND SILICON CARBIDE.

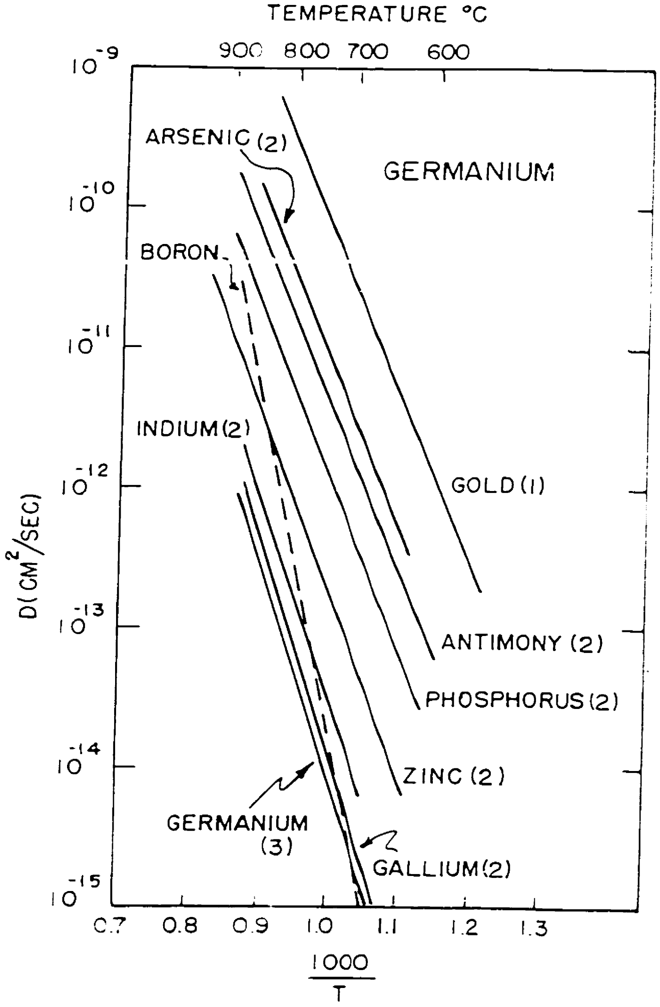

FIG. 28 DIFFUSION COEFFICIENTS, D, OF IMPURITY ELEMENTS IN GERMANIUM AS A FUNCTION OF TEMPERATURE. (1) AFTER (40) (2) AFTER (83) (3) AFTER (16).

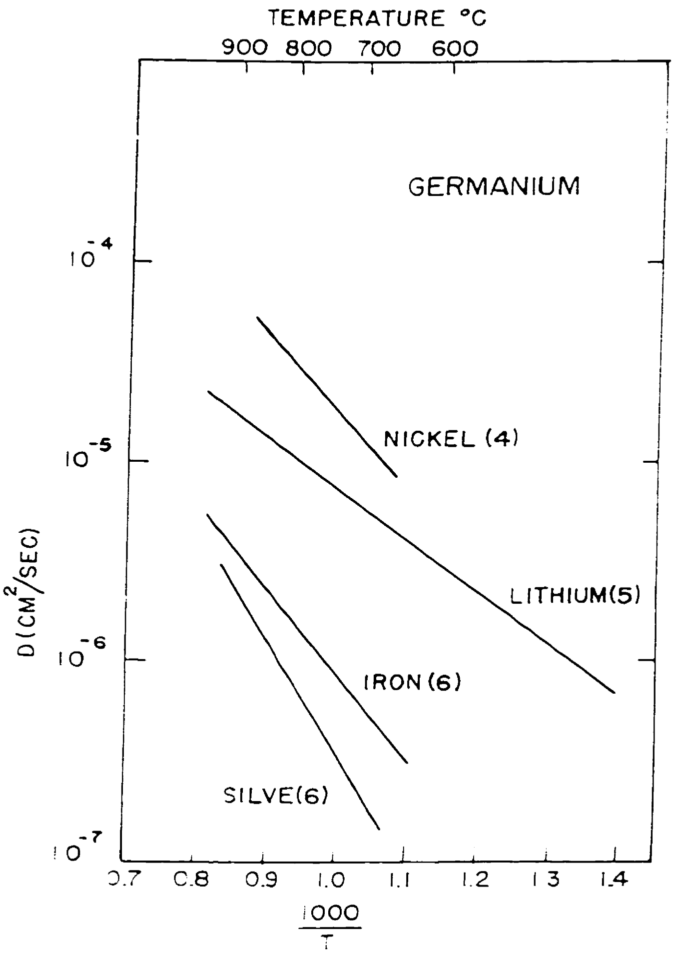

FIG 29 DIFFUSION COEFFICIENTS OF IMPURITY ELEMENTS IN GERMANIUM AS A FUNCTION OF TEMPERTURE (4) AFTER [41], (5) AFTER [92], (6) AFTER [93]

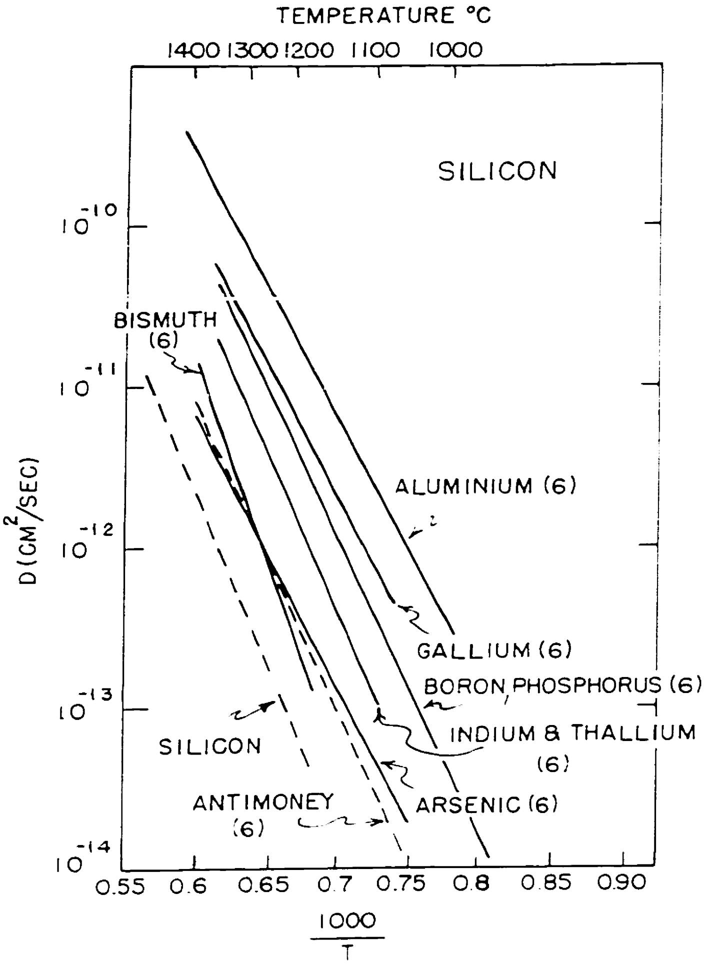

FIG 30 DIFFISION COEFFICIENTS OF IMPURITY ELEMENTS IN SILICON AS A FUNCTION OF TEMPERATURE (6) AFTER (98)

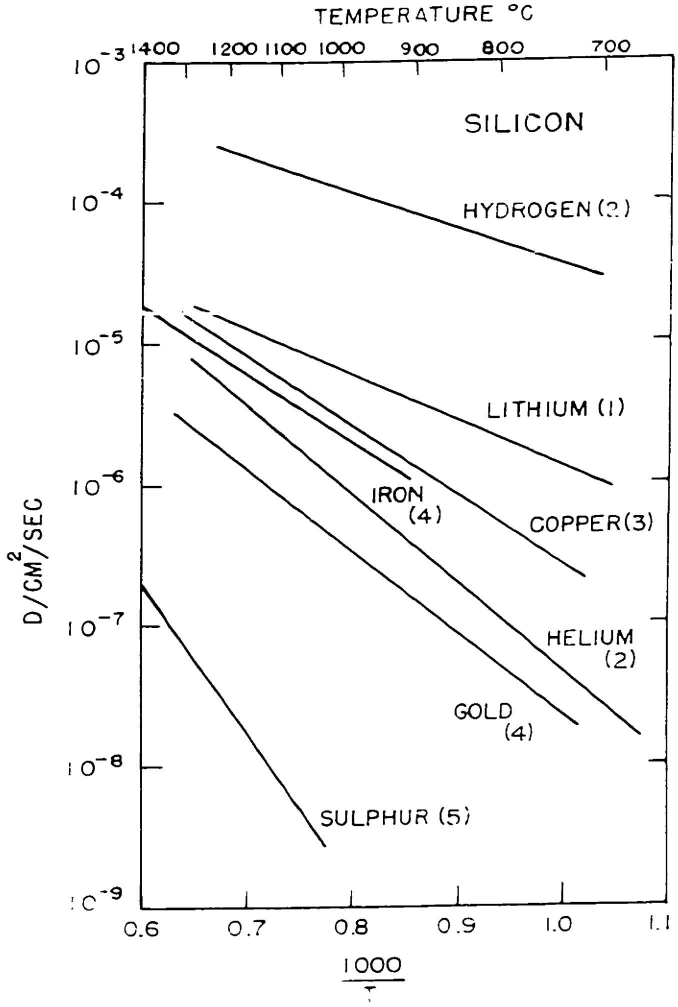

FIG 31 DIFFUSION COEFFICIENTS OF IMPURITY ELEMENTS IN SILICON AS A FUNCTION OF TEMPERATURE. (1) AFTER(92), (2) AFTER(94), (3) AFTER(95), (4) AFTER(96), (5) AFTER(97)

Band gaps (E_G) of the Group IV semiconductors are plotted as a function of their unit cell dimensions in Fig. 27, whereas the available diffusion data of various acceptor and donor elements in germanium and silicon are reproduced in Figs. 28-31(69). From these property values, silicon carbide is found to be intermediate in position between diamond and silicon.

(b) Diamond, Germanium and Silicon Semiconductors and the Nature of their Vacancies:

1. Diamond. Diamond has been least investigated as a Group IV semiconductor(70). Structurally, it is the ideal of all cubic Group IV semiconductors. However, from the presence of a (222) x-ray reflection, it can be said that the charge distribution surrounding carbon atoms is not spherically symmetrical. In Fig. 32, each solid line connecting two atoms represents a single orbital, whereas each dotted line represents only one electron. To a first approximation, at a point such as A, the atoms are still supported by normal bonds, whereas the nearest neighbors to the vacancy, B,C,D, and E are each left with one unpaired electron. One way these unpaired electrons can behave is to attempt to form quasi-covalent bond (or paired orbital) with the unpaired electrons of the two nearest atoms surrounding the vacancy as shown in Fig. 32. Or each may remain associated with its particular carbon nucleus or it may orbit around all the four unsatisfied atoms. A wave mechanical solution will involve a certain probability in all these configurations (final positions of the nearest neighbors are shown in

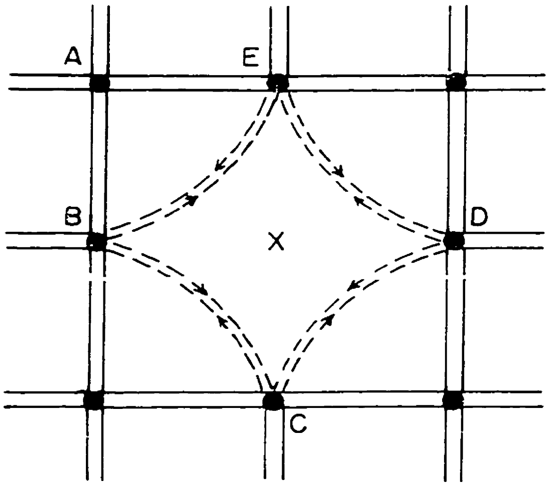

FIG. 32 A SCHEMATIC OF A LATTICE VACANCY IN DIAMOND LATTICE.

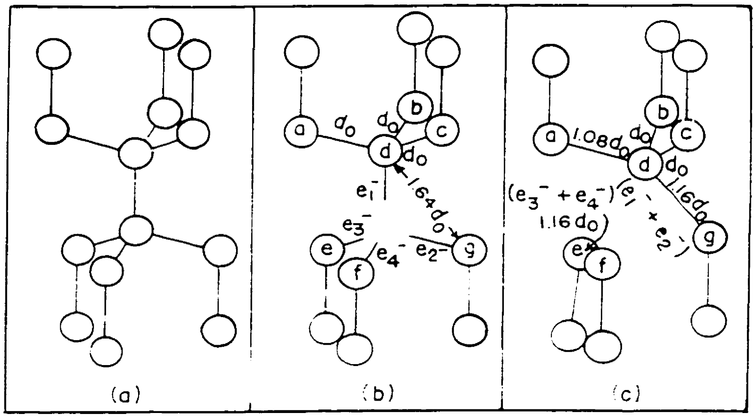

FIG. 33 FORMATION OF VACANCY IN A DIAMOND CUBIC LATTICE.
(a) NORMAL SITE, (b) REMOVAL OF ATOM, (c) RELAXATION OF NEIGHBORS

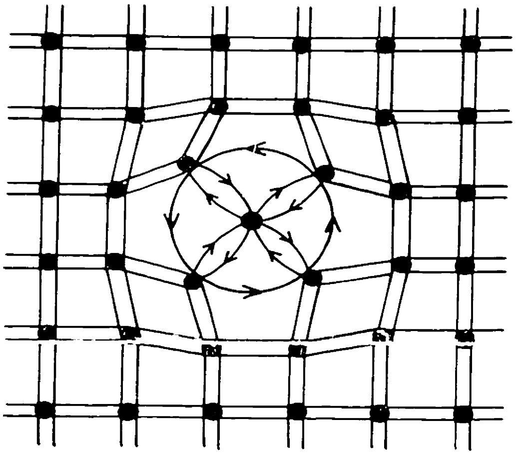

FIG. 34 A SCHEMATIC DIAGRAM OF AN INTERSTITIAL CARBON ATOM IN DIAMOND LATTICE.

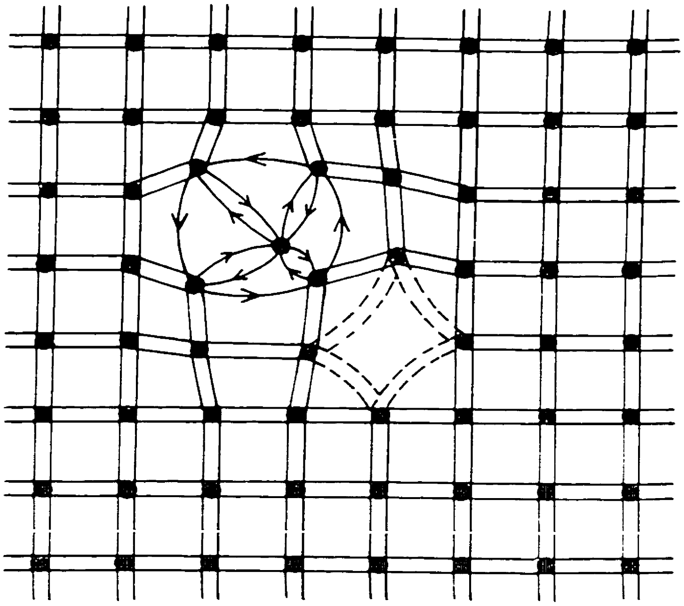

FIG. 35 A SCHEMATIC DIAGRAM OF DIAMOND LATTICE SHOWING AN EMBEDDED VACANCY-INTERSTITIAL PAIR (NOTE THE LOSS OF SYMMETRY)

Fig. 33).(71) But all of them will have the common feature that the unpaired orbital will be less tightly bound to the solid than those electrons which constitute a normal bond. Atoms like B, C, D, and E will have higher potential energy than the normal lattice atoms. A vacant site will normally be neutral. But by trapping holes from the valence bonds, they will acquire virtual donor properties in diamond(70). A good percentage will also trap electrons (or exitons finally) from the conduction bond. The effective ionization energy of this electron is about 0.2 eV(70).

Fig. 34 shows the interaction of an interstitial carbon atom into a normal lattice. The surrounding atoms of an interstitial carbon atom would necessarily suffer bond distortion and a variety of defect bonds are created. These levels are all higher than those for normal bonds and, hence, these too would act as positive hole traps by the same reasoning as that applied to vacant sites. Considering the open structure of diamond, the diagram of Fig. 34 is probably a little exaggerated. Both the positive hole trapping level and the electron affinity levels associated with an interstitial atom are, therefore, likely to be even shallower than those for the corresponding vacant site. Fig. 35 shows the presence of a vacancy-interstitial pair inside the diamond lattice. No diffusion measurements have been reported in diamond. But nitrogen impurity has been shown to be present at the lattice sites of natural diamond as a double layer of nitrogen every 6000 atomic planes. Impurity bands in diamond lie between 0.3 and 0.5 eV above the valence band, leading to p-type conduction.

2. Germanium. Germanium, as a semiconductor, has been most extensively investigated in Group IV. It has the same cubic structure as diamond and thus the formation of atomic and/or electronic defects can be similarly visualized. However, the electrical nature of the lattice vacancies are completely opposite in germanium, where the vacancies behave as acceptors (in contrast to the virtual donor properties of diamond vacancies). This fact has been confirmed by the self-diffusion studies of Valenta and Ramasastry(18) in heavily doped (arsenic and gallium) material. They observed n-type material (As-doped) to possess higher diffusivity than p-type material (Ga-doped) and the activation energy for self-diffusion a function of impurity type and level. If self-diffusion does occur by means of vacancies, the diffusion coefficient at a given temperature will be proportional to the concentration of vacancies. By changing the concentration of vacancies by a known amount, one would then be able to predict the variation in the self-diffusion coefficient. A method for varying the concentration of vacancies is suggested in the work of Reiss and Fuller(20,72) if one further assumes that vacancies act as acceptors. They(72) have been able to confirm the predictions of the former author(20), namely that the solubility of a donor increases with increasing acceptor content and that the solubility of a donor decreases in the presence of another donor. Similarly, Reiss(20) predicts that an acceptor would be more soluble in a donor environment than in an acceptor environment. Consequently, if vacancies behave as acceptors, one would expect that at a given temperature

the equilibrium concentration of vacancies in n-type germanium would be greater than in p-type germanium(73), i.e., germanium self-diffusion should be greater in n-type than p-type germanium in the case of diffusion via vacancies. That, indeed, has been observed by Valenta and Ramasasty(18) whose data are reproduced in Fig. 36. These authors explained their observed dependence of activation energy for self-diffusion in germanium on the volatilization of the dopants at the diffusion annealing temperatures. Boltaks(1) attributed the effect to a change of the position of the Fermi level from the intrinsic to doped material. As discussed in Chapter II:

$$D = D_o \exp \left[\frac{-(Q - \Delta\mu)}{RT} \right] \qquad \text{(II.7)}$$

where the change in Fermi level ($\Delta\mu$) is dependent on the impurity type and concentration, Q is the activation energy in intrinsic material.

Further evidence indicating that vacancies act as acceptors is found in data obtained from irradiated germanium(74,75). A good fraction of the acceptors generated by quenching germanium from high temperatures have been interpreted as vacancies(76,77).

3. Silicon. Silicon, being the second member of Group IV, is in the boarderland of metals and non-metals. Its properties are intermediate with respect to diamond and germanium. This is also the case for the electrical nature of its vacancies. From the diffusion data reported in Figs. 28-31, Swalin(77) has recently pointed out that the apparent inconsistencies shown by the rates of diffusion of various

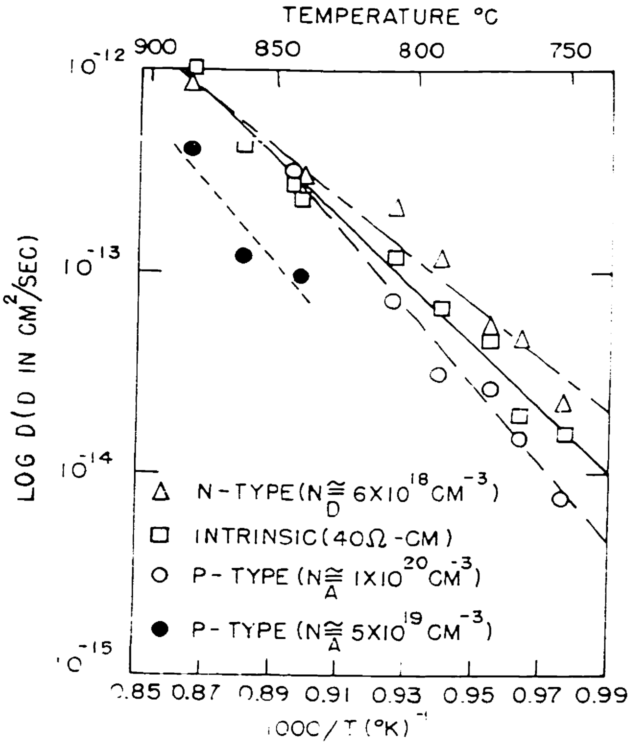

FIG. 36 SELF-DIFFUSION COEFFICIENTS IN Ge, AT VARIOUS TEMPERATURES FOR DIFFERENT DOPINGS.

elements in germanium and silicon are attributable to a difference between the energy levels of vacancies in the two semiconductors.

Vacancies in the crystal lattices of both silicon and germanium behave as acceptors. However, the acceptor level of vacancies in germanium is located in the lower half of the forbidden band, 0.26 eV above the valence band, whereas in silicon this level is found in the upper half of the forbidden band, 0.16 eV below the bottom of the conduction band(78). At comparable temperatures, therefore, there will be more charged vacancies in germanium than in silicon. This situation must be reflected in the mechanism of diffusion in the two semiconductors which involves the neighboring vacancies for elements of Group III and V. In germanium, this gives rise to Coulomb interactions between the charged impurities and the charged vacancies; positively charged impurity ions are attracted towards the negatively charged vacancies, which thus assist their motion, whilst negatively charged ions are repelled. This effect, of course, hinders the motion of negative ions through the crystals. In silicon, on the other hand, most of the vacancies are neutral and there is no Coulomb interaction between vacancies and impurity ions.

(c) Interpretation of Diffusion Data in Si and Ge.

1. Comments on the Available Experimental Data: In contrast to diamond, silicon and germanium have been intensively investigated mainly because of their practical utility. Table XV shows the position of the donor and acceptor levels in silicon and germanium in terms of

their ionization energies. The levels due to other impurities generally lie further from the valence or conduction bands. Imperfections introduced into Ge and Si by bombardment with high energy particles (equal number of interstitials and vacancies) behave differently: n-type Ge is converted to p-type, and with further exposure, the conductivity increases while both n-type and p-type Si tend to become more nearly intrinsic with prolonged bombardment.

TABLE XV(79)

IONIZATION ENERGIES OF GROUP III AND GROUP V IMPURITIES IN Ge AND Si (T INDICATES VALUES OBTAINED BY A THERMAL METHOD AND O BY AN OPTICAL METHOD

Impurity	Donor (D) or Acceptor (A)	Ionization Energy (eV)	
		Ge	Si
B	A	0.0104(T)	0.045(T), 0.046(0)
Al	A	0.0102(T)	0.047(T), 0.067(0)
Ga	A	0.0108(T)	0.065(T), 0.071(0)
In	A	0.0112(T)	0.16 (T), 0.154(0)
P	D	0.0120(T)	0.044(T), 0.046(0)
As	D	0.0127(T)	0.049(T), 0.056(0)
Sb	D	0.0096(T)	0.0039(T), 0.043(0)
Bi	D	----	0.069(T), ----

This shows that in Ge acceptor centers are created with energy levels just above the top of the valence band. The situation is more complex for silicon; it is clear that both deep lying hole traps and electron traps are created(80). Silicon-germanium alloys have also been looked into(81). The band gap (Ge and Si alloy) increases to 0.93 eV at 15% silicon and then at a slower rate to the E_g value for pure silicon. The segregation coefficients for Group III and V impurities in Si and Ge are also different but decrease in the same direction in either of them(80). In silicon and germanium, Group III and V elements have relatively higher solubilities but lower diffusion coefficients than other elements, whereas group I and transition elements have the lowest solubilities and highest diffusivities of all the elements studied(69).

The III-V active impurity elements are incorporated in substitutional positions in the semiconductor lattice while the transition and Group I elements tend to occupy interstitial positions. It might reasonably be assumed, therefore, that the transport or motion in the lattice of these two types of atoms will be governed by different mechanisms. In the first case, a substitutional diffusion process takes place, while in the second, a mechanism of interstitial diffusion is believed to occur.

Investigations have been carried out on a wide variety of impurity elements in both Ge and Si and, depending on their activation energies, they can roughly be divided into two groups: a) those elements with energies less than or approximately equal to 1 eV; and b) those with energies greater than 2 eV. The first group includes the group I and transition elements which presumably diffuse by an interstitial mechanism, whereas the second comprises the III-V elements which diffuse by a substitutional mechanism including the additional energy due to vacancy formation. The experimentally determined values of the diffusion coefficients of various impurity elements as a function of temperature are shown in Figs. 28 and 29 for Ge and in Figs. 30 and 31 for silicon. In the case of Ge, it is evident from the data that the donor impurities diffuse faster than the acceptors, whereas the opposite appears to hold in silicon with the exception of phosphorus.

No experimental data are available for self-diffusion in silicon. However, Boltaks(1) assumed the relation:

$$D = 10 \exp\left(\frac{-97\ \text{Kcal}}{RT}\right)\ \text{cm}^2/\text{sec} \qquad \text{(V.15)}$$

for self-diffusion in silicon. The value of Q in this relation lies between that predicted by Fuller and Ditzenberger(98) (110 Kcal/mole) and that assumed by Elbaum(101) (90 Kcal/mole).

2. Possible diffusion mechanisms operating in Si and Ge:

The most probable mechanism, accounting for the relatively high activation energies of diffusion of the substitutional impurities, is one involving vacancy reaction. By this means the movement of the solute atoms in the crystal, or the solvent atoms in the case of self-diffusion, takes place in a particular direction by a sequency of jumps into vacant lattice sites. This can be regarded as a drift of the vacancies in the opposite direction in a manner somewhat analogous to the behavior of the electrons and holes in the electrical conduction. On the assumption that the binding energy between the solute atom and its neighboring solvent atoms is less than that between the atoms of the host lattice, it has been shown that it is energetically easier to produce a vacancy near to an impurity site(82). Since both the solute atoms and the vacancies individually strain the lattice structure, this reduction of energy presumably results from the decrease of the strain produced by closely associated impurities and vacancies. The vacancies will, therefore, associate preferentially with the impurity atoms and the lattice can be regarded as containing a certain concentration of solute-vacancy molecules. This hypothesis appears to be supported by the fact that the activation energies for the diffusion of the substitutional impurities in germanium [Sb(2.3 eV), As(2.4 eV), In(3.0 eV), Ga(2.6 eV)](83) are relatively low compared to that for self-diffusion (3.0 eV)(16).

This idea has been further developed theoretically(77). These calculations have indeed shown that the diffusion rate of the n-type impurities in Ge is about 2 orders of magnitude greater than that of the p-type impurities, in excellent agreement with the experimental data shown in Figs. 28 and 29. In the case of Si, in which the acceptors diffuse about an order of magnitude faster than the donors, reasonable agreement between theory and experiment was also obtained by taking into consideration the contribution to the activation energy due to the lattice strain energy of the ions. There is strong evidence that self-diffusion in Ge also occurs by a vacancy mechanism. The enhanced effect of vacancies on the diffusion of impurities has been demonstrated by the enhanced diffusion of As in irradiated Ge(84) and of Ga in irradiated Si(85). According to James and Lark-Horovitz(99), di-vacancies are probable with high impurity content to some extent.

(c) The Mechanism of Self-Diffusion in SiC. Before drawing any conclusion about the possible mechanism of self-diffusion in SiC, a few salient points of this work are recapitulated below:

1. p-type (black) Al-doped material is observed to have higher diffusivity of carbon than the N-doped n-type (green) material.
2. The data is assumed to lie in an impurity controlled range.
3. The average impurity content of the p-type SiC used was about 4.28×10^{20} Al/cm^3 ($\approx$600 ppm) and that of the n-type SiC used was about 1.38×10^{19} ($\approx$100 ppm).
4. Silicon has a much higher diffusion coefficient than Carbon in SiC.
5. Diffusion data obtained for carbon in SiC are all along [0001] in 6H SiC.

1. Some available informations pertinent to the Conclusion of the Mechanism of Carbon Self-Diffusion in SiC.

Compared to Silicon and Germanium, the electronic and other properties of SiC are very little known and understood(86). The donor energy levels of Group V elements are all about 0.08 eV below the conduction band and the acceptor energy levels of the Group III elements are all about 0.25 eV above the valence band. Other than the present work, only aluminum diffusion data along [0001] in 6H SiC are available(65). As expected, the activation energy for this impurity diffusion has been found lower than that of carbon in SiC. The absolute D values at a given temperature (within the range of experimental measurements) are higher than (but near to) that of carbon in SiC following a pattern as in silicon (Fig. 30).

Woodbury and Ludwig(87) have studied the position of boron and nitrogen in 6H SiC by electron-spin resonance. They conclude that both these impurities substitute for carbon and occupy the three non-equivalent carbon sites with equal probability. These three carbon sites are shown in Fig. 37. Again, from the work of Seace and Slack(88) on the solubility of carbon in liquid silicon and from the thermodynamic study of the binary system carbon-silicon by Drowart and De Maria(89), it is concluded that there is a certain amount of carbon in solid solution& ismost probably placed substitutionally in silicon lattice sites. Moreover, a good amount of stacking faults are known to be present(47,91) in all SiC structures. Thus, the SiC samples used have a considerable number of structural imperfections.

Calculations have been made(90) of the nature of Si—C bond. This showed that SiC can be considered as a resonance hybrid of the following two structures of which the ionic structure (A) contributes about 12% to the final hybrid at room temperature:

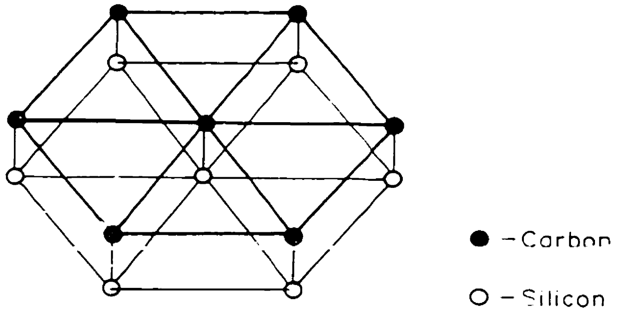

(a) Basic silicon-carbon layer "A sites

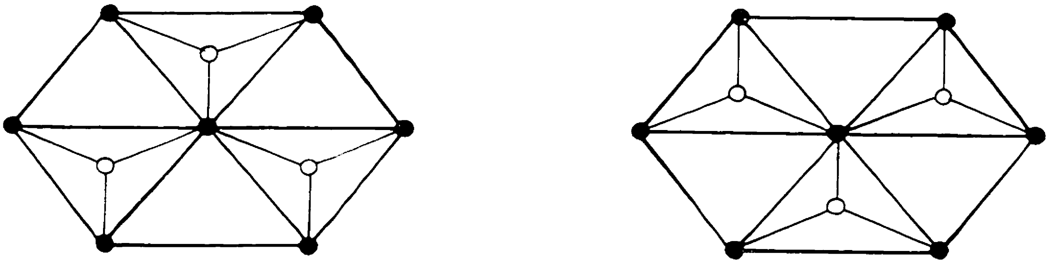

(b) "B" sites for next layer

c) "C" sites for next layer

FIG. 37 THREE TYPES OF CARBON LATTICE SITES IN 6H SILICON CARBIDE CRYSTALS.

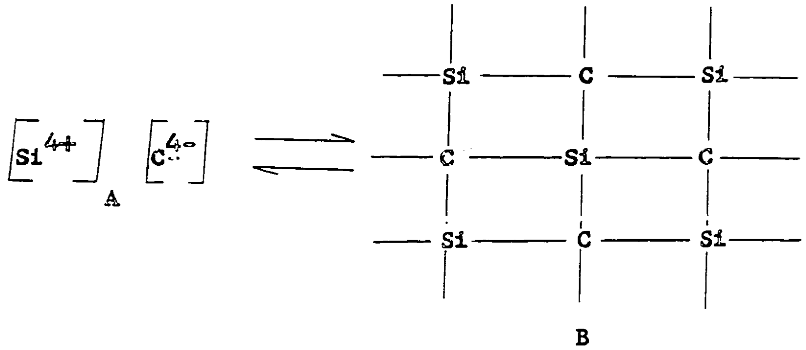

An experimental fact pertinent to this point will be mentioned here. During dislocation etching (either electrolytically in 20% KOH or in fused NaOH and/or in Borax) always only one side of a single crystal was etched at random. Since only silicon was dissolved out of the crystal (under the etching conditions) leaving a graphite residue it is conceivable that the negatively charged OH ions attacked only the surface containing an outermost layer of partially positively charged Si^{+x} ions and probably establish an electrical double layer on the crystal.

The electrical nature of the lattice vacancies in Group IV semiconductors changes from the virtual donor nature in diamond to almost fully acceptor character in germanium with silicon vacancies occupying an intermediate position of partial acceptor to near neutral nature. Thus, carbon vacancies in silicon carbide can be conceived of being partially virtual-donor in nature though to a less extent than carbon vacancies in diamond. This would produce a higher self-diffusivity in the p-type material than in n-type material with a change in the position of the Fermi level following Eq. (II.7), if the diffusion of carbon in SiC is assumed to occur by a vacancy mechanism.

According to Friedel(82) the proximity of an impurity centre lowers the energy for the formation of a vacancy by an amount ΔH_s given approximately by the formula:

$$\Delta H_s \cong \frac{6\pi(r_s - r_s')^2 r_s'}{Z(1 + \alpha)\chi'} \qquad (V.16)$$

where

$$\alpha = \frac{(1 + p)\chi \; r_s'}{2(1 - 2p)\chi' r_s}$$

with r_s' and r_s the ionic radii of the impurity and of the semiconductor particle, respectively, χ' and χ are the compressibilities of the two substances, p is Poisson's ratio for the semiconductor, and Z is the coordination number of the semiconductor crystal. A typical calculated value of ΔH_s is 0.25 eV at 790°K for the case where Mg is dissolved in Ca. For elements with widely different valencies, sizes and crystal structures, the value of ΔH_s may be of the order of an eV.

2. Concluded Mechanism of Carbon self-diffusion in SiC. Combining an extension of Woodbury and Ludwig's(87) observation to Al and N impurities in SiC (i.e., Al and N both substitute for carbon in lattice sites of SiC) with Friedel's(82) idea of relative ease of vacancy formation adjacent to a substitutional impurity, it can be said from the experi-

mental data that all the measured D values lie in an extrinsic or impurity controlled region exactly as in germanium(18). Thus, carbon lattice vacancies can be created (at high temperatures) in the immediate vicinity of the impurity sites. These vacancies assume virtual donor properties by subsequent hole-trapping. This is a Schottky-type atomic defect and electronic defect complex and can be produced independently of silicon lattice vacancies (there is no requirement to charge balance by equating vacancy concentrations). The donor or acceptor impurity being positively charged will be repelled by the positively charged vacant carbon lattice site; thus, impurity atom-vacancy complex production is ruled out. Again, due to the fact that Si-C bond is more than 50% stronger than Si-Si bond, there will be practically no substitutional disorder between the vacant carbon site and the neighboring lattice silicon atoms; C on Si site leads to bond energy higher than SiC however.

$$\left[277.2(=69.3 \times 4) \text{ Kcal/mole} > 250.6(=83.1 \times 4/2 + 42.2 \times 4/2) \text{ Kcal/mole}\right]$$

This consideration also suggests that few or no multiple carbon vacancy complexes would exist except at high impurity content and at low temperatures (if the decrease in strain energy for multiple vacancy complex formation exceeds the Coulombic repulsion energy between like-charged carbon vacancies plus the energy required to produce substitutional disorder of the type mentioned).

A fraction of the impurities occupying carbon lattice sites may form strong impurity-impurity complex (viz., of the form AlN). Therefore, the entire concentration of impurity sites may not be availalbe for the formation of adjacent vacant carbon lattice sites at high temperatures. In other words. due to considerable strengths of N-Si. Al-Si, and N-Al bonds, the removal of lattice carbon adjacent to the impurity centres to produce lattice vacancies (carbon) will be a function of temperature. From the experimental fact that the diffusion coefficients of carbon in both p-and n-type SiC become almost identical at around 2100°C, it can be guessed that aluminum and nitrogen impurity controlled vacancy formation is complete at about that temperature.

From the fact that some amount of carbon is soluble in SiC (about 10-50 ppm at 2000°C) some disorder is expected in the ideal 6H SiC structure which will provide more carbon lattice sites for occupancy by the Group III and V impurities if the carbon in solid solution in SiC is taken to be substitutional. Because of the high volatility of Si compared to carbon more carbon is expected in SiC (in solid solution) than the stoichiometry of SiC demands.

The order of value of the activation energy obtained in this work (which is more than twice the Si-C bond strength) appears to support the vacancy mechanism of carbon diffusion in SiC. Dienes(26) made theoretical calculations for the activation energies for different mechanismsof self-diffusion in graphite. His treatment is based on carbon-carbon bond strengths and their variation with carbon-carbon distances. His values 119.4 Kcal/mole for the formation of a vacancy and 71.4 Kcal/mole for the motion of a vacancy do not take into account the possible relaxation of atoms around the vacancy. The activation energies for the different possible mechanisms of self-diffusion in graphite are:

Q(Kcal/mole)	Mechanism
190.8	Vacancy
90.4	Direct Interchange
417.0	Energy of formation of interstitials for interstitial mechanism.

giving direct exchange as the probable mechanism in graphite. Kanter(27) observed Q = 163 Kcal/mole for the diffusion of C-14 in natural graphite crystals, very near to that calculated for vacancy mechanism . Kanter recalculated the activation energies following Dienes (using a different value (170 Kcal/mole) for the heat of sublimation of graphite). His value is Q = 263 Kcal/mole for self-diffusion in graphite by a vacancy mechanism.

Following the same line of reasoning as Dienes, the vacancy formation energy is estimated to be 138.6 Kcal/mole in SiC (69.3 × 2 = 138.6 Kcal/mole where 69.3 Kcal/mole is the C-Si bond strength(66)). Since the strength of SiC bond is not known as a function of their interatomic distance and since Si-C distance along C-direction in SiC is about double the value of C-C distance in graphite perpendicular to the C-direction (3.08 Å vs. 1.42 Å)(26,91), about 60 Kcal/mole or more can be estimated to be required for the motion of a vacancy in SiC. This makes a total of about 200 Kcal/mole required for the self-diffusion of carbon in SiC which is about the value expected for carbon diffusion in intrinsic SiC from the experimental data (between 141 and 302 Kcal/mole). Thus, a sequence of zig-zag jump-motions of carbon between lattice vacancy sites created around the impurities at high temperature (as also the intrinsic carbon lattice vacancies controlled by the impurity type and level) is concluded to be the mechanism of carbon diffusion in SiC. This vacancy mechanism also explains why p-type SiC has higher diffusivity for carbon than n-type SiC whereas n-type germanium produces higher diffusion coefficient of Ge than the p-type material. It is hard to speculate on the nature of the moving carbon species but with all probability it is atomic carbon with about 0.12 e of negative charge (attracted by the positive vacancy) rather than an ion (due to high ionization energy of carbon).

So far as the region of the experimental data is concerned, the use of the term extrinsic is probably improper. The extrinsic range for self-diffusion in ionic materials refers to that where the vacancy concentration is fixed by the impurity concentration (at any temperature) and the activation energy for diffusion involves only the energy required for mobility. Whereas in SiC in this so-called extrinsic range, the activation energy term includes the energy necessary for mobility and for the formation of carbon lattice vacancies around the impurity centres (probably temperature, and impurity level and type dependent to some extent).

3. Postulated mechanism of Silicon self-diffusion in SiC. From the aforementioned mechanism for the diffusion of carbon in SiC some idea can be made of the mechanism of silicon diffusion in Silicon Carbide. If we assume a lattice vacancy (silicon) mechanism for the diffusion of Si in silicon carbide the experimental findings of higher absolute D values for silicon in SiC compared to that of carbon in SiC (at any given temperature) can be explained. According to the atomic theory of diffusion, the D value is directly proportional to the concentration of vacant sites. Since even at the lowest experimental temperature (about 1850°C) silicon carbide has been observed to decompose substantially with the volatilization of silicon and the deposition of spongy graphite(102), a larger amount of Si vacancy creation (compared to carbon) at the SiC surface and their subsequent diffusion inwards is very probable.

Group III and V impurities do not affect the silicon lattice sites and the silicon vacancies are partly negatively charged to neutral in character with practically no effect by the presence of either donor or acceptor impurities on vacancy concentration. The concentration can be described by an equation of the Schottky-type involving only one species, i.e., silicon. Thus, the concentration of silicon lattice vacancies in SiC is much larger than that of carbon. Even without this inward diffusion of silicon lattice vacancies it should be much easier to form a vacant silicon site (which are closer to an impurity center than the lattice carbons nearest to the impurity site) than a vacant carbon site. However, due to larger size of silicon compared to carbon, the energy required for diffusion mobility should be somewhat higher for silicon than for carbon in SiC. Again, in general, the energy required for vacancy formation is a much larger fraction (about two-thirds) of the total activation energy than the energy required for mobility (about one-third Q or less). Therefore, due to presumably lower energy requirement for the formation of silicon vacancies in SiC (and consequently higher vacancy concentration than that of carbon vacancies in SiC at a given temperature) silicon should have higher diffusivity in SiC than carbon. This is what is observed experimentally.

From this mechanism, it can also be concluded that the activation energy for the diffusion of Si in SiC should be lower than that for carbon in the so-called extrinsic range. This conclusion falls in exact line with the observation that in compound semiconductors, in general, the higher electropositive species has a lower activation energy for self-diffusion (Chapter II). However, in the intrinsic range (or at all temperatures in the intrinsic material) both silicon and carbon will require the same energy for vacancy formation under the proposed vacancy mechanism of self-diffusion. But partly due to the opposite electrical nature of carbon lattice vacancy and of the carbon diffusing species and partly due to the smaller size of the carbon diffusing species (than that of silicon) energy for mobility will be lower for carbon self-diffusion than for silicon self-diffusion either in intrinsic range in doped material, or in intrinsic material at all temperatures.

4. Projected mechanism of Aluminum Diffusion in SiC. From the preceeding discussion of the mechanisms of carbon and silicon self-diffusion in SiC and keeping in line with the existing interpretations of the diffusion mechanism of Group III and V impurities in silicon and germanium, a proposal can be made of the mechanism of aluminum diffusion in SiC. This is suggested to be a vacancy mechanism proceeding in a manner exactly as carbon self-diffusion in SiC (in the extrinsic range). But, covalent SiC structure is quite open (which permits interstitial movement of aluminum) and the diffusing aluminum species is much smaller than the carbon species (radius of Al^{+3} = 0.5 Å and radius of C = 0.77 Å).(66) Therefore, the difference in the diffusivity of these two species (in the extrinsic range) lies in the energy required for mobility which is concluded to be much higher for carbon than for aluminum. Most of the aluminum, however, diffuses through intrinsic carbon lattice vacancies whose concentration is progressively increased with increased aluminum content. Thus, the diffusivity of aluminum in SiC should a function of the impurity content of the sample and at very low impurity concentrations even the minute amount of concentration change produced by diffusing aluminum might lower aluminum diffusion rate further along the direction of diffusion. Since donors increase the solubility of acceptors in semiconductors, they should decrease the diffusion rate of acceptors(20,36).

Finally, it should be remembered that the above discussion of impurity effects on diffusion (by vacancy mechanism) in SiC is in addition to the effect of impurities in increasing or decreasing (as the case may be) the intrinsic lattice vacancy concentration. Thus, donors (by contributing an extra electron to the conduction band) decrease the intrinsic carbon lattice vacancy concentration (which are virtual-donors in SiC) and acceptors (by accepting an electron from the valence band) increase the intrinsic carbon lattice vacancy concentration in SiC(20). It also follows from this conclusion that there would be a considerable association of intrinsic carbon and silicon lattice vacancies in SiC (from the considerations of both the factors responsible for vacancy association viz., reduction of lattice strain energy and possession of opposite electrical charge).

VI. CONCLUSIONS

1. From the measured diffusion coefficients it is evident that silicon, the higher electropositive component of SiC, is the higher diffusing species (in the temperature range 1853°C to 2060°C).

2. Carbon diffusion coefficients measured in SiC single and polycrystals were characteristic of lattice diffusion in the temperature range 1853°C to 2060°C.

3. Carbon lattice diffusion coefficients measured appear to be in the extrinsic (or impurity-controlled) range.

4. The experimental results for carbon self-diffusion in black hexagonal SiC single crystals (≃600 ppm Al-doped) along [0001] in the temperature range 1853°C to 2060°C are given by:

$$D = 3.014 \times 10^{2} \exp\left[\frac{-141.5 \pm 16.6 \text{ Kcal}}{RT}\right] \text{cm}^2/\text{sec.}$$

The same data in a light-green hexagonal crystal along [0001] is given by:

$$D = 2 \times 10^{17} \exp\left[\frac{-302.4 \pm 48.6 \text{ Kcal}}{RT}\right] \text{cm}^2/\text{sec.}$$

The carbon lattice diffusion coefficients measured in black dense (>99%) polycrystalline material are given by:

$$D = 2.36 \times 10^{2} \exp\left[\frac{-137.1 \pm 14.2 \text{ Kcal}}{RT}\right] \text{ cm}^{2}/\text{sec.}$$

5. Carbon diffusivity in SiC is found to be higher in p-type black material than in n-type green material (in the temperature range 1853°C to 2060°C) and becomes equal at around 2100°C. This is in exact reverse order to that found in Germanium in the extrinsic range.

6. From the existing interpretation of the electrical nature of the lattice vacancy sites in diamond, silicon and germanium, the author concludes that a carbon vacancy site in SiC lattice has virtual donor properties and is thus opposite in nature to that of germanium lattice vacancy in germanium.

7. In the absence of any contradictory evidence, it is suggested that the self-diffusion of carbon in SiC proceeds by a vacancy mechanism involving the intrinsic vacancies plus the gradual formation of carbon lattice vacancy in the vicinity of the impurity sites (which occupy the three non-equivalent carbon lattice sites with equal probability) and movement of carbon along the vacant lattice sites by a sequence of jumps. Other than the imperfections already present in SiC crystals only carbon lattice vacancy-hole complex is concluded to be formed at high temperatures (significantly affecting carbon diffusion).

VII. SUGGESTIONS FOR FUTURE WORK

1. A detailed and precise study of silicon self-diffusion in SiC can be made using radioactivation analysis technique in conjunction with Silicon-30 stable isotope (rather than Silicon-28 used in this study). This will increase the sensitivity of silicon detection many fold.

2. From this study (in both intrinsic and doped single crystals) a verification can be made of the proposed mechanism of silicon diffusion in SiC.

3. Different authors have predicted different rates of self-diffusion in semiconducting silicon (intrinsic). These can now be verified using the technique developed here. This will considerably clarify the mechanism of self-diffusion in intrinsic Group IV semiconductors which are of immense practical utility.

4. In the near future, better impurity type and level controlled (as also intrinsic) silicon carbide single crystals of different structural modifications may be available. This would allow more accurate determination of self-diffusion coefficients (for both silicon and carbon) as a function of impurity type and level, crystal orientation and crystal structure.

5. For a better understanding of the mechanism of carbon self-diffusion in SiC single crystals, studies on different types of defect formation (in SiC) are required.

6. Diffusivity studies of different commonly encountered impurities in SiC will considerably help to understand the diffusional properties of SiC in comparison with other Group IV semiconductors.

7. Segregation coefficients of acceptors and donors as a function of temperature and the determination of the exact positions of impurity energy levels have not been ascertained to date. These determinaations, in conjunction with the diffusivity studies suggested above, will produce a firm basis for developing SiC as a practical special-purpose semiconductor (with controlled properties for high temperature applications).

VIII. BIBLIOGRAPHY

1. Boltaks, B. I., DIFFUSION IN SEMICONDUCTORS, English Translation by J. I. Carasso, Academic Press, New York (1963).

2. Jost, W., DIFFUSION IN SOLIDS, LIQUIDS AND GASES, Revised Edition, Academic Press, New York (1960).

3. Nernst, W., "Thermodynamics of Very Dilute Gases and Solutions," *Preurs. Akad. Wiss. Berlin*, Ber. 13, 467 (1933).

4. Einstein, A., "Motion of Particles Suspended in a Static Liquid Described by the Molecular Kinetic Theory of Heat," *Ann. Physik*, *17*, 549 (1905).

5. Frenkel, J., "Heat Motion in Solids and Liquids," *Z. Physik*, *35*, 652 (1926).

6. Friauf, R. J., "Diffusion of Silver in Silver Bromide and Evidence for Interstitialcy Migration," *Phys. Rev.*, *105*, 843 (1957).

7. Wagner, C., and Schottky, W., "Theory of Regular Mixed Phases," *Zeits. F. physik Chem.*, *11*, Abt. B, 163 (Dec. 1930).

8. Lidiard, A. B., HANDBUCH DER PHYSIK, ELECTRICAL CONDUCTIVITY II, Edited by S. Flugge, Vol. XX, Springer, Berlin (1957).

9. Berard, M. F., DIFFUSION IN CERAMIC SYSTEMS; A SELECTED BIBLIOGRAPHY, U.S. AEC R & D Report TID 4500, Dec. 15, 1960. Published by Ames Laborotary at I.S.U., May 1962 (No. IS-448).

10. Crank, J., MATHEMATICS OF DIFFUSION, Oxford Univ. Press, Fair Lawn, N.J., 1956.

11. Tomizuka, C., in Lark-Horowitz, K., and Johnson, V.A., (Editors), METHODS OF EXPERIMENTAL PHYSICS, *Vol. 6A*, 364-373, Academic Press, New York, 1959.

12. Hoffman, R. E., in ATOM MOVEMENTS, pp. 51-68, ASM, Cleveland, 1951.

13. Zener, C., "Theory of Diffusion," pp. 289-314, in IMPERFECTIONS IN NEARLY PERFECT CRYSTALS, Edited by W. Shockley, John Wiley, New York, 1952.

14. Shewmon, P.G., DIFFUSION IN SOLIDS, McGraw-Hill, New York, 1963..

15. Zaromb, S., "An Analysis of Diffusion in Semiconductors," I.B.M. J. Res. Dev., 1, 57 (1957).

16. Letaw, H., Portnoy, W.M., and Slifkin, L.M., "Self-Diffusion in Germanium," Phys. Rev., 102, 636 (1956); Bull. Am. Phys. Soc., 30(2), 13 (1955).

17. Mayburg, S. and Rotondi, L., "Thermal Acceptors in Vacuum Heat-Treated Germainum," Phys. Rev., 91, 1015 (1953).

18. Valenta, W. M. and Ramasastry, C., "Effect of Heavy Doping on the Self-Diffusion of Germanium," Phys. Rev., 106, 73 (1957).

19. Cleland, J.W., Crawford, J.H. and Holmes, D.K., "Effects of Gamma Radiation on Germanium," Phys. Rev., 102, 722 (1956).

20. Reiss, H., "Chemical Effects Due to the Ionization of Impurities in Semiconductors," J. Chem. Phys., 21, 1209 (1953).

21. Cuddeback, R.B. and Drickamer, H.G., "Diffusion in Solid Sulfur," J. Chem. Phys., 19, 790 (1951).

22. Hanffe, K., REACTIONEN IN UND FESTEN STOFFEN, Berlin, 1955.

23. Boltaks, B.I. and Plachenov, B.T., "Self-Diffusion in Selenium," Zhur. Tekh. Fiz., 27, 2229 (1957).

24. Nachtrieb, N.H. and Handler, G.S., "Self-Diffusion in α-White Phosphorus," J. Chem. Phys., 23, 1187 (1955).

25. Feldman, M.H., Geoddel, W.V., Dienes, G.J. and Gossen, W., "Studies of Self-Diffusion in Graphite using C-14 Tracer," J. Appl. Phys., 23, 1200 (1952).

26. Dienes, G.J., "Mechanism for Self-Diffusion in Graphite," J. Appl. Phys., 23, 1194 (1952).

27. Kanter, M.A., "The Mechanism for Atom Motion in Graphite Crystals," in KINETICS OF HIGH TEMPERATURE PROCESSES, W. D. Kingery, Ed., Tech. Press of M.I.T. and John Wiley, New York (1959), 61-66.

28. Anderson, J.S. and Richards, J.R., "The Self-Diffusion of Lead in Lead Sulfide," J. Chem. Soc., p. 537 (1946).

29. Bloem, J., "Controlled Conductivity in Lead Sulfide Single Crystals," *Philips Res. Reports*, *11*, 273 (1956).

30. Boltaks, B.I. and Mokhov, I.N., "Self-Diffusion and Diffusion of Impurities in Lead Telluride and Selenide," *Zhur. Tekh. Fiz.*, *28*, 1046 (1958); "The Diffusion of Lead in Lead Telluride," *Zhur. Tekh. Fiz.*, *26*, 2448 (1956).

31. Secco, E.A., "Diffusion and Exchange of Zinc in Crystalline Zinc Sulfide," *J. Chem. Phys.*, *29*, 406 (1958).

32. Lindner, R., "Diffusion of Radioactive Zinc in Zinc-Iron Spinel and Zinc Oxide," *Acta Chem. Scand.*, *6*, 457 (1952).

33. Moore, W.J. and Lee, J.K., "Kinetics of the Formation of Oxide Films on Zinc Foil," *Trans. Farad. Soc.*, *47*, 501 (1951).

34. Secco, E.A. and Moore, W.J., "Diffusion and Exchange of Zinc in Crystalline Zinc Oxide," *J. Chem. Phys.*, *26*, 942 (1957).

35. Boltaks, B.I. and Kulikov, G., "On the Diffusion of Indium, Antimony and Tellurium in Indium Antimonide," *Zhur. Tekh. Fiz.*, *27*, 82 (1957).

36. Boltaks, B.I. and Gutorov, Yu.A., "Some Results on the Diffusion of Impurities and their Effect on the Electrical Properties of Gallium Antimonide," *Fiz. Tverdogo Tela.*, *1*, 1015 (1959).

37. Eisen, F.H., and Birchenall, C.E., "Self-Diffusion in Indium Antimonide and Gallium Antimonide," *Acta Metallurgica*, *5*, 265 (1957).

38. Goldstein, B., SYMPOSIUM ON IMPURITIES IN III-V ELEMENTS AND COMPOUNDS, B.M.I., Columbus, Ohio (1960).

39. Goldstein, B., "Diffusion of Cadmium and Zinc in Gallium Arsenide," *Phys. Rev.*, *118*, 1024 (1960).

40. Dunlap, W.C., "Gold as an Acceptor in Germanium," *Phys. Rev.*, *97*, 614 (1955).

41. Maesen, F. van der, and Brenkman, J.A., "The Solid Solubility and the Diffusion of Nickel in Germanium," *Philips Res. Reports*, *9*, 225 (1954).

42. Keyes, R.W., "Morphology of Commercial Silicon Carbide Crystals," in Ref. No. 44, pp. 217-20.

43. Carrol, P., "Resistivity of Granular Silicon Carbide-Impurity and Crystal Structure Difference," in Ref. No. 44, pp. 341-6.

44. O'Connor, J.R. and Smiltens, J., (Editors), SILICON CARBIDE: A HIGH TEMPERATURE SEMICONDUCTOR, Proc. Conf. on Silicon Carbide, Boston, Mass., Pergamon Press, New York (1960).

45. Fetterley, F.G., "Electrical Conduction in SiC," *J. Electrochem. Soc.*, *104*, 322 (1957).

46. Dilion, J.A., Jr., "The Interaction of Oxygen with Silicon Carbide Surfaces," in Ref. No. 44, pp. 225-9.

47. Farnsworth, P.L., "Deformation and Fracture of Silicon Carbide," Sc.D. Thesis, Dept. of Metallurgy, M.I.T., Cambridge, Mass., (1964).

48. Paladino, A.E., Jr., "Aluminum Ion Diffusion in Aluminum Oxide," Sc.D. Thesis, Dept. of Metallurgy, M.I.T., Cambridge, Mass., (1962).

49. Freeman, M.S., "Gold Radioactivity in Neutron-Irradiated Diamond," *J. Chem. Phys.*, *20*, 1040 (1952).

50. Tomonari, T., "On the Manufacturing Method of Carborundum (Part 2): On the Reaction Mechanism of SiC Formation," *J. Electrochem. Soc. Japan*, *24*, 27 (1956).

51. Williams, G.P., Jr. and Slifkin, L., "Diffusion Along Dislocations," *Phys. Rev. Letters*, *1*, 243 (1958).

52. Rothman, S.J., Gray, J., Jr., Hughes, J.P. and Harkness, A.L., "Self-Diffusion in Beta Uranium," *J. Nucl. Materials*, *3*, 72 (1961).

53. Rothman, S.J., Hines, J.J., Gray, J.,Jr., and Harkness, A.L., "Anisotropy of Self-Diffusion in Alpha Uranium," *J. Appl. Phys.*, *33*, 2113 (1962).

54. Williams, G.P., Jr. and Slifkin, L., "Tracer Insolubility and the Anomalous Diffusion of Rare Earths in Silver and Lead," *Acta Met.*, *11*, 319 (1963).

55. Wajda, E., "Grain Boundary Self-Diffusion in Zinc," *Acta Met.*, *2*, 184 (1954).

56. Ballufi, R.W. and Ruoff, A.L., "On Strain-Enhanced Diffusion in Metals. I. Point Defect Models," *J. Appl. Phys.*, *34*, 1634 (1963).

57. Ballufi, R.W. and Ruoff, A.L., "On the Strain-Enhanced Diffusion in Metals. II. Dislocation and Grain-Boundary Short Circuiting Models," *J. Appl. Phys.*, *34*, 1848 (1963).

58. Ballufi, R.W. and Ruoff, A.L., "On Strain-Enhanced Diffusion in Metals. III. Interpretation of Recent Experiments," J. Appl. Phys., 34, 2863 (1963).

59. Melngailis, J. and O'Hara, S., "Diffusion of Vacancies during Quenching of Ge and Silicon," J. Appl. Phys., 33, 2596 (1962).

60. Lazarev, B.G. and Ovcharenko, O.N., "Energy of Formation and of Displacement of Vacancies in Gold and Platinum," Zhur. Ekspt1. i Zeoret. Fiz., 36, 60 (1959).

61. Bacchella, G.A., Germagnoli, E. and Granata, S., "The Kinetics of Quenched-in Lattice Vacancies in Platinum," J. Appl. Phys., 30, 748 (1959).

62. Kelley, K.K., CONTRIBUTIONS TO THE DATA ON THEORETICAL METALLURGY, U.S. Bur. Mines Bull. 584, U.S. Gov't. Printing Office, Washington, D.C. (1960).

63. Lely, J.A., "Darstellung von Einkristallen von Silicium-carbid und Beherrschung von Art und Menge der eingebauten Verunreinigungen," Ber. dent. Keram. Ges., 32, 229-31 (1955).

64. Bartdorf, R.L. and Smits, F.M., "Diffusion of Impurities into Evaporating Silicon," J. Appl. Phys., 30, 259 (1959).

65. Chang, Hung-chi, LeMay, C.Z. and Wallace, L.F., "Use of Silicon Carbide in High Temperature Transistors," pp. 496-507 in Ref. No. 44.

66. Pauling, L., THE NATURE OF THE CHEMICAL BOND, Cornell Univ. Press, Ithaca (1962).

67. Cottrell, T.L., STRENGTH OF CHEMICAL BONDS, Butterworths, London (1954).

68. Hodgman, C.D. (Ed.), HANDBOOK OF CHEMISTRY AND PHYSICS, 36th Edition, Chem. Rubber Pub. Co., Cleveland, Ohio (1954).

69. Rhodes, R.G., IMPERFECTIONS AND ACTIVE CENTRES IN SEMICONDUCTORS, McMillan & Co., New York (1954), pp. 228-235.

70. Champion, F.C., ELECTRONIC PROPERTIES OF DIAMONDS, Butterworths, London, (1963).

71. Swalin, R.A., "Theoretical Calculations of the Enthalpies and Entropies of Diffusion and Vacancy Formation in Semiconductors," J. Phys. Chem. Solids, 18, 290 (1961).

72. Reiss, H. and Fuller, C.S., "Influence of Holes and Electrons on the Solubility of Lithium in Boron-Doped Silicon," J. Metals, 8, 276 (1956).

73. Longini, R.L., Greene, R.F., "Ionization Interaction between Impurities in Semiconductors and Insulators," Phys. Rev., 102, 992 (1956).

74. Fan, H.Y., and Lark-Horovitz, K., REPORT OF BRISTOL CONFERENCE ON DEFECTS IN CRYSTALLINE SOLIDS. The Physical Society, London, p. 232.

75. Blank, Von K., Geist, D. and Seiler, K.," Uber den Einfluss spezieller Gitterstörungen auf die elektrischen Eigenschaften von Germanium," Z. Naturforsch., 9a, 515 (1954).

76. Logan, R.A., "Thermally Induced Acceptors in Germanium," Phys. Rev., 101, 1455 (1956).

77. Swalin, R.A., "Model for Solute Diffusion in Crystals with the Diamond Structure," J. Appl. Phys., 29, 670 (1958).

78. Wertheim, G., "Energy Levels in Electron-Bombarded Silicon,". Phys. Rev., 105, 1730 (1957).

79. Kohn, W., SOLID STATE PHYSICS, 5, p. 262, Academic Press, New York (1957).

80. Smith, R.A., SEMICONDUCTORS, Cambridge Univ. Press, England (1961), pp. 365-81.

81. Herman, F., Glicksman, M. and Parmenter, R.A., in PROGRESS IN SEMICONDUCTORS, 2, 1, Heywood & Co., 1957.

82. Friedel, J., "Electronic Structure of Primary Solid Solutions in Metals," Adv. Phys., 3, 446 (1954); "Deviations from Vegard's Law," Phil. Mag., 46, 514 (1955).

83. Dunlap, W.C., "Diffusion of Impurities in Germanium," Phys. Rev., 94, 1531 (1954).

84. Peterson, N.L. and Ogilvie, R.E., "TheEffect of Radiation on The Rate of Diffusion of Arsenic in Germainum," Trans. AIME, 215, 873 (1959).

85. Baruch, P., Constantin, C., Pfister, J.C. and Saintesprit, Mme. R., "Vacancy Enhanced Diffusion in Silicon; Effects of Irradiation and of Chemical Impurities," Disc. Farad. Soc., No. 31, 76 (1961).

86. Keyes, R.W., "Review of Section IV" in Ref. No. 44, p. 395.

87. Woodbury, H.H., and Ludwig, G.W., "Electron Spin Resonance (EPR) Studies in SiC," *Phys. Rev.*, 124, 1083-9 (1961).

88. Scace, R.I. and Slack, G.A., "The Si-C and Ge-C Phase Diagrams," p. 24 in Ref. No. 44.

89. Drowart, J. and De Maria, G., "Thermodynamic Study of the Binary System Carbon-Silicon using a Mass Spectrometer," p. 16 in Ref. No. 44.

90. Tsertsvadge, A.A., Chkhartishvili, Y.V. and Kachlishvili, Z.S., "Calculation of Ionic and Atomic Contributions to Bonding in SiC Crystals," *Fiz. Tverd. Tela*, 4, pp. 1743-7 (1962).

91. Taylor, A. and Jones, R.M., "The Crystal Structure and Thermal Expansion of Cubic and Hexagonal Silicon Carbide," p. 147 in Ref. No. 44.

92. Fuller, C.S., and Severiens, J.C., "Mobility of Impurity Ions in Germanium and Silicon," *Phys. Rev.*, 96, 21 (1954).

93. Bugai, A.A., Kosenko, V.E. and Miseliuk, E.G., "Diffusion and Solubility of Iron in Germanium," *Soviet Phys., -Tech. Phys.*, 2, 183 (1957); "Diffusion and Solubility of Silver in Germanium," *Soviet Phys., - Tech. Phys.*, 1553 (1957).

94. Wieringen, A. van, and Warmoltz, N., "On the Permeation of Hydrogen and Helium in Single Crystal Silicon and Germanium at Elevated Temperatures," *Physica*, 22, 849 (1956).

95. Boltaks, B.I. and Sozinov, I.I., "The Diffusion of Copper in Silicon," *Soviet Phys., - Tech. Phys.*, 3, 636 (1958).

96. Struthers, J.D., "Solubility and Diffusivity of Gold, Iron and Copper in Silicon," *J. Appl. Phys.*, 28, 516 (1957); 27, 1560 (1956).

97. Carlson, R.O., Hall, R.N. and Pell, E.M., "Sulfur in Silicon," *J. Phys. Chem. Solids*, 8, 81 (1959).

98. Fuller, C.S. and Ditzenberger, J.A., "Diffusion of Donor and Acceptor Elements in Silicon," *J. Appl. Phys.*, 27, 544 (1956).

99. James, H.M. and Lark-Horovitz, Karl, "Localized Electronic States in Bombarded Semiconductors," *Z. Phys. Chem.*, 198, 107 (1951).

100. Taylor, A. and Kagle, B.J., CRYSTALLOGRAPHIC DATA ON METAL AND ALLOY STRUCTURES, Dover Publications, New York, 1963.

101. Elbaum, C., "On Dislocations formed by the Collapse of Vacancy Discs," Phil. Mag., 5, 669 (1960).

102. Badami, D.V., "Graphitization of α-SiC," Nature, 193, 569 (1962).

103. LeClaire, A.D., "Diffusion in Metals," in PROGRESS IN METAL PHYSICS, Vol. 4, Pergamon Press, New York (1953) pp. 265-332.

104. LeClaire, A.D., "Diffusion of Metals in Metals," in ibid, Vol. 5, Pergamon Press, New York (1956), pp. 306-379.

A 1. Mott, N.F. and Gurney, R.W., ELECTRONIC PROCESSES IN IONIC CRYSTALS, Oxford, England, 1957.

A 2. Oishi, Y. and Kingery, W.D., "Self-Diffusion of Oxygen in Single Crystal and Polycrystalline Aluminum Oxide," J. Chem. Phys., 33, 480 (1960).

A 3. Glasstone, S., Laidler, K.J., and Eyring, H., THE THEORY OF RATE PROCESSES, McGraw-Hill, New York, 1941.

A 4. Kingery, W.D., INTRODUCTION TO CERAMICS, John Wiley, New York, 1960.

A 5. Mapother, D., Crooks, H.N. and Maurer, R., "Self-Diffusion of Sodium in Sodium Chloride and Sodium Bromide," J. Chem. Phys., 18, 1231 (1950).

A 6. Kinkkola, K., and Wagner, C., "Measurement on Galvanic Cells Involving Solid Electrolytes," J. Electrochem. Soc., 104, 379 (1957).

A 7. Kingery, W.D., Pappis, J., Doty, M.E. and Hill, D.C., "Oxygen ion Mobility in Cubic $Zr_{0.85}Ca_{0.15}O_{1.85}$," J. Am. Ceram. Soc., 42, 393 (1959).

A 8. Nabarro, F.R.N., "Report on Conference on the Strength of Solids," Physical Society, London, 75 (1948).

A 9. Herring, C, "Diffusional Viscosity of a Polycrystalline Solid," J. Appl. Phys., 21, 437 (1950).

A 10. Coble, R.L., "Sintering in Solids. I. Intermediate and Final State Diffusion Models," J. Appl. Phys., 32, 787 (1961).

A 11. Coble, R.L., "Sintering Crystalline Solids. II. Experimental Test of Diffusion Models in Powder Compacts," ibid, 32, 799 (1961).

A 12. Burke, J.E., "Role of Grain Boundaries in Sintering," J. Am. Ceram. Soc., 40, 80 (1957).

A 13. Kingery, W.D. and Berg, M., "Study of Initial Stages of Sintering Solids by Viscous Flow, Evaporation-Condensation and Self-Diffusion." J. Appl. Phys., 26, 1205 (1955).

A 14. Coble, R.L., "Initial Sintering of Alumina and Hematite," J. Am. Ceram. Soc., 37, 55 (1958).

A 15. Bowen, H.J.M. and Gibbons, D, RADIOACTIVATION ANALYSIS, Oxford at the Clarendon Press, 1963.

A 16. Koch, R.C., ACTIVATION ANALYSIS HANDBOOD, Academic Press, New York, 1960.

A 17. Proceedings of the RADIOACTIVATION ANALYSIS SYMPOSIUM, Vienna, Austria, June (1959); Butterworths, London, 1960.

A 18. Boyd, G.E., "Method of Activation Analysis," Anal. Chem., 21, 335 (1949).

A 19. Leddicotte, G.W. and Reynolds, S.A., "Neutron Activation Analysis," ORNL Report No. CF-56-7-106, May 3, 1957.

A 20. Meinke, W.W., "Trace-Element Sensitivity: Comparison of Activation Analysis with other Methods," Science, 121, 177 (1955).

A 21. Ryskin, G. Ya., "Diffusion Coefficient Measurement by the Radioactivation Analysis and Isotope Dilution Methods," Fiz. Tverdogo Tela, 1, 952-4 (1959).

B 1. Lyon, W.S. and Manning, J.J., "Radioactive Si^{31}," Phys. Rev., 93, 501 (1954).

B 2. Motz, H.T., "Beta-Activity of Si^{31} and the Masses of the Al and Si Isotopes," Phys. Rev., 85, 501 (1952).

B 3. Wapstra, A.H., "The Decay Energies of Pb^{209} and Si^{31}," Arkiv. Fys., 6, 263 (1953).

B 4. Seaborg, G., Perlman, I. and Hollander, J., TABLE OF ISOTOPES, Univ. of Calif., Lawrence Radiation Laboratory (1956).

B 5. U.S. Department of Health, Education and Welfare, RADIOLOGICAL HEALTH HANDBOOK, OTS, U.S. Dept. of Commerce, (1960), PB 121784 R.

APPENDIX A

SUPPLEMENT TO THE GENERAL THEORY

(a) Diffusion Theory

Although a satisfactory theory for diffusion in simple solids has not been derived, there are at least qualitative theories available to provide a rational basis for discussing atomic mobility.

Mott and Gurney(A1) have discussed a simple model for the diffusion of vacancies or interstitials in a simple sodium chloride lattice. If U is the energy barrier for an ion to jump to a neighboring site (vacancy or interstitial) and ν is the frequency of its vibration, the probability p_i per unit time that it moves to a neighboring position is given by

$$p_i \sim \nu \exp(-U/kT) \tag{A.1}$$

where k is the Boltzmann constant and T the absolute temperature. Let us consider two planes separated by a distance λ equal to the distance between adjacent sites, and a concentration gradient dC/dx between the planes. One plane has a concentration of C ions per cc and the other has a concentration of $(C + \lambda\, dC/dx)$. The number of ions contained in a slab of thickness λ will be $\lambda\,(C)$ and $\lambda\,(C + \lambda\, dC/dx)$, respectively. The difference between the latter two times the jump probability p_i, will be the net number of ions migrating across the slab per unit area per unit time.

$$J \sim p_i\, \lambda^2\, \frac{dC}{dx} \tag{A.2}$$

Using Fick's first law for the definition of flux J from equation (I.2)

$$J = D_i \frac{dC}{dx} \qquad (I.2)$$

the ion diffusion coefficient will be

$$\begin{aligned} D_i &= p_i \lambda^2 \\ &= \nu \lambda^2 e^{-U/kT} \end{aligned} \qquad (A.3)$$

Equation (A.3) is the diffusion coefficient of the ions (vacancies or interstitials) diffusing, but only a fraction of the lattice ions are adjacent to a vacancy. From Frenkel's(5) and Schottky's(7) thermodynamic treatment of the formation of interstitials or vacancies in simple lattices, the ratio of the number of vacancies or interstitials, n, to the number of normal lattice sites, N , is given by

$$\frac{n}{N} = e^{-F/2kT} \qquad (A.4)$$

where F is the free energy of formation of a pair of Frenkel or Schottky defects. Therefore, the observed diffusion coeffecient D is equal to D_i times the fraction of defects present.

$$D = \frac{n}{N} D_i = \nu \lambda^2 \exp\left[-\left(\frac{F}{2kT} + \frac{U}{kT}\right)\right] \qquad (A.5)$$

Now, since from thermodynamics F = H + TS the above equation reduces to

$$D = \nu \lambda^2 \exp \frac{S}{2k} \exp\left[-(U + \tfrac{1}{2} H)/kT\right] \qquad (A.6)$$

where H and S are the enthalpy and entropy of formation of vacancies or interstitials, respectively. Equation (A.6) is subject to considerable refinement, but its qualitative features are considered to be correct.

Comparison with the Arrhenius equation (I.4) provides some basis for interpreting the pre-exponential term, D_o, the frequency factor, and the activation energy, Q. The energy required for diffusion is made up of two parts: the energy necessary for the formation of the defects and the energy necessary for the migration of the defects. Diffusion data in alkali halides$^{(8)}$ and in some oxides$^{(A2)}$ overwhelmingly support such a viewpoint.

A second approach to the problem of developing a suitable diffusion theory is found in the application of absolute reaction rate theory to the diffusion process by Glasstone, Laidler and Eyring$^{(A3)}$. (See Kingery$^{(A4)}$ for a brief summary of the theory applied to diffusion).

The diffusion coefficient for defects is given by:

$$D = \lambda^2 \frac{kT}{h} \exp \frac{\Delta S^*}{R} \exp \left(- \frac{\Delta H^*}{RT}\right) \qquad (A.7)$$

where ΔS^* and ΔH^* are the entropy and enthalpy of complex formation. Equation (A.7) is the diffusion coefficient for motion of either vacancies or interstitials. Only the process of passing over an energy barrier was considered in the activation process, and the disordering process was not included.$^{(2)}$ This equation, as does equation (A.6), shows that the diffusion coefficient has an exponential temperature dependence, consistent with the experimentally observed results. Although comparison of experimental results can be made with the fundamental terms in equation (A.7), the atomistic details of the diffusion process cannot be obtained from this analysis. If the activated complex is relatively simple, ΔS^* in equation (A.7) is small and sometimes negative, and if it is complicated in atomic configuration, ΔS^* is large.$^{(A.3)}$

(b) Diffusion coefficient from other Measurements.

1. Nernst-Einstein Relationship(3,4): The relationship between the diffusion coefficient and ionic conductivity has been given in equation (I.5).

$$\frac{D_i}{\sigma} = \frac{t_i kT}{n_i (z_i e)^2} \qquad (I.5)$$

This has been a particularly fruitful relationship in the study of atomic mobility in alkali halides, specially sodium chloride.(A5) The only oxide system which have been successfully studied using this relationship is ZrO_2-CaO solid solution.(A6,A7)

2. Diffusion Coefficients From Creep Data: An important kinetic process requiring diffusional flow of material is the high temperature deformation of oxides under an applied stress. Nabarro(A8) and Herring(A9) model postulates that in a polycrystalline material deformation results from diffusional flow (due to the self-diffusion of the slowest diffusing species) within each grain away from these boundaries where there is a normal compressive force (high chemical potential) toward boundaries having a normal tensile stress.

The Nabarro-Herring theory predicts an effective viscosity for aggregates of quasi-spherical grains with tangential stresses relieved at the boundaries by the relation

$$\eta = \frac{kT\ (GS)^2}{10 D \Omega_o} = \frac{\sigma}{\dot{\epsilon}} \qquad (A.8)$$

from which the diffsuion coefficient is given by

$$D = \frac{\dot{\epsilon} kT \ (GS)^2}{10 \Omega_o \sigma} \qquad (A.9)$$

where,

GS = grain size

η = effective viscosity

k = Boltzmann constant

T = absolute temperature

Ω_o = atomic volume of diffusing vacancy

$\dot{\epsilon}$ = strain rate

Recently, Farnsworth(47) has made creep measurements on polycrystalline silicon carbide from which diffusion coefficients can be calculated and compared to those measured directly.

<u>3. Diffusion Coefficients from Sintering Data</u>: Sintering is another kinetic process which is controlled by bulk diffusion in many systems(A10,A11) toward grain boundaries(A12) acting as vacancy sinks. The models proposed for diffusion sintering contain within them explicit expressions for the bulk diffusion coefficient in terms of geometric and surface tension parameters. The two approaches for studying sintering are by measuring neck growth between two spheres, or a sphere and a plate, or by isothermal shrinkage studies of powder compacts. The two models widely in use are proposed by Kingery and Berg(A13) and Coble.(A10,A14)

(c) Radioactivation Analysis(A15,A16,A17) as Applied to Diffusion.

The technique of radioactivation analysis is based on the formation of radioactive nuclides as a net result of reactions between nuclear particles and the isotopes of the trace elements of interest. There are many nuclear reactions which, in principle, can be utilized for this purpose. However, only some of these reactions are of practical interest. In the great majority of cases, two particle reactions are utilized; one particle being a reactant, and the other being a product. The particles which are available in sufficient intensity for general use as reactants are neutrons, protons, deuterons, tritons, alpha particles, and photons (or electrons). However, irradiation by thermal neutrons in a moderated nuclear reactor is the most convenient and widely used technique for radioactivation.

The rate of formation of a particular activation product, R_F, in a given sample is given by the equation

$$R_F = \phi n\sigma = \frac{\phi m N^o f\sigma}{A} \qquad (A.10)$$

where;

n = the number of target atoms

ϕ = the neutron flux (n/cm^2-sec.)

m = the mass of the trace element in the specimen (gm)

A = the atomic weight of the trace element (gm/gm-atom)

f = the fractional isotopic abundance of the target nuclide

N^o = Avogadro's number (atoms/gm-atom)

σ = the reaction cross-section (cm^2/atom)

The decay rate, D, expressed in atomic disintegrations per second of the product radionuclide in the specimen is given by

$$D = \lambda N \tag{A.11}$$

where N = the number of atoms (radioactive) of the nuclide in the specimen.

λ = the decay constant of the nuclide (sec^{-1})

Therefore, the rate of change of the quantity of the activation product in the sample during the irradiation is given by

$$\frac{dN}{dt} = R_F - D = \frac{\phi m N^o f \sigma}{A} - N\lambda \tag{A.12}$$

which upon integration over the irradiation interval, t, yields

$$N = \frac{\phi m N^o f \sigma}{\lambda A} \quad (1 - e^{-\lambda t}) \tag{A.13}$$

Therefore, the amount of activity, D_t, in units of disintegrations per second, exhibited by the atoms N produced up to a time, t, is given by the expression

$$D_t = \lambda N = \frac{\phi m N^o f \sigma}{A} \quad (1 - e^{-\lambda t}) \tag{A.14}$$

$$= D_\infty \quad (1 - \exp(\frac{-0.693t}{T_{\frac{1}{2}}})) \tag{A.15}$$

where $D_\infty = \frac{\phi m N^o f \sigma}{A}$ = saturation activity, produced by an infinitely long irradiation and $\lambda = 0.693/T_{\frac{1}{2}}$ with $T_{\frac{1}{2}}$ the half-life of the radioisotope.

The use of equation (A.15) for the estimation of trace elements by radioactivation was first suggested by Boyd(A18) whereupon Ledicotte(A19) reported his initial success for a few elements to a much higher sensitivity than was available by the most sensitive physico-chemical method.(A20)

Recently, Ryskin(A21) indicated the possibility of using this method to determine concentrations of a diffusing element in successive sections of a diffusion couple subjected to a suitable stable isotope diffusion. This would free the tracer technique of half-life limitations and would extend the experimental determination of D values up to 10^{-17} cm^2/sec. or smaller. The determination of concentration profile of an annealed specimen can be carried out either by mass spectrometry or by radioactivation analysis depending on the particular system. In combination with gamma scintillation spectrometry radioactivation of diffusion annealed specimens provides a non-destructive and non-interferring (by impurity atoms easily activated under the irradiation conditions) method for the determination of D values even with isotopes of aluminum ($T_{\frac{1}{2}}$ = 2.3 mins.).

APPENDIX B

DETAILED DESCRIPTION OF MATERIALS AND EQUIPMENTS

I. Isotopes.

(a) Silicon: As far as it is known, silicon has seven isotopes of which only three are stable.$^{(B1,B2,B3,B4)}$

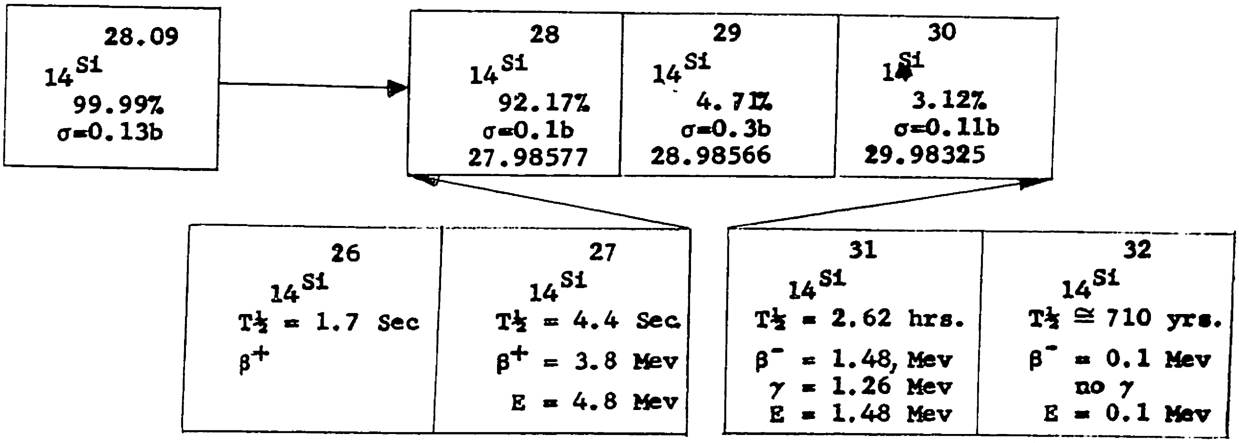

For the application of the radioactivation technique to determine concentration profiles in diffusion annealed samples, the use of a stable isotope (of highest available purity) which can be irradiated to a radioisotope of sufficiently long half-life, is necessary. Since the most conveniently available irradiation in a thermal reactor (n,γ) is chosen, silicon-30 is the desired stable isotope:

$$ {}^{30}_{14}\mathrm{Si} + {}^{1}_{0}\mathrm{n} \rightarrow {}^{31}_{14}\mathrm{Si} + \gamma \qquad \text{(B.1)} $$

Silicon-31 has sufficiently long half-life (2.62 hrs.) for post-irradiation counting purposes. Silicon-32, if available, is the most useful isotope of silicon since it can be used as a direct tracer. The different nuclear reactions for producing silicon isotopes with other associated isotopes are shown below:

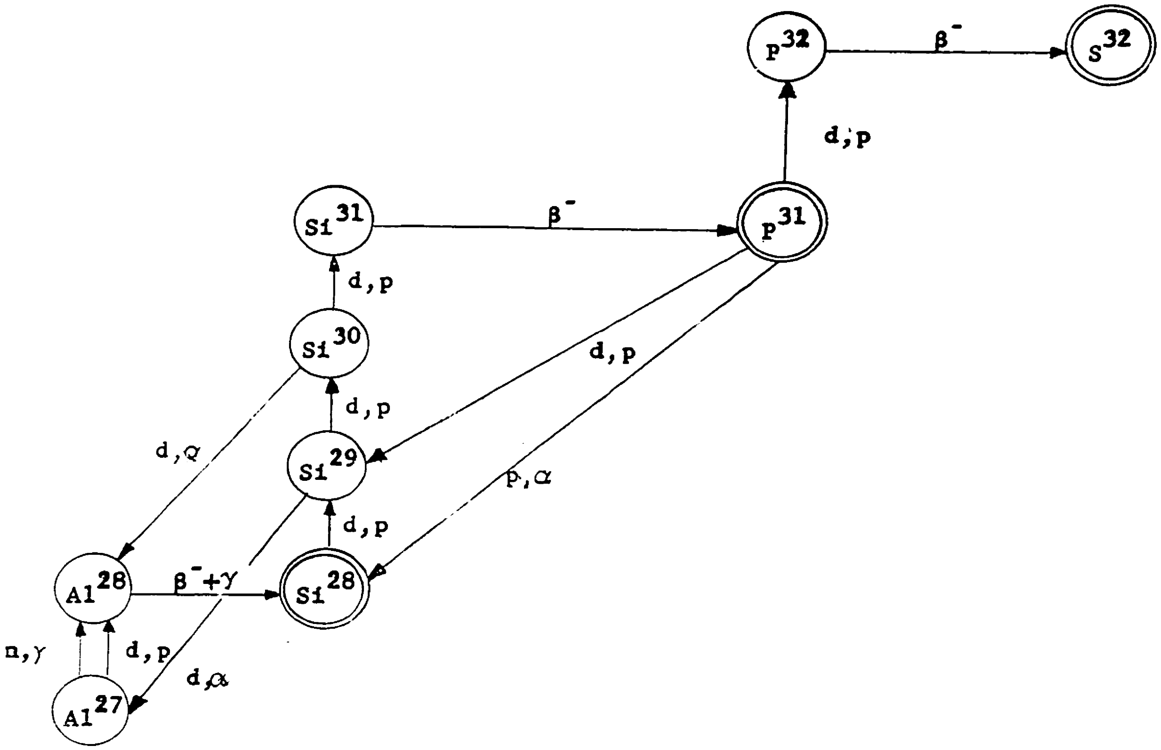

Other important nuclear reactions frequently used for producing silicon-31 are:

a) $${}^{31}_{15}P + {}^{1}_{0}n \text{ (thermal)} \longrightarrow {}^{31}_{14}Si + {}^{1}_{1}P \qquad (B.2)$$

b) $$\left.\begin{aligned} {}^{28}_{14}Si + {}^{2}_{1}d &\longrightarrow {}^{29}_{14}Si + {}^{1}_{1}P \\ {}^{29}_{14}Si + {}^{2}_{1}d &\longrightarrow {}^{30}_{14}Si + {}^{1}_{1}P \\ {}^{30}_{14}Si + {}^{2}_{1}d &\longrightarrow {}^{31}_{14}Si + {}^{1}_{1}P \end{aligned}\right\} \qquad (B.3)$$

c) $${}^{32}_{16}S + {}^{1}_{0}n \longrightarrow {}^{31}_{14}Si + {}^{2}_{2}\alpha \qquad (B.4)$$

Decay product of ${}^{31}_{14}Si$ by β^--emission is ${}^{31}_{15}P$ according to the reaction and scheme:

$${}_{14}Si^{31} \rightarrow {}_{15}P^{31} + \beta^- \qquad (B.5)$$

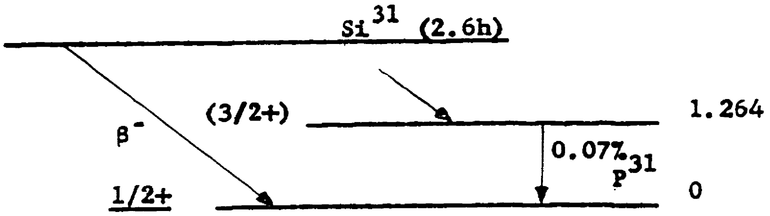

with only 0.07% of the disintegration producing γ-radiation of 1.26 Mev.

Instead of silicon-30 source on the surface, silicon-28 sink was used. The material contained 0.07 ±0.02% silicon-30 and was supplied by the Oak Ridge National Laboratory in the powdered elemental form. A complete analysis of the sample used in given in the Appendix E.

(b) Carbon: Carbon has the following six isotopes with only two stable isotopes:(B4,B5)

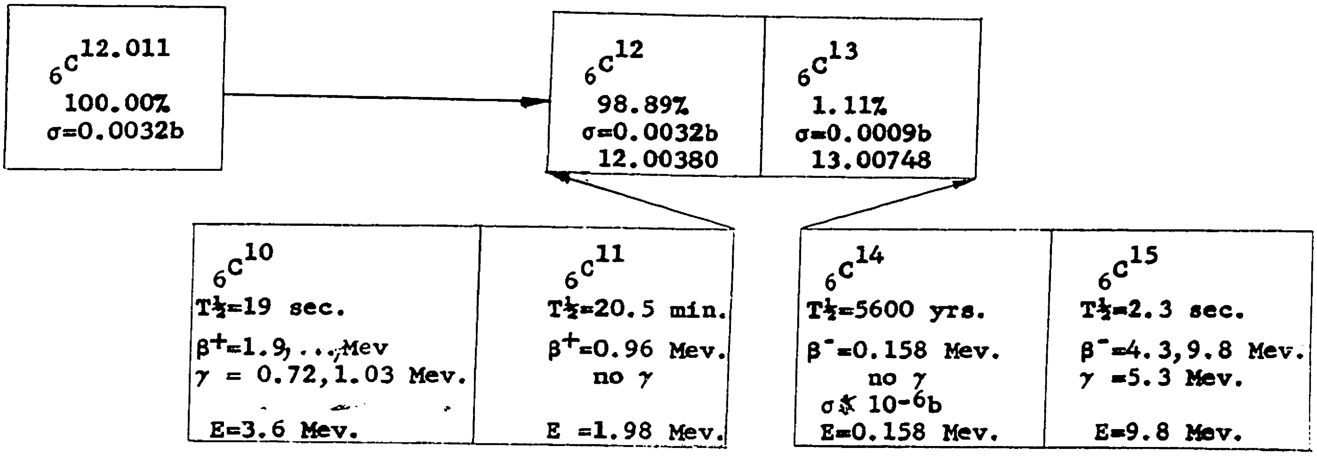

Of these four radioisotopes, only carbon-14 (having a T½=5,600 yrs.) is of any importance for experimental use.

The carbon C-14 tracer used was obtained from the Nuclear-Chicago Corporation, Des Plaines, Illinois, in the amorphous elemental form having a specific activity of 1.07 millicuries/millimole (Sample CFA75, lot 8). An analysis of the material, as provided by the supplier, is given in the Appendix E. Carbon-14 disintegrates to nitrogen-14 according to the following reaction and scheme:

$$ {}_{6}C^{14} \longrightarrow {}_{7}N^{14} + \beta^{-} \qquad (B.6) $$

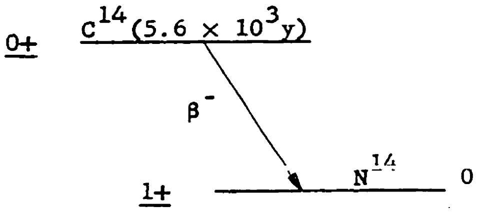

II. Furnace Assembly.

In order to obtain and maintain temperatures above 2000°C in special atmospheres, an induction furnace was employed. The furnace assembly was designed to meet the following objectives:

1) Allow the use of vacuum and purified gases up to about 9/10 of an atmospheric pressure (static).
2) Allow the attainment and maintenance of constant temperatures up to at least 2350°C for extended periods of days.
3) Allow the visual observation of the sample temperature continuously without disturbing the temperature equilibrium.
4) Allow the removal of traces of oxygen from the furnace atmosphere and at the same time withstand the corrosive atmosphere of reactive metallic vapors (such as silicon and titanium) inside the furnace chamber.
5) Allow very rapid heating and cooling of the sample.

The entire furnace design is shown in Figs. B-1 and B-2.

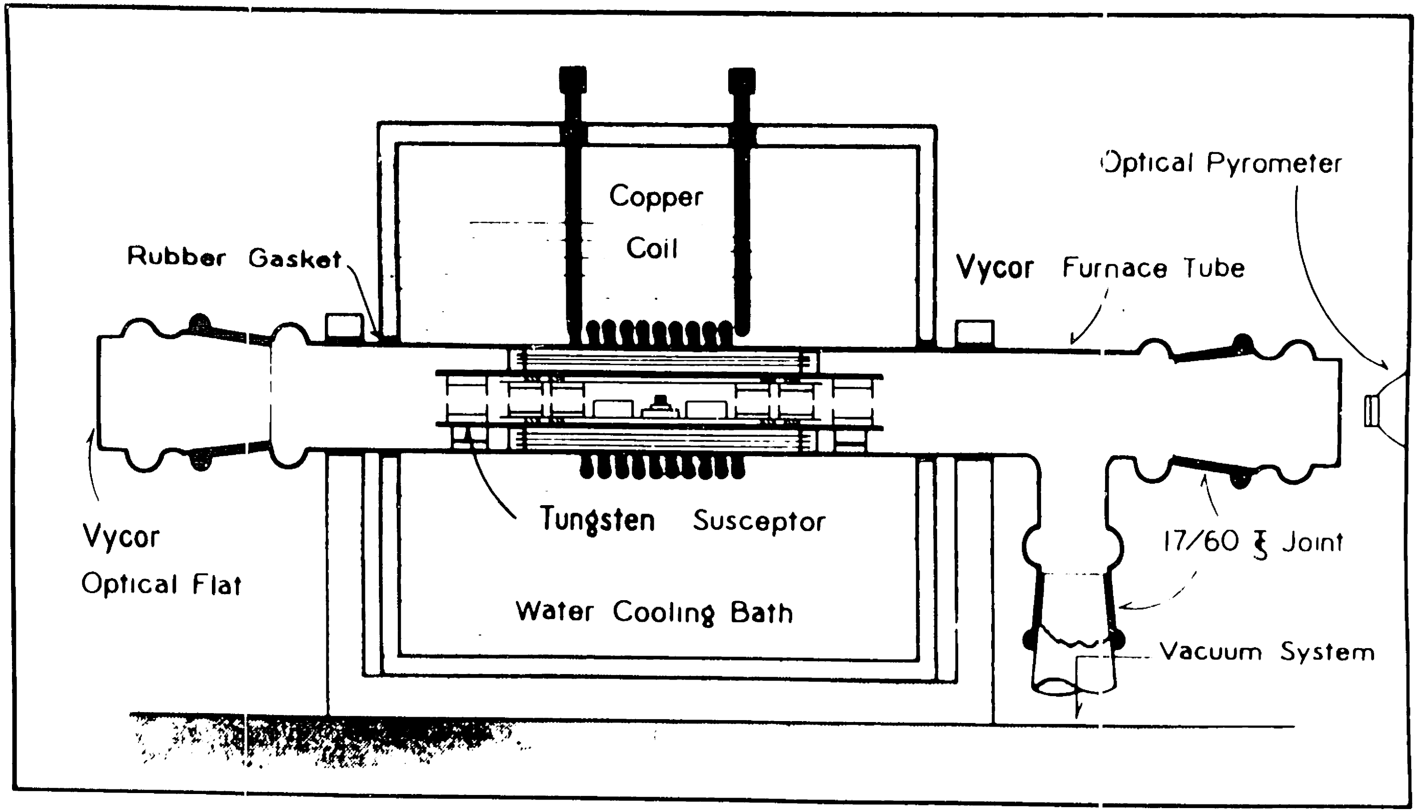

FIG. B-1 FURNACE ASSEMBLY CROSS SECTION

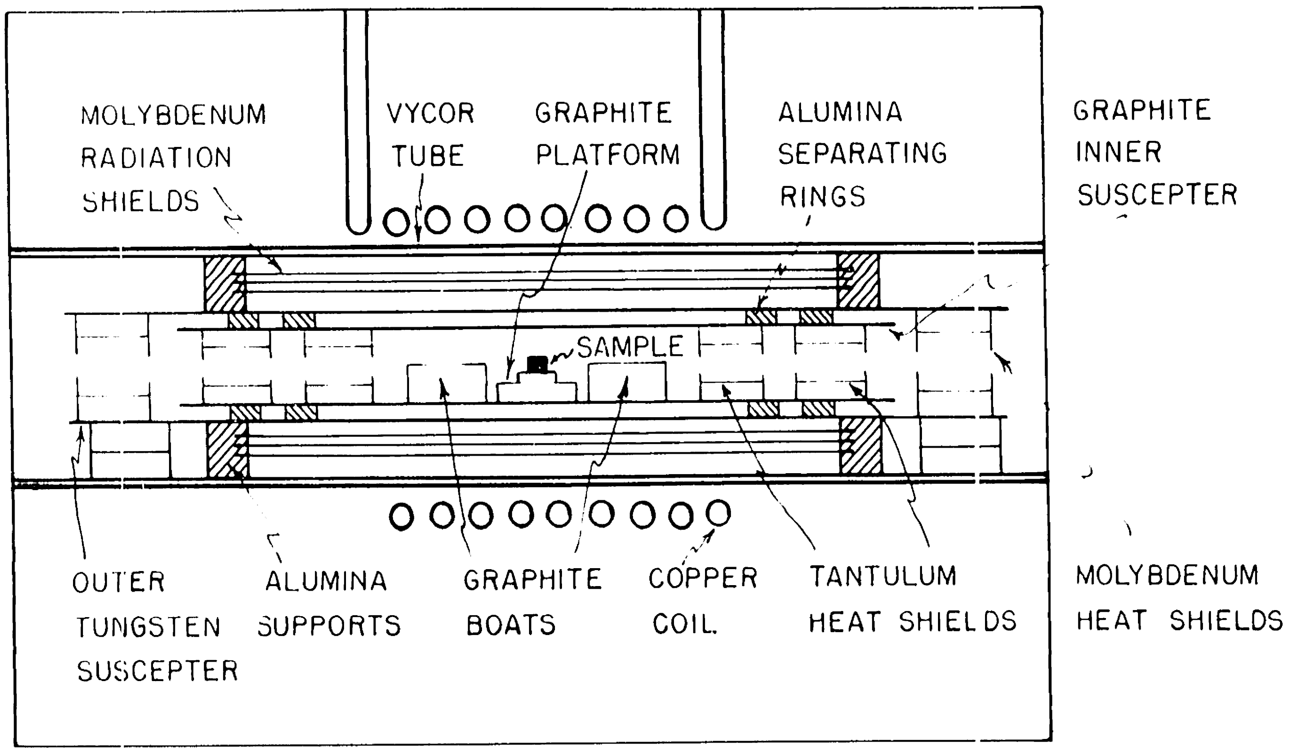

FIG B-2 HEATING ZONE CROSS SECTION

The furnace heating element consists of a pair of concentric cylindrical susceptors. The outer tungsten susceptor is 1.50" I.D. × 12" long, constructed by welding of 0.40" thick tungsten sheet. The inner graphite susceptor is machined out of Grade AUC "National" Graphite rod. It has a dimension of 1.00" I.D. × 0.10" wall × 10" long. They are separated from each other by pure alumina end rings. The susceptors are supported at two ends by molybdenum supports horizontally inside the vycor furnace tube. Three rolled sheets of 0.10" thick molybdenum (separated from each other as also from the susceptors by alumina separators) around the susceptors serve as radial radiation shields. At each end of the dual susceptors, three supported 0.10" thick tantalum and molybdenum disc-shaped fixtures (with a central 5/16" dia. sight hole) serve as end heat-shields. The entire furnace assembly, as shown in Fig. B.1, is enclosed in a water cooled vycor furnace tube of 2.5" in diameter with vycor optical flats sealing both ends by full length standard taper joints. A silicon high vacuum grease is used for sealing the ground glass joints.

Power is supplied to the susceptors by a copper induction coil wound around the furnace tube for about 5 inches and dipped directly into the water bath. The powder unit is a 100 H.P., 50 KW, 10 Kilocycle Tocco motor-generator set type 50 PMG10B manufactured by the Ohio Crankshaft Company. At one end of the furnace tube a Leeds and Northrup Opitcal pyrometer is mounted for sighting directly on the sample.

The two susceptors have been used from efficiency considerations. Metallic susceptors, like that of tungsten, are very efficient in induction heating from room temperature up to about 1800°C; whereas, a graphite susceptor has poor efficiency up to about 1600°C but is very efficient at higher temperatures. When both are employed together the outer tungsten susceptor heats up the inner graphite susceptor very rapidly which then takes over to make the attainment of temperatures above 2000°C possible in about half-an-hour.

A D.P.I Model GW 25 oil diffusion pump in conjunction with a Cenco Megavac forepump is used to evacuate the furnace chamber to about 10^{-6} cm of mercury before the introduction of the desired atmosphere. This low pressure can be obtained since the entire furnace tube is water cooled. Water cooling also permits the use of a vycor furnace tube instead of quartz. A schematic drawing of the vacuum system is shown in Fig. B.3. The entire furnace assembly, including the vauuum and pyrometer systems, is mounted on an angle iron-transite frame which in turn is mounted on shock absorbers to eliminate any vibrations.

Purified gas atmospheres are obtained by evacuating the system with prolonged degassing while the furnace is slowly heated to about 900°C and then adding the desired gas (argon, helium or hydrogen) which is purified with phosphorus pentoxide, activated alumina, and platinized asbestos (5%) catalyst. Last traces of oxygen and nitrogen are removed from the furnace chamber by absorption in spongy -8 + 35 mesh titanium turnings at 850°C placed into two graphite boats on two sides of the graphite sample platform.

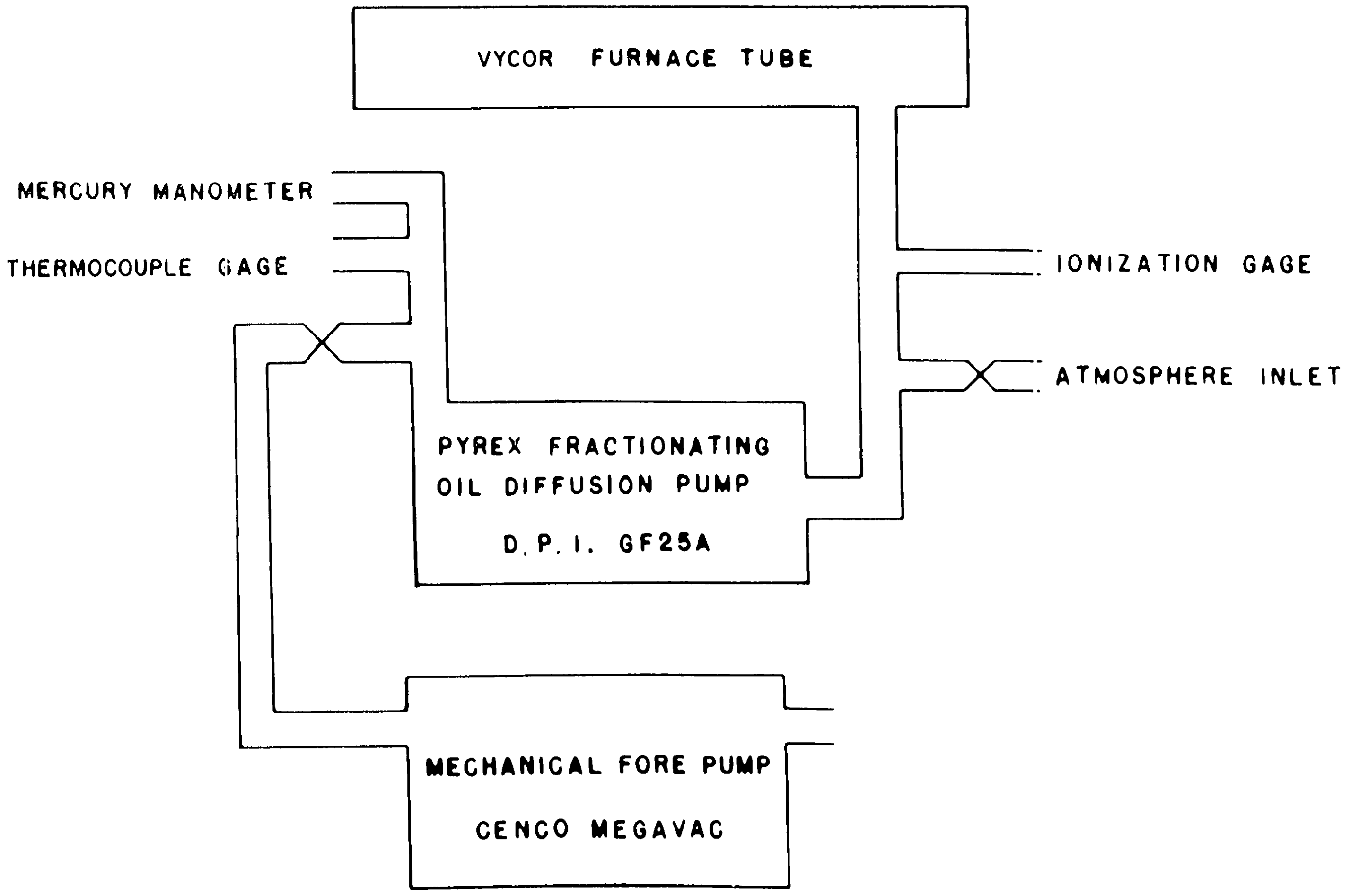

FIG B-3 SCHEMATIC OF VACUUM SYSTEM

In operation, the furnace temperature is controlled manually by controlling the percentage rated field voltage of the motor generator. A mercury arc type voltage stabilizer ("Clark Control") is used alongside. Control circuits are interlocked for safety purposes so that the inductor is automatically shut off if the water supply fails, if the motor or generator bearings overheat, etc. Furnace pressure during the pumpdown is determined in stages by mercury manometer to thermocouple gauge to ionization gauge.

Temperature limitations of the furnace assembly had not been determined although the maximum temperature obtained at about 80% of the rated voltage was 2350°C. The power output at this temperature is approximately 15 kilowatts.

III. Radiation Counting Equipments.

Counting of 0.155 MeV β^--radiation from carbon C-14 was done in a windowless gasflow proportional counter Model PCC-11A manufactured by the Nuclear Measurements Corporation of Indianapolis, Indiana. This is a manual equipment having 2-1/4" diameter chamber working in a P-10 gas (90% Argon + 10% Methane) atmosphere and equipped with a built-in transistorized amplifier-discriminator. This converter is suitable for use in environments where a high and variable background is present, or where extremely low activity levels are being measured. The detection chamber is shielded by an equivalent of 2" of lead; thus giving an almost constant background of about 26 counts/minute. Its efficiency of detection of alpha is about 51%, beta about 55-75%, and for gamma (preferably of low energy) varies inversely as energy around 0.5%. This is from thin samples with a geometry of two pi plus backscattering less self-absorption. Even though it was used for only beta-counting, it is capable of discriminating alpha in the presence of beta or count both.

The signals from the proportional detector is counted by an Atomic Instruments Company Model 1070A scaler and Model 1228 timer assembly. This scaler is equipped with Model 1201B high voltage power supply continuously variable from 400 to 2500 volts by a pair of coarse and fine controls. It has a mechanical four-digit recorder in conjunction with three scaling strips with a scale selector of 10, 40, 100, 400, and 1000. It is equipped with manual, preset time (up to 20 minutes continuously variable) and three preset count selectors: ×10, ×100 and ×1000. Among other controls are the pulse height selector and attenuator. It has a sensitivity of 1 mv minimum with 5 microseconds resolving time. The timer unit has an accuracy of ±1 sec. with the smallest graduation of 1 sec.

Gamma scintillation spectrometry for 1.26 Mev gamma from silicon-31 was done at the Department of Nuclear Chemistry, Massachusetts Institute of Technology. Fig. B.4 presents a block diagram of this counting apparatus. It consists of a gamma ray source, or the sample, and a large 6" × 4" NaI (Tℓ) cylindrical well crystal detector. The fluorescence from the crystal is amplified with three photomultiplier tubes from which the signals are linearly preamplified and amplified to an analog to digital converter. This data is analyzed with a RIDL Model 34-12B 400 channel analyzer and

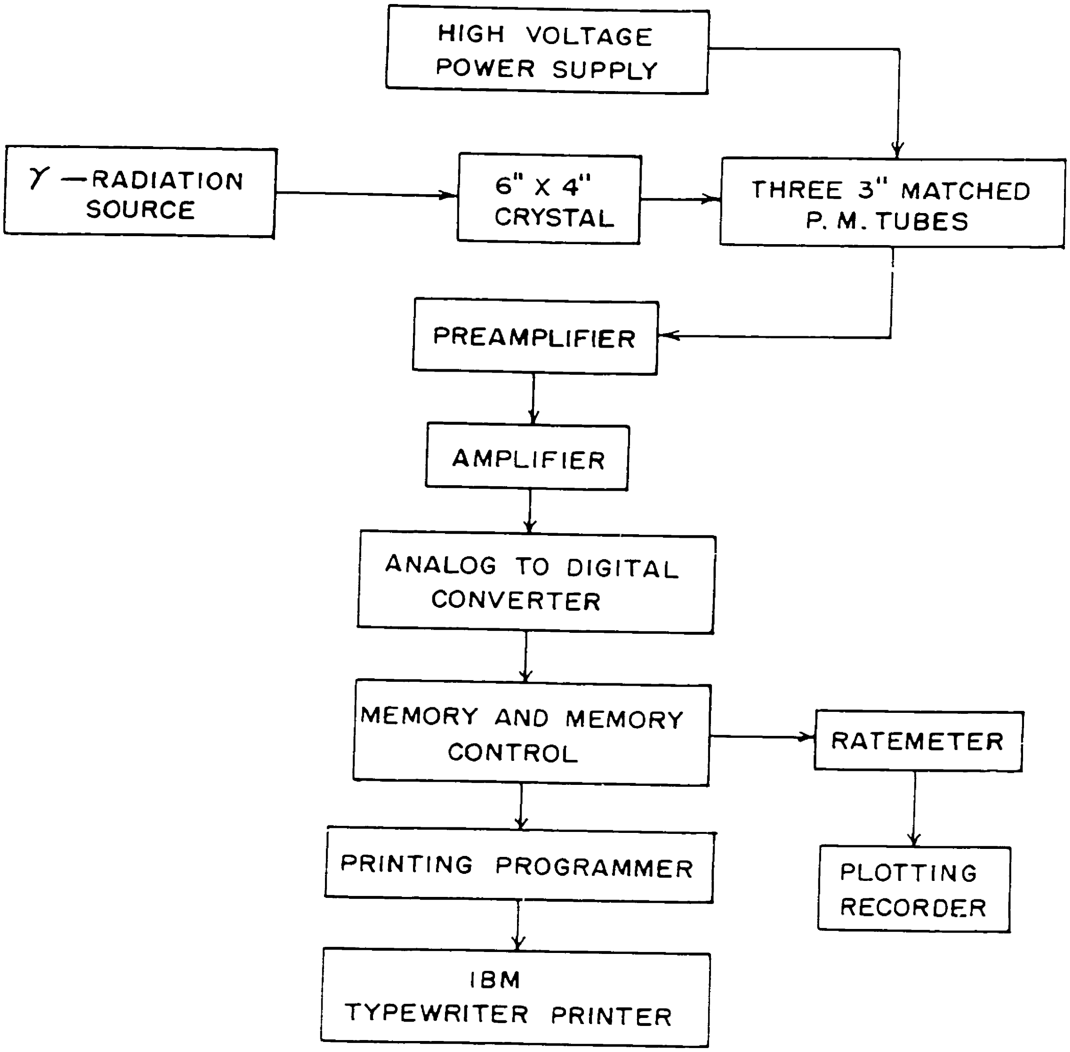

FIG. B-4 BLOCK DIAGRAM OF ELECTRONIC EQUIPMENT EMPLOYED AT THE NUCLEAR CHEMISTRY DEPARTMENT OF M.I.T.

printed out by an IBM typewriter set with a printing programmer. The data can be stored in the analyzer's memory system for a simultaneous comparative display on the analyzer's monitor oscilloscope or for later print out or record on a plotter.

The system is capable of measuring the quanta emitted as a function of the energy of the quanta from 0.1 to 2.8 Mev in 400 channels with an accuracy of ±10 KeV. This allows for measuring a very small energy range of the radiation above a corresponding small range of energies in the background.

APPENDIX C

TABLE C I

DATA FOR CALCULATING CONCENTRATION PROFILES of C-14 in Single Crystal SiC

Sample Number	Section Number	Activity (C/M)	Weight (mg)	Specific Activity (C/M/mg)	Avg. Penetration (microns)	$\bar{X}^2$ (cm^2)
S/N_B/8 (2235°K)	I	308.2	0.11	2,801.8	0.81	0.065×10^{-7}
	II	64.3	0.17	378.2	2.89	0.837×10^{-7}
	III	58.9	0.23	256.2	5.85	3.42×10^{-7}
	IV	26.0	0.15	173.3	8.66	7.50×10^{-7}
	V	21.1	0.17	124.1	11.03	12.18×10^{-7}
	VI	15.7	0.24	65.4	14.06	19.75×10^{-7}
S/N_B/5 (2290°K)	I	282.0	0.14	2,014.3	1.05	0.11×10^{-7}
	II	111.7	0.10	1,117.0	2.86	0.82×10^{-7}
	III	136.6	0.22	620.9	5.28	2.79×10^{-7}
	IV	52.9	0.14	377.8	7.99	6.38×10^{-7}
	V	31.7	0.15	211.3	10.18	10.36×10^{-7}
	VI	21.4	0.26	80.1	13.27	17.61×10^{-7}
	VII	3.2	0.16	20.0	16.45	27.06×10^{-7}

TABLE C I (continued)

DATA FOR CALCULATING CONCENTRATION PROFILES OF C-14 IN SINGLE CRYSTAL SiC

Sample Number	Section Number	Activity (C/M)	Weight (mg)	Specific Activity (C/M/mg)	Avg. Penetration (microns)	$\bar{X}^2$ (cm^2)
S/N$_B$/14/A (2311°K)	I	1,270.2	0.18	7,056.7	1.16	0.134×10^{-7}
	II	71.3	0.15	475.3	3.29	1.08×10^{-7}
	III	29.9	0.20	149.5	5.55	3.12×10^{-7}
	IV	29.2	0.19	153.7	8.08	6.52×10^{-7}
	V	12.6	0.19	66.3	10.54	11.10×10^{-7}
	VI	9.2	0.18	51.1	12.93	16.73×10^{-7}
	VII	6.2	0.18	34.4	15.25	23.20×10^{-7}
S/N$_B$/12 (2333°K)	I	820.3	0.07	11,718.6	0.545	0.297×10^{-8}
	II	44.0	0.26	169.2	3.115	0.97×10^{-7}
	III	11.5	0.25	46.0	7.09	5.03×10^{-7}
	IV	1.0	0.39	2.6	12.08	14.57×10^{-7}
S/N$_B$/7 (2210°K)	I	678.2	0.10	6,782.0	0.75	0.056×10^{-7}
	II	33.0	0.12	275.0	2.42	0.58×10^{-7}
	III	25.6	0.16	160.0	5.54	3.07×10^{-7}
	IV	17.5	0.14	125.0	7.81	6.10×10^{-7}
	V	14.6	0.16	91.3	10.08	10.16×10^{-7}
	VI	10.6	0.18	58.9	12.65	16.00×10^{-7}
	VII	6.0	0.22	27.3	15.69	24.62×10^{-7}

TABLE C I (continued)

DATA FOR CALCULATING CONCENTRATION PROFILES OF C-14 IN SINGLE CRYSTAL SiC

Sample Number	Section Number	Activity (C/M)	Weight (mg)	Specific Activity (C/M/mg)	Avg. Penetration (microns)	$\bar{X}^2$ (cm²)
$S/N_B/10$	I	122.8	0.11	1,116.4	0.82	0.067×10^{-7}
(2126°K)	II	40.9	0.13	314.6	2.60	0.676×10^{-7}
	III	25.2	0.12	210.0	4.45	1.98×10^{-7}
	IV	28.1	0.13	216.2	6.31	3.98×10^{-7}
	V	18.9	0.15	126.0	8.39	7.04×10^{-7}
	VI	23.9	0.21	113.8	11.06	12.23×10^{-7}
	VII	16.2	0.26	62.3	14.55	21.17×10^{-7}
$S/N_B/14/B$	I	3,625.5	0.12	30,212.5	0.79	0.062×10^{-7}
(2165°K)	II	158.4	0.13	1,218.5	2.45	0.60×10^{-7}
	III	73.9	0.16	461.9	4.37	1.91×10^{-7}
	IV	62.5	0.18	347.2	6.52	4.38×10^{-7}
	V	40.3	0.20	201.5	9.14	8.35×10^{-7}
	VI	21.3	0.23	92.6	11.99	14.38×10^{-7}
$S/N_B/2/A$	I	687.7	0.27	2,547.0	2.10	0.44×10^{-7}
(2180°K)	II	92.0	0.16	575.0	5.46	2.98×10^{-7}
	III	26.7	0.14	190.7	7.80	6.08×10^{-7}
	IV	7.3	0.27	27.0	11.01	12.10×10^{-7}

TABLE C I (continued)

DATA FOR CALCULATING CONCENTRATION PROFILES OF C-14 IN SINGLE CRYSTAL SiC

Sample Number	Section Number	Activity (C/M)	Weight (mg)	Specific Activity (C/M/mg)	Avg. Penetration (microns)	$\bar{x}^2$ (cm^2)
$S/N_B/2/B$ (2361°K)	I	1,782.5	0.25	7,130.0	2.03	0.412×10^{-7}
	II	255.8	0.29	882.1	6.40	4.10×10^{-7}
	III	108.4	0.20	542.0	10.37	10.75×10^{-7}
	IV	34.3	0.34	100.9	14.75	21.76×10^{-7}
	V	2.9	0.17	17.1	18.88	35.65×10^{-7}
$S/N_G/5/B$ (2361°K)	I	73.8	0.12	615.0	0.78	0.061×10^{-7}
	II	73.1	0.23	317.8	3.04	0.924×10^{-7}
	III	49.8	0.25	199.2	6.13	3.76×10^{-7}
	IV	19.3	0.25	77.2	9.35	8.74×10^{-7}
	V	6.3	0.26	24.2	12.64	15.98×10^{-7}
$S/N_G/5/E$ (2336°K)	I	109.9	0.14	785.0	1.58	0.25×10^{-7}
	II	43.7	0.18	242.8	3.57	1.27×10^{-7}
	III	39.6	0.20	198.0	6.52	4.25×10^{-7}
	IV	24.8	0.17	145.9	9.40	8.84×10^{-7}
	V	16.8	0.15	112.0	11.88	14.11×10^{-7}
	VI	14.3	0.21	68.1	14.68	21.55×10^{-7}
	VII	10.5	0.25	42.0	18.25	33.31×10^{-7}

TABLE C I (continued)

DATA FOR CALCULATING CONCENTRATION PROFILES OF C-14 IN SINGLE CRYSTAL SiC

Sample Number	Section Number	Activity (C/M)	Weight (mg)	Specific Activity (C/M/mg)	Avg. Penetration (microns)	$\bar{X}^2$ (cm²)
$S/N_G/5/A$ (2311°K)	I	875.5	0.20	4,377.5	1.26	0.157×10^{-7}
	II	88.9	0.24	370.4	4.02	1.62×10^{-7}
	III	25.8	0.23	112.1	6.98	4.87×10^{-7}
	IV	7.9	0.18	43.8	9.55	9.12×10^{-7}
	V	4.1	0.29	10.6	12.50	15.62×10^{-7}
$S/N_G/5/F$ (2280°K)	I	190.8	0.16	1,192.5	1.25	0.156×10^{-7}
	II	36.5	0.21	173.8	4.15	1.72×10^{-7}
	III	28.4	0.22	129.1	7.52	5.66×10^{-7}
	IV	16.2	0.19	85.3	10.74	11.53×10^{-7}
	V	10.4	0.20	52.0	13.79	19.03×10^{-7}
	VI	6.5	0.22	29.5	17.08	29.17×10^{-7}
$S/N_G/5/C$ (2225°K)	I	20.70	0.11	188.2	0.82	0.067×10^{-7}
	II	13.13	0.13	101.0	2.62	0.686×10^{-7}
	III	9.82	0.13	75.5	4.57	2.088×10^{-7}
	IV	6.86	0.14	49.0	6.60	4.356×10^{-7}
	V	3.65	0.14	26.1	8.70	7.569×10^{-7}
	VI	2.05	0.15	13.7	10.87	11.816×10^{-7}

TABLE C I (continued)

DATA FOR CALCULATING CONCENTRATION PROFILES OF C-14 IN SINGLE CRYSTAL SiC

Sample Number	Section Number	Activity (C/M)	Weight (mg)	Specific Activity (C/M/mg)	Avg. Penetration (microns)	$\bar{X}^2$ (cm^2)
$S/N_C/4/B$ (2361°K)	I	2,485.1	0.71	3,500.1	2.75	0.756×10^{-7}
	II	367.2	0.28	1,311.4	6.59	4.34×10^{-7}
	III	249.3	0.38	656.1	9.15	8.37×10^{-7}
	IV	177.8	0.52	341.9	12.65	16.00×10^{-7}
	V	52.4	0.44	119.1	16.38	26.83×10^{-7}
$S/N_C/4/C$ (2280°K)	I	223.2	0.28	797.1	1.10	0.121×10^{-7}
	II	76.2	0.32	238.1	3.47	1.20×10^{-7}
	III	88.2	0.45	196.0	6.52	4.25×10^{-7}
	IV	49.4	0.38	130.0	9.80	9.60×10^{-7}
	V	42.6	0.58	73.4	13.59	18.47×10^{-7}
	VI	20.5	0.64	32.0	18.41	33.89×10^{-7}
$S/N_C/4/A$ (2210°K)	I	252.8	0.29	871.7	1.08	0.116×10^{-7}
	II	19.3	0.21	92.2	2.93	0.856×10^{-7}
	III	12.0	0.25	48.0	4.64	2.153×10^{-7}
	IV	3.3	0.21	15.7	6.34	4.019×10^{-7}

TABLE C II

DATA FOR CALCULATING CONCENTRATION PROFILES of C-14 in Polycrystalline SiC

Sample Number	Section Number	Activity (C/M)	Weight (mg)	Specific Activity (C/M/mg)	Avg. Penetration (microns)	$\bar{x}^2$ (cm^2)
$P/A_B/1/B$	I	4,284.6	0.25	1.71×10^4	1.30	0.017×10^{-6}
(2200°K)	II	688.2	0.61	1.13×10^3	5.77	0.333×10^{-6}
	III	322.9	0.36	8.97×10^2	10.80	1.166×10^{-6}
	IV	308.9	0.44	7.02×10^2	14.95	2.235×10^{-6}
	V	241.2	0.51	4.73×10^2	19.89	3.956×10^{-6}
	VI	112.1	0.38	2.95×10^2	24.51	6.007×10^{-6}
	VII	88.2	0.42	2.10×10^2	28.67	8.22×10^{-6}
	VIII	119.5	0.72	1.66×10^2	34.59	11.96×10^{-6}
$P/A_B/2/B$	I	2,276.4	0.42	5.42×10^3	2.19	0.048×10^{-6}
(2200°K)	II	346.6	0.48	7.22×10^2	6.88	0.47×10^{-6}
	III	269.6	0.57	4.73×10^2	12.36	1.53×10^{-6}
	IV	145.9	0.51	2.86×10^2	18.00	3.24×10^{-6}
	V	109.4	0.64	1.71×10^2	24.00	5.76×10^{-6}
	VI	69.8	0.45	1.55×10^2	29.69	8.81×10^{-6}
	VII	90.2	0.71	1.27×10^2	35.74	12.77×10^{-6}
	VIII	72.6	0.84	8.64×10^1	43.83	19.21×10^{-6}

TABLE C II

DATA FOR CALCULATING CONCENTRATION PROFILES OF C-14 IN POLYCRYSTALLINE SiC (continued)

Sample Number	Section Number	Activity (C/M)	Weight (mg)	Specific Activity (C/M/mg)	Avg. Penetration (microns)	$\bar{X}^2$ (cm^2)
P/A_B/1/A (2250°K)	I	6,708.2	0.52	1.29×10^4	2.63	0.069×10^{-6}
	II	1,331.0	0.55	2.42×10^3	8.06	0.650×10^{-6}
	III	1,232.2	0.61	2.02×10^3	13.93	1.94×10^{-6}
	IV	744.0	0.48	1.55×10^3	19.45	3.78×10^{-6}
	V	672.6	0.57	1.18×10^3	24.77	6.14×10^{-6}
	VI	481.8	0.73	6.60×10^2	31.36	9.83×10^{-6}
	VII	236.3	0.63	3.75×10^2	38.25	14.63×10^{-6}
	VIII	151.4	0.58	2.61×10^2	44.38	19.70×10^{-6}
	IX	136.5	0.78	1.75×10^2	51.27	26.29×10^{-6}
P/A_B/2/A (2250°K)	I	4,048.0	0.46	8.8×10^3	2.39	0.057×10^{-6}
	II	790.5	0.51	1.55×10^3	7.41	0.55×10^{-6}
	III	652.8	0.48	1.36×10^3	12.53	1.57×10^{-6}
	IV	550.0	0.55	1.00×10^3	17.87	3.19×10^{-6}
	V	360.5	0.50	7.21×10^2	23.31	5.43×10^{-6}
	VI	195.6	0.46	4.25×10^2	28.29	8.00×10^{-6}
	VII	161.8	0.68	2.38×10^2	34.19	11.69×10^{-6}
	VIII	75.1	0.62	1.21×10^2	40.93	16.75×10^{-6}
	IX	56.8	0.71	8.0×10^1	47.82	22.87×10^{-6}

TABLE C II

DATA FOR CALCULATING CONCENTRATION PROFILES OF C-14 IN POLYCRYSTALLINE SiC
(continued)

Sample Number	Section Number	Activity (C/M)	Weight (gm)	Specific Activity (C/M/gm)	Avg. Penetration (microns)	$\bar{X}^2$ (cm^2)
$P/A_B/1/C$ (2336°K)	I	2,560.8	0.44	5.82×10^3	2.36	0.06×10^{-6}
	II	268.6	0.41	6.55×10^2	6.91	0.48×10^{-6}
	III	254.3	0.49	5.19×10^2	11.73	1.38×10^{-6}
	IV	208.0	0.52	4.00×10^2	17.15	2.94×10^{-6}
	V	136.7	0.68	2.01×10^2	23.58	5.56×10^{-6}
	VI	77.5	0.62	1.25×10^2	30.55	9.33×10^{-6}
	VII	23.1	0.70	3.30×10^1	37.63	14.16×10^{-6}
	VIII	12.1	1.12	1.08×10^1	46.40	21.51×10^{-6}
$P/A_B/2/C$ (2336°K)	I	2,313.6	0.48	4.82×10^3	2.59	0.067×10^{-6}
	II	548.6	0.72	7.62×10^2		

TABLE D I

SECTIONING DATA FOR SAMPLE S/N_B/2/A

Sample Weight Before Sectioning = 62.82 mg.

Section Number	Wt. of 4-8 μ Amplex Diamond Powder Used (mg.)	Duration of Hand Lapping (mins.)	Sample weight After Lapping (mg.)	(mg.) Weight of the Section Removed	Thickness of the Section (μ)	Avg. Distance of Section from Surface (μ)
I	5.00	10 + 30 + 5[(a)]	62.55	0.27	4.21	2.10
II	5.00	8 + 25 + 5[(a)]	62.39	0.16	2.49	5.46
III	5.00	7 + 25 + 5[(a)]	62.25	0.14	2.19	7.80
IV	5.00	10 + 35 + 5[(a)]	61.98	0.27	4.21	11.01

(a) The first number denotes the duration of lapping with light finger pressure on the plunger, the second number denotes the duration of lapping without any finger pressure, and the third number denotes the duration of blanc lapping with the guard ring only (i.e., with the plunger containing the mounted sample removed). They were also done in this order.

TABLE D II

COUNTING DATA FOR SAMPLE $S/N_B/2/A$

Section Number	Activity of Section Counts/time = rate (Counts / Minute)	Background (For the Section) Counts/time = rate (Counts / Minute)	Activity of Cleaner Counts/time = rate (Counts / Minute)	Background (For the Cleaner) Counts/time = rate (Counts / Minute)	Net Activity		
					Section (C/M)	Cleaner (C/M)	Total (C/M)
I	6,276/ 10 = 627.6	2,555/60 = 42.6	i) 15,035/120 = 125.3 ii) 7,517/120 = 62.6	2,555/60 = 42.6	585.0	82.7 20.0	687.7
II	3,587/30 = 119.6	2,522/60 = 42.0	i) 5,545/105 = 52.8 ii) 5,151/110 = 46.8	2,555/60 = 42.6 2,555/60 = 42.6	77.6	10.2 4.2	92.0
III	4,038/60 = 67.3	4,263/100 = 42.6	4,910/110 = 44.6	2,555/60 = 42.6	24.7	2.0	26.7
IV	11,549/240 = 48.1	7,342/180 = 40.8	3,410/80 = 42.6	2,555/60 = 42.6	7.3	0	7.3

TABLE D III

SECTIONING DATA FOR SAMPLE $S/N_B/2/B$

Sample Weight before Sectioning = 57.92 mg.

Section Number	Wt. of 4-8 μ Amplex Diamond Powder Used (mg.)	Duration of Hand Lapping (mins)	Sample weight After Lapping (mg)	(mg.) Weight of the Section Removed	(μ) Thickness of the Section	(μ) Avg. Distance of Section from Surface
I	3.00	5 + 5 + 5(a)	57.67	0.25	4.05	2.03
II	3.00	5 + 5 + 5(a)	57.38	0.29	4.70	6.40
III	3.00	3 + 5 + 5(a)	57.18	0.20	3.24	10.37
IV	3.00	6 + 5 + 5(a)	56.84	0.34	5.51	14.75
V	3.00	2 + 5 + 5(a)	56.67	0.17	2.76	18.88

(a) The first number denotes the duration of lapping with light finger pressure on the plunger, the second number denotes the duration of lapping without any finger pressure, and the third number denotes the duration of blanc lapping with the guard ring only (i.e., with the plunger containing the mounted sample removed). They were also done in this order.

TABLE D IV

COUNTING DATA FOR SAMPLE $S/N_B/2/B$

Section Number	Activity of Section Counts/time = rate (Counts / Minute)	Background (For the Section) Counts/time = rate (Counts / Minute)	Activity of Cleaner Counts/time = rate (Counts / Minute)	Background (For the Cleaner) Counts/time = rate (Counts / Minute)	Net Activity		
					Section (C/M)	Cleaner (C/M)	Total (C/M)
I	49,959/30 = 1,665.3	1,965/60 = 32.8	3,657/20 = 182.9	1,645/50 = 32.9	1,632.5	150.0	1782.5
II	16,498/60 = 275.0	1,968/60 = 32.8	2,095/45 = 46.5	1,645/50 = 32.9	242.2	13.6	255.8
III	8,272/60 = 137.9	1,968/60 = 32.8	2,172/60 = 36.2	1,645/50 = 32.9	105.1	3.3	108.4
IV	3,564/60 = 59.4	2,428/90 = 27.0	2,582/70 = 36.9	3,147/90 = 35.0	32.4	1.9	34.3
V	5,981/200 = 29.9	2,428/90 = 27.0	3,504/100 = 35.0	3,147/90 = 35.0	2.9	0.0	2.9

TABLE D V

SECTIONING DATA FOR SAMPLE S/N_B/5

Sample Weight before Sectioning = 66.86 mg.

Section Number	Wt. of 4-8 μ Amplex Diamond Powder Used (mg.)	Duration of Hand Lapping (mins.)	Sample weight After Lapping (mg.)	(mg.) Weight of the Section Removed	(μ) Thickness of the Section	(μ) Avg. Distance of Section from Surface
I	4.00	0 + 15 + 8[a]	66.72	0.14	2.11	1.05
II	4.00	0 + 15 + 5[a]	66.62	0.10	1.51	2.86
III	4.00	3 + 12 + 5[a]	66.40	0.22	3.32	5.28
IV	4.00	1 + 14 + 5[a]	66.26	0.14	2.11	7.99
V	4.00	3 + 12 + 5[a]	66.11	0.15	2.26	10.18
VI	4.00	5 + 10 + 5[a]	65.85	0.26	3.93	13.27
VII	4.00	3 + 12 + 5[a]	65.69	0.11	2.42	16.45

(a) The first number denotes the duration of lapping with light finger pressure on the plunger, the second number denotes the duration of lapping without any finger pressure, and the third number denotes the duration of blanc lapping with the guard ring only (i.e., with the plunger containing the mounted sample removed). They were also done in this order.

TABLE D VI

COUNTING DATA FOR SAMPLE S/N_B/5

Section Number	Activity of Section Counts/time = rate (Counts / Minute)	Background (For the Section) Counts/time = rate (Counts / Minute)	Activity of Cleaner Counts/time = rate (Counts / Minute)	Background (For the Cleaner) Counts/time = rate (Counts / Minute)	Net Activity		
					Section (C/M)	Cleaner (C/M)	Total (C/M)
I	3,000/10 = 300.0	1,117/30 = 37.2	3,392/60 = 56.5	1,493x40 = 37.3	262.8	19.2	282.0
II	3,997/30 = 133.2	1,539/45 = 34.2	i) 2,732/60 = 45.5 ii) 2,065/60 = 34.4	2,018/60 = 33.6 2,018/60 = 33.6	99.0	11.9 0.8	111.7
III	9,893/60 = 164.9	2,102/60 = 35.0	3,619/90 = 40.2	3,018/90 = 33.5	129.9	6.7	136.6
IV	7,613/90 = 84.6	3,298/90 = 36.6	4,793/120 = 39.9	4.202/120 = 35.0	48.0	4.9	52.9
V	9,007x150 = 60.0	6,321/180 = 35.1	6,125/150 = 40.8	6,116/180 = 34.0	24.9	6.8	31.7
VI	10,059/180 = 55.9	6,212/180 = 34.5	6,216/180 = 34.5	4,489/130 = 34.5	21.4	0.0	21.4
VII	8,747/240 = 36.4	7,963/240 = 33.2	3,409/100 = 34.1	3,414/100 = 34.1	3.2	0.0	3.2

TABLE D VII

SECTIONING DATA FOR SAMPLE $S/N_B/7$

Sample Weight before Sectioning = 64.79 mg

Section Number	Wt. of 4-8 μ Amplex Diamond Powder Used (mg)	Duration of Hand Lapping (mins)	Sample weight After Lapping (mg)	(mg.) Weight of the Section Removed	(μ) Thickness of the Section	(μ) Avg. Distance of Section from Surface
I	4.00	2 + 4 + 5(a)	64.69	0.10	1.51	0.75
II	4.00	2 + 4 + 5(a)	64.57	0.12	1.82	2.42
III	4.00	3 + 5 + 5(a)	64.41	0.16	2.42	5.54
IV	4.00	2 + 5 + 5(a)	64.27	0.14	2.12	7.81
V	4.00	3 + 5 + 5(a)	64.11	0.16	2.42	10.08
VI	4.00	3 + 5 + 5(a)	63.93	0.18	2.73	12.65
VII	4.00	5 + 5 + 5(a)	63.71	0.22	3.33	15.69

(a) The first number denotes the duration of lapping with light finger pressure on the plunger, the second number denotes the duration of lapping without any finger pressure, and the third number denotes the duration of blanc lapping with the guard ring only (i.e., with the plunger containing the mounted sample removed). They were also done in this order.

TABLE D VIII

COUNTING DATA FOR SAMPLE $S/N_B/7$

Section Number	Activity of Section Counts/time = rate (Counts / Minute)	Background (For the Section) Counts/time = rate (Counts / Minute)	Activity of Cleaner Counts/time = rate (Counts / Minute)	Background (For the Cleaner) Counts/time = rate (Counts / Minute)	Net Activity		
					Section (C/M)	Cleaner (C/M)	Total (C/M)
I	19,053/30 = 635.1	2,882/100 = 28.8	6,098/60 = 101.6	3.565/120 = 29.7	606.3	71.9	678.2
II	6,832/120 = 56.9	2,882/100 = 28.8	3,464/100 = 34.6	3,565/120 = 29.7	28.1	4.9	33.0
III	12,486/240 = 52.0	8,526/300 = 28.4	5,612/180 = 31.2	10,524/300 = 29.2	23.6	2.0	25.6
IV	11,474/250 = 45.9	8,526/300 = 28.4	-------	-------	17.5	—	17.5
V	10,322/240 = 43.0	8,526/300 = 28.4	-------	-------	14.6	—	14.6
VI	11,714/300 = 39.0	8,526/300 = 28.4	-------	-------	10.6	—	10.6
VII	12,377/360 = 34.4	8,526/300 = 28.4	-------	-------	6.0	—	6.0

TABLE D IX

SECTIONING DATA FOR SAMPLE $S/N_B/8$

Sample Weight before Sectioning = 62.11 mg

Section Number	Wt. of 4-8 μ Amplex Diamond Powder Used (mg.)	Duration of Hand Lapping (mins.)	Sample weight After Lapping (mg.)	(mg.) Weight of the Section Removed	(μ) Thickness of the Section	(μ) Avg. Distance of Section from Surface
I	3.00	0 + 15 + 5 (a)	62.00	0.11	1.63	0.81
II	3.00	2 + 13 + 5 (a)	61.83	0.17	2.52	2.89
III	3.00	2 + 13 + 5 (a)	61.60	0.23	3.40	5.85
IV	3.00	2 + 13 + 5 (a)	61.45	0.15	2.22	8.66
V	3.00	2 + 13 + 5 (a)	61.28	0.17	2.52	11.03
VI	3.00	2 + 13 + 5 (a)	61.04	0.24	3.55	14.06

(a) The first number denotes the duration of lapping with light finger pressure on the plunger, the second number denotes the duration of lapping without any finger pressure, and the third number denotes the duration of blanc lapping with the guard ring only (i.e., with the plunger containing the mounted sample removed). They were also done in this order.

TABLE D X

COUNTING DATA FOR SAMPLE $S/N_B/8$

Section Number	Activity of Section Counts/time = rate (Counts / Minute)	Background (For the Section) Counts/time = rate (Counts / Minute)	Activity of Cleaner Counts/time = rate (Counts / Minute)	Background (For the Cleaner) Counts/time = rate (Counts / Minute)	Net Activity Section (C/M)	Net Activity Cleaner (C/M)	Net Activity Total (C/M)
I	3,139/10 = 313.9	2,059/60 = 34.3	i) 2,738/60 = 45.1 ii) 2,463/60 = 41.0	1,742/60 = 29.0 1,742/60 = 29.0	279.6	16.6 12.0	308.2
II	26,191/30 = 87.3	3,854/120 = 32.1	i) 4,685/130 = 36.0 ii) 4,307/130 = 33.1	3,006/100 = 30.0 3,006/100 = 30.0	55.2	6.0 3.1	64.3
III	25,802/30 = 86.0	7,441/240 = 31.0	6,628/200 = 33.1	4,386/150 = 29.2	55.0	3.9	58.9
IV	6,512/125 = 52.1	9,182/300 = 30.6	6,740/200 = 33.7	4,386/150 = 29.2	21.5	4.5	26.0
V	5,988/120 = 49.9	7,178/230 = 31.2	4,861/150 = 32.4	3,619/120 = 30.0	18.7	2.4	21.1
VI	6,225/150 = 41.5	14,083/480 = 29.3	8,346/300 = 27.8	4,382/180 = 24.3	12.2	3.5	15.7

TABLE D XI

SECTIONING DATA FOR SAMPLE $S/N_B/10$

Sample Weight before Sectioning = 65.64 mg.

Section Number	Wt. of 4-8 μ Amplex Diamond Powder Used (mg)	Duration of Hand Lapping (mins)	Sample weight After Lapping (mg)	(mg.) Weight of the Section Removed	(μ) Thickness of the Section	(μ) Avg. Distance of Section from Surface
I	2.50	2 + 5 + 5(a)	65.53	0.11	1.63	0.82
II	2.50	3 + 5 + 5(a)	65.40	0.13	1.93	2.60
III	2.50	3 + 4 + 5(a)	65.28	0.12	1.78	4.45
IV	2.50	3 + 5 + 5(a)	65.15	0.13	1.93	6.31
V	2.50	4 + 5 + 5(a)	65.00	0.15	2.23	8.39
VI	2.50	6 + 5 + 5(a)	64.79	0.21	3.12	11.06
VII	2.50	7 + 6 + 5(a)	64.53	0.26	3.86	14.55

(a) The first number denotes the duration of lapping with light finger pressure on the plunger, the second number denotes the duration of lapping without any finger pressure, and the third number denotes the duration of blanc lapping with the guard ring only (i.e., with the plunger containing the mounted sample removed). They were also done in this order.

TABLE D XII

COUNTING DATA FOR SAMPLE $S/N_B/10$

Section Number	Activity of Section Counts/time = rate (Counts / Minute)	Background (For the Section) Counts/time = rate (Counts / Minute)	Activity of Cleaner Counts/time = rate (Counts / Minute)	Background (For the Cleaner) Counts/time = rate (Counts / Minute)	Net Activity		
					Section (C/M)	Cleaner (C/M)	Total (C/M)
I	23,629/180 = 131.27	5,341/180 = 29.67	10,482/200 = 52.41	6,243/200 = 31.21	101.6	21.2	122.8
II	11,849/180 = 65.80	5,207/180 = 28.9	6,980/200 = 34.9	6,183/200 = 30.9	36.9	4.0	40.9
III	9,831/180 = 54.6	5,299/180 = 29.4	6,250/200 = 31.2	6,252/200 = 31.2	25.2	0.00	25.2
IV	11,581/200 = 57.9	5,953/200 = 29.8	--------	---------	28.1	—	28.1
V	11,506/240 = 47.9	6,970/240 = 29.0	--------	---------	18.9	—	18.9
VI	12,694/240 = 52.9	6,970/240 = 29.0	--------	---------	23.9	—	23.9
VII	10,851/240 = 45.2	6,970/240 = 29.0	--------	---------	16.2	—	16.2

TABLE D XIII

SECTIONING DATA FOR SAMPLE $S/N_B/12$

Sample Weight before Sectioning = 73.44 mg.

Section Number	Wt. of 4-8 μ Amplex Diamond Powder Used (mg.)	Duration of Hand Lapping (mins.)	Sample Weight After Lapping (mg.)	(mg.) Weight of the Section Removed	(μ) Thickness of the Section	(μ) Avg. Distance of Section from Surface
I	2.00	0 + 30 + 5[(a)]	73.37	0.07	1.09	0.545
II	3.00	0 + 90 + 10[(a)]	73.11	0.26	4.05	3.115
III	3.00	5 + 15 + 5[(a)]	72.86	0.25	3.90	7.09
IV	3.00	10 + 20 + 5[(a)]	72.47	0.39	6.08	12.08

(a) The first number denotes the duration of lapping with light finger pressure on the plunger, the second number denotes the duration of lapping without any finger pressure, and the third number denotes the duration of blanc lapping with the guard ring only (i.e., with the plunger containing the mounted sample removed). They were also done in this order.

TABLE D XIV

COUNTING DATA FOR SAMPLE $S/N_B/12$

Section Number	Activity of Section Counts/time = rate (Counts / Minute)	Background (For the Section) Counts/time = rate (Counts / Minute)	Activity of Cleaner Counts/time = rate (Counts / Minute)	Background (For the Cleaner) Counts/time = rate (Counts / Minute)	Net Activity		
					Section (C/M)	Cleaner (C/M)	Total (C/M)
I	820.7/10 = 820.7	1,231/30 = 41.0	3,019/40 = 75.5 2,120/45 = 47.1	2,461/60 = 41.0 2,464/60 = 41.0	779.7	34.5 6.1	820.3
II	2,461/30 = 82.0	4,204/100 = 42.0	5,404/120 = 45.0	2,462/60 = 41.0	40.0	4.0	44.0
III	10,000/198.02 = 50.5	10,000/243.90 = 41.0	10,000/232.56 = 43.0	2,462/60 = 41.0	9.5	2.0	11.5
IV	10,000/238.67 = 41.9	10,000/244.50 = 40.9	-------	-------	1.0	—	1.0

TABLE D XV

SECTIONING DATA FOR SAMPLE S/N$_B$/14/A

Sample Weight before Sectioning = 45.82 mg.

Section Number	Wt. of 4-8 μ Amplex Diamond Powder Used (mg)	Duration of Hand Lapping (mins.)	Sample weight After Lapping (mg)	(mg.) Weight of the Section Removed	(μ) Thickness of the Section	(μ) Avg. Distance of Section from Surface
I	2.00	0 + 10 + 5(a)	45.64	0.18	2.32	1.16
II	2.00	2 + 6 + 5(a)	45.49	0.15	1.94	3.29
III	2.00	3 + 10 + 5(a)	45.29	0.20	2.59	5.55
IV	2.00	3 + 7 + 5(a)	45.10	0.19	2.46	8.08
V	2.00	3 + 7 + 5(a)	44.91	0.19	2.46	10.54
VI	2.00	3 + 7 + 5(a)	44.73	0.18	2.32	12.93
VII	2.00	5 + 5 + 5(a)	44.55	0.18	2.32	15.25

(a) The first number denotes the duration of lapping with light finger pressure on the plunger, the second number denotes the duration of lapping without any finger pressure, and the third number denotes the duration of blanc lapping with the guard ring only (i.e., with the plunger containing the mounted sample removed). They were also done in this order.

TABLE D XVI

COUNTING DATA FOR SAMPLES S/N$_B$/14/A

Section Number	Activity of Section Counts/time = rate (Counts / Minute)	Background (For the Section) Counts/time = rate (Counts / Minute)	Activity of Cleaner Counts/time = rate (Counts / Minute)	Background (For the Cleaner) Counts/time = rate (Counts / Minute)	Net Activity Section (C/M)	Net Activity Cleaner (C/M)	Net Activity Total (C/M)
I	12,080/10 = 1,208.0	930/30 = 31.0	7,417/60 = 123.6	1,766/60 = 29.4	1,177.0	93.2	1,270.2
II	2,689/30 = 89.6	952/30 = 31.7	2,570/60 = 42.8	1,766/60 = 29.4	57.9	13.4	71.3
III	3,590/60 = 59.8	1,876/60 = 31.3	2,261/65 = 34.8	2,340/70 = 33.4	28.5	1.4	29.9
IV	14,264/240 = 59.4	2,263/75 = 30.2	5,840/200 = 29.2	5,836/200 = 29.2	29.2	0.00	29.2
V	2,568/60 = 42.8	2,263/75 = 30.2	--------	--------	12.6	----	12.6
VI	8,448/200 = 42.2	6,597/200 = 33.0	--------	--------	9.2	----	9.2
VII	6,679/200 = 33.4	19,581/720 = 27.2	--------	--------	6.2	----	6.2

TABLE D XVII

SECTIONING DATA FOR SAMPLE S/N$_B$/14/B

Sample weight before Sectioning = 34.52 mg.

Section Number	Wt. of 4-8 μ Amplex Diamond Powder Used (mg)	Duration of Hand Lapping (mins)	Sample weight After Lapping (mg)	(mg.) Weight of the Section Removed	(μ) Thickness of the Section	(μ) Avg. Distance of Section from Surface
I	3.00	3 + 5 + 5(a)	34.40	0.12	1.59	0.79
II	3.00	3 + 5 + 5(a)	34.27	0.13	1.72	2.45
III	3.00	4 + 5 + 5(a)	34.11	0.16	2.12	4.37
IV	3.00	5 + 5 + 5(a)	33.93	0.18	2.39	6.62
V	3.00	5 + 5 + 5(a)	33.73	0.20	2.65	9.14
VI	3.00	8 + 4 + 5(a)	33.50	0.23	3.05	11.99

(a) The first number denotes the duration of lapping with light finger pressure on the plunger, the second number denotes the duration of lapping without any finger pressure, and the third number denotes the duration of blanc lapping with the guard ring only (i.e., with the plunger containing the mounted sample removed). They were also done in this order.

TABLE D XVIII

COUNTING DATA FOR SAMPLE $S/N_B/14/B$

Section Number	Activity of Section Counts/time = rate (Counts / Minute)	Background (For the Section) Counts/time = rate (Counts / Minute)	Activity of Cleaner Counts/time = rate (Counts / Minute)	Background (For the Cleaner) Counts/time = rate (Counts / Minute)	Net Activity		
					Section (C/M)	Cleaner (C/M)	Total (C/M)
I	97,378/30 = 3245.9	2,780/100 = 27.8	12,728/40 = 318.2 5,106/35 = 145.8	2,831/100 = 28.3	3218.1	289.9 117.5	3625.5
II	9,278/60 = 154.6	2,780/100 = 27.8	3,593/60 = 59.9	2,831/100 = 28.3	126.8	31.6	158.4
III	9,414/100 = 94.1	2,780/100 = 27.8	4,304/120 = 35.9	2,831/100 = 28.3	66.3	7.6	73.9
IV	14,593/180 = 81.1	6,458/240 = 26.9	8,862/240 = 36.9	6,287/220 = 28.6	54.2	8.3	62.5
V	15,095/240 = 62.9	6,458/240 = 26.9	8,226/250 = 32.9	6,287/220 = 28.6	36.0	4.3	40.3
VI	14,460/300 = 48.2	6,458/240 = 26.9	6,872/240 = 28.6	6,287/220 = 28.6	21.3	0.0	21.3

APPENDIX E

Calculation of Si-30 Detection Sensitivity

Lowest concentration of Si-30 that will be required to determine

$= 0.07\%$ of total Silicon Isotope

$\cong 0.1\%$ of total Si

Let us assume:

Minimum Sample Surface Area $\cong 0.2\ \text{cm}^2$.

Minimum thickness of a section = $1\mu = 10^{-4}$ cm.

Density of SiC $\cong 3.2\ \text{gm/cm}^3$.

Total weight of a 1μ SiC section

$\cong 0.2 \times 10^{-4} \times 3.2$ gm.

$= 0.64 \times 10^{-4}$ gm.

$= 0.64 \times 10^{-4} \times \frac{28}{40}$ gm of silicon.

Therefore, total amount of Si-30 in a 1μ SiC section

$\cong 0.64 \times 10^{-4} \times \frac{28}{40} \times 0.1$ gm

$= 0.64 \times 7 \times 10^{-4} \times 10^{-2}$ gm

$= 4.48 \times 10^{-6}$ gm

Now, according to Leddicotte(A19) the sensitivity of detection of silicon = 10^{-6} gm

So, the sensitivity of detection of Silicon-30

$= 3.12 \times 10^{-2} \times 10^{-6}$ gm

$= 0.0312 \times 10^{-6}$ gm

Thus the factor of safety for the detection of silicon in a 1μ SiC section of $0.2\ \text{cm}^2$ area $= \frac{4.48 \times 10^{-6}}{0.0312 \times 10^{-6}} \cong 1.44 \times 10^2$

TABLE E I

Spectrochemical Impurities in Commerical SiC (ppm)(44)

Element	Black	Green	Colorless
Al	10,000	370	16
B	10	0	0
Fe	10	10	1
Ni	3	3	1
Ti	22	23	15
U	15	18	25

TABLE E II

SPECTROGRAPHIC ANALYSIS OF THE MATERIALS USED

Impurity Element	Black SiC (Norton)(1) (in ppm)	Pure-Al sectioning(2) block(Untd.Minl.)ppm	Silicon-28(3) (Oak Ridge) %	Amorphous C-14(4) (Nuclear-Chicago)
Ag	---	0.1	---	---
Al	600	Major	0.05*	---
B	40	---	0.02*	---
Ba	---	---	0.02*	---
Be	---	---	0.001*	---
Ca	50	1.0	0.02+	---
Cb	---	---	0.1*	---
Cd	---	---	---	Faint Trace
Co	---	---	0.05*	---
Cr	---	---	0.05*	---
Cu	---	20.0	0.05+	---
Fe	40	3.0	0.02*	Faint Trace
Hg	---	---	---	Not Detected
In	---	3.0	---	---
K	10	---	0.01*	---
Li	---	---	0.01*	---
Mg	20	10.0	0.05*	Major Impurity
Mn	---	---	0.02*	Not Detected
Mo	---	---	0.02*	---
N	100	---	---	---
Na	30	---	0.1	---

TABLE E II

SPECTROGRAPHIC ANALYSIS OF THE MATERIALS USED (continued)

Impurity Element	Black SiC (Norton)(1) (in ppm)	Pure-Al sectioning(2) block(Untd.Minl.)ppm	Silicon-28(3) (Oak Ridge)7%	Amorphous C-14(4) (Nuclear-Chicago)
Ni	5	---	0.05*	Trace
P	20	---	---	---
Pb	---	5.0	0.1*	---
Si	Major	3.0	Major	---
Sn	---	---	0.05*	---
Ti	25	---	0.02*	---
V	20	---	0.02*	---
Zn	---	---	0.2	---
Zr	---	---	0.1*	---
TOTAL:	0.096%	0.00451%	0.4%	---

Notes:

1. Analysis done by Jarrell-Ash Company, Newtonville, Mass. Error Estimated: ±20%.
2. Lot No. 1709. Analysis supplied by the United Mineral & Chemical Corporation.
3. Series 1A, Sample 973(b). Analysis supplied. Isotopic analysis:

   Si-28 = 99.83 ± 0.02% ; Si-29 = 0.10 ± 0.02% ; Si-30 = 0.07 ± 0.02%
4. Semi-quantitative analysis supplied by Nuclear-Chicago Corp. Sample: CFA-76, Lot 7.

* No spectrum line visible. Probably absent or definitely less than the value given.

+ Present but less than the value given.

TABLE E III

A Comparison of the Suspending Media Studied

Medium	Character of film	Drying		Any flow to back	Minm. obtd. Density of film(mg/cm^2)	Adherence to sample	Effect with ammonia	Effect with acid	Add'l. Comments
		Temp	Time						
Ethanol	Considerable Segregation	Rm.	V. Sm.	Little	28.0	V. poor	Good Segregation & agglomeration	Almost same as NH_4OH	Very uniform film. Useless Hard to apply (uniformly)
Butanol	V. Little Segregation (if any)	$84^{o}C$	About 5 mins.	Considerable	5.6	Poor	Little Segregation & agglomeration	Little more than with NH_4OH	Ununiform film. Almost useless. Hard to apply.
Ethylene Glycol	Almost Uniform	$84^{o}C$	About 10 mins.	Practically none	14.0	Satisfactory	Same as above.	more than with NH_4OH	Pretty uniform film. can be used. not too hard to apply. (uniformly)
Glycerol	quite uniform	$84^{o}C$	About 30 mins.	not at all	11.2	quite good	Same as above	more than with	Very uniform film. Best usable of all Easy to apply.

TABLE E IV

DATA ON DECOMPOSITION OF SILICON CARBIDE

1. Black Hexagonal Single Crystals:

Sample Number	Temp (^oK)	Time (sec)	Tracer coated surface area (cm^2)	Total surface area (cm^2)	Decomposition (mg)	Equivalent thickness decomposed (microns)	Rate of decomposition ($Mg/cm^2/sec$)
$S/N_B/10$	2126°	3.900×10^5	0.2100	0.6380	0.45	2.20	1.81×10^{-6}
$S/N_N/14/B$	2165°	9.000×10^4	0.2351	0.6087	0.09	0.46	1.64×10^{-6}
$S/N_B/2/A$	2180°	0.972×10^5	0.1999	0.5668	1.13	6.21	2.05×10^{-5}
$S/N_B/7$	2210°	9.360×10^4	0.2057	0.5717	1.50	8.18	2.80×10^{-5}
$S/N_B/3$	2216°	2.015×10^5	0.2284	0.6380	3.99	19.48	3.10×10^{-5}
$S/N_B/8$	2235°	1.049×10^5	0.2105	0.6384	2.21	10.79	3.30×10^{-5}
$S/N_B/5$	2290°	2.070×10^4	0.2062	0.6274	0.10	0.50	7.70×10^{-6}
$S/N_B/14/A$	2311°	3.240×10^4	0.2405	0.6203	1.94	9.74	9.65×10^{-5}
$S/N_B/12$	2333°	3.600×10^3	0.1998	0.5689	0.55(?)	3.01	2.68×10^{-4}(?)
$S/N_B/2/B$	2361°	6.000×10^3	0.1922	0.5533	0.09	0.51	2.61×10^{-5}

TABLE E IV

DATA ON DECOMPOSITION OF SILICON CARBIDE (continued)

Sample Number	Temp(^{o}K)	Time(sec)	Tracer coated surface area (cm^2)	Total surface area (cm^2)	Decomposition (mg)	Equivalent thickness decomposed (microns)	Rate of decomposition (Mg/cm^2/sec)
2. Light Green Hexagonal Crystal:							
$S/N_G/5/C$	2250°	1.500×10^5	0.2081	0.5292	0.26	1.52	3.27×10^{-6}
$S/N_G/5/F$	2280°	1.440×10^5	0.1986	0.4628	0.72	4.85	1.08×10^{-5}
$S/N_G/5/A$	2311°	3.240×10^4	0.2480	0.5880	1.54	8.16	8.08×10^{-5}
$S/N_G/5/E$	2336°	3.420×10^4	0.2006	0.4863	0.46	2.95	2.76×10^{-5}
$S/N_G/5/B$	2361°	6.000×10^3	0.2420	0.5752	0.09	0.50	2.61×10^{-5}
3. Faint Yellow-Green Hexagonal Crystal:							
$S/N_C/4/A$	2210°	9.360×10^4	0.4193	0.9334	2.71	9.05	3.10×10^{-5}
$S/N_C/4/C$	2280°	1.440×10^5	0.3942	0.8832	1.45	5.14	1.14×10^{-5}
$S/N_C/4/B$	2361°	6.00×10^3	0.4011	0.8970	0.15	0.51	2.79×10^{-5}
4. Black Polycrystalline Material (Dense):							
$P/A_B/1/B$	2200°	1.62×10^5	0.3057	0.7427	1.65	6.99	1.37×10^{-5}
$P/A_B/2/B$	2200°	1.62×10^5	0.3041	0.7388	1.54	6.55	1.28×10^{-5}
$P/A_B/1/A$	2250°	1.50×10^5	0.3105	0.7498	1.02	4.28	9.07×10^{-6}
$P/A_B/2/A$	2250°	1.50×10^5	0.3096	0.7502	0.96	4.02	8.53×10^{-6}
$P/A_B/1/C$	2336°	3.42×10^4	0.2933	0.7368	0.36	1.54	1.43×10^{-5}
$P/A_B/2/C$	2336°	3.42×10^4	0.2906	0.7312	0.38	1.65	1.53×10^{-5}

TABLE E V

INITIAL AND FINAL SURFACE TRACER CONCENTRATIONS

(used in the correction of concentration profiles of C-14 in black single crystals of SiC)

Sample	Surface Count (counts/min.) (dN/dt)	Starting Surface Concentration: Corresponding No. of atoms of C-14 ($N=4.247\times10^9\times dN/dt$)	Starting Surface Concentration: Tracer Density (atoms/cm^2)	Final Surface Concentration: Sp. Activity 1st Section (C/M/mg)	Final Surface Concentration: Corresponding No. atoms of C-14 (Atoms/mg)	Final Surface Concentration: Final Tracer Concentration (Atoms/cm^3)
$S/N_B/5$	1,790	7.60×10^{12}	3.686×10^{13}	2.014×10^{3}	8.553×10^{12}	2.746×10^{16}
$S/N_B/8$	42,097	1.79×10^{14}	8.503×10^{14}	2.802×10^{3}	1.190×10^{13}	3.820×10^{16}
$S/N_B/14/A$	25,000	1.06×10^{14}	4.407×10^{14}	7.053×10^{3}	2.995×10^{13}	9.614×10^{16}
$S/N_B/12$	28,532	1.21×10^{14}	6.056×10^{14}	1.265×10^{4}	5.372×10^{13}	1.724×10^{17}
$S/N_B/10$	1,884	8.00×10^{12}	3.810×10^{13}	1.116×10^{3}	4.739×10^{12}	1.521×10^{16}
$S/N_B/14/B$	77,400	3.29×10^{14}	1.399×10^{15}	3.021×10^{4}	1.283×10^{14}	4.118×10^{17}
$S/N_B/7$	55,340	2.35×10^{14}	1.142×10^{15}	6.782×10^{3}	2.880×10^{13}	9.245×10^{16}
$S/N_B/2/A$	34,830	1.48×10^{14}	7.404×10^{14}	2.550×10^{3}	1.083×10^{13}	3.476×10^{16}
$S/N_B/2/B$	20,700	8.79×10^{13}	4.573×10^{14}	7.130×10^{3}	3.028×10^{13}	9.720×10^{16}

Program used in IBM 7094 Computer for the Correction of Concentration Profiles at M.I.T. Computation Center

```
*M4014-3459,FMS,DEBUG,2,2,2000,0
*             XEQ
*             MAD
              DIMENSION CA(300),CB(300)
              INTEGER IMIN,IMAX,JMAX,I,J
START         R'A
             R
             R DATA=XP,XPP,DELX,TTOT,Q,CF,D
             R XP=DEPTH OF SURFACE DECOMPOSITION,CM.
             R XPP= ASSUMED MINIMUM DEPTH OF DIFFUSION, CM.
             R TTOT=TOTAL TIME FOR DIFFUSION, SECONDS.
             R CO=INITIAL SURFACE CONCENTRATION,NUMBER PER CMSQ.
             R CF=FINAL SURFACE CONCENTRATION, NUMBER PER CC.
             R D=DIFFUSION COEFFICIENT, CMSQ PER SECOND.
             R Q=TOTAL AMOUNT OF DIFFUSING MATERIAL, NUMBER PER CMSQ.
             R
              CO=Q/DELX
              DELT=DELX*DELX*.5/D
              JMAX=TTOT/DELT
              IMAX=XPP/DELX
              RS=XP/((JMAX-1)*DELT)
              RCS=(CO-CF)/((JMAX-1)*DELT)
              P'S DELT,IMAX,JMAX,RS,RCS,CO
              T'H LOOPA, FOR I=1, 1,I.G.(IMAX+1)
LOOPA         CA(I)=0.
              T'H LOOPD, FOR J=0,1,J.G.(JMAX-1)
              IMIN=(RS*J*DELT/DELX+.5)
              CA(IMIN)=CO-RCS*J*DELT
              T'H LOOPB, FOR I=(IMIN+1),1,I.G.IMAX
LOOPB         CB(I)=(CA(I-1)+CA(I+1))/2.
              T'H LOOPC, FOR I=(IMIN+1),1,I.G.IMAX
LOOPC         CA(I)=CB(I)
LOOPD         CONTINUE
              P'S IMIN
              PRINT COMMENT $ IMIN=SUBSCRIPT OF SURFACE COORDINATE
             1 AT TIME=TTOT.$
              P'S CA(IMIN)...CA(IMAX)
              T'O START
              E'M
*             DATA
```

Program used in IBM 7094 Computer for the Calculation of Ideal Concentration Profiles at M.I.T. Computation Center

```
*M4014-3459,FMS,DEBUG,1,2,500,0
*             XEQ
*             MAD
              DIMENSION CA(600),CB(600)
              INTEGER IMAX,JMAX,I,J
START         R'A
             R
             R DATA=XPP,DELX,TTOT,Q,D
             R XPP= ASSUMED MINIMUM DEPTH OF DIFFUSION, CM.
             R TTOT= TOTAL TIME FOR DIFFUSION, SECONDS.
             R CO= INITIAL SURFACE CONCENTRATION, NUMBER PER CC.
             R D= DIFFUSION COEFFICIENT, CMSQ PER SECOND.
             R Q= TOTAL AMOUNT OF DIFFUSING MATERIAL, NUMBER PER CMSQ.
             R
              PI=3.14159
              CO=Q/DELX
              DELT=DELX*DELX*.5/D
              JMAX=TTOT/DELT
              IMAX=XPP/DELX
              P'S DELT,JMAX,IMAX,CO
              CA(0)=CO
              T'H LOOPA, FOR I=1,1,I.G.(IMAX+1)
LOOPA         CA(I)=0.
              T'H LOOPD, FOR J=0,1,J.G.(JMAX-1)
              SUM=0.
              T'H LOOPB, FOR I=1,1,I.G.IMAX
              CB(I)=(CA(I-1)+CA(I+1))/2.
LOOPB         SUM=SUM+CB(I)
              CB(0)=CO-SUM
              T'H LOOPC, FOR I=0,1,I.G.IMAX
LOOPC         CA(I)=CB(I)
LOOPD         CONTINUE
              TIMES=J
              P'S TIMES
              P'S CA(0)...CA(IMAX)
              CAOCAL=Q/((PI*D*J*DELT).P..5)
              P'S CAOCAL
              PRINT COMMENT $ CAOCAL=ANALYTICAL VALUE OF FINAL
             1  SURFACE CONCENTRATION, AND SHOULD=CA(0).$
              T'O START
              E'M
*             DATA
```

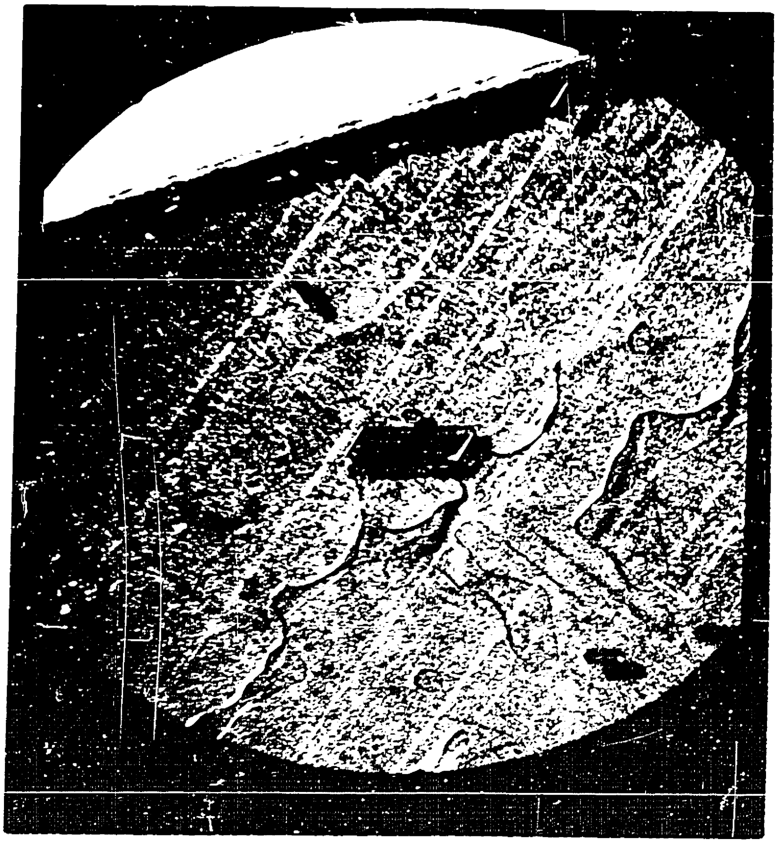

FIG. E-1 ISOORIENTED GROWN-IN CRYSTALLITES INSIDE AN INDUSTRIAL GREEN SiC SINGLE CRYSTAL. 50X.

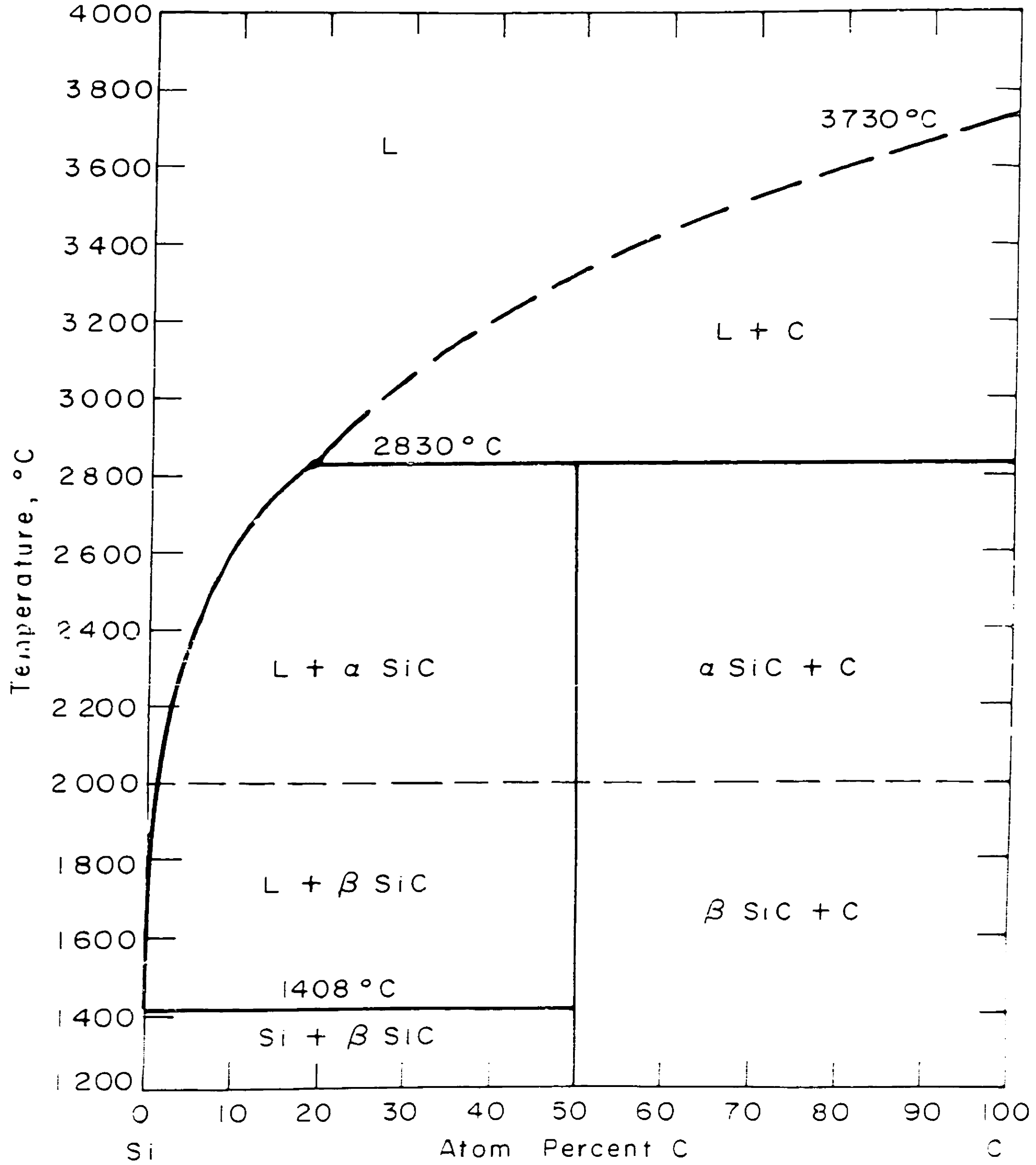

α = Hexagonal and Rhombehedral Polytypes
β = Cubic 3C Polytype

FIGURE E2. Si – C BINARY PHASE DIAGRAM

BIOGRAPHICAL NOTE

The author was born on July 7, 1937 in the village of Sribari, East Bengal, India (now in East Pakistan). He is the eldest of the two sons of Professor Rabindra Nath Ghoshtagore and Ashoka Uma Basumajumder. He was brough up and educated by his maternal family while his father was fighting with the Japanese in the Far East in World War II. He joined his parents in January, 1950, after his father returned from the Indian Army and had only three years of formal schooling before he graduated from Bindubasini High School, Tangail, East Pakistan, in 1953, securing 3rd position in order of merit among 35,000 students (under East Bengal Secondary Education Board).

Then he migrated to India to attend several colleges in Calcutta. He graduated with his Bachelor's Degree in Chemistry (with Honors) in 1957 from Presidency College, Calcutta (under the University of Calcutta) securring top position in order of merit in 1st Class. He then attended the University of Calcutta, College of Science and Technology. He graduated in 1960 with his Master's Degree in Applied Chemistry leading the list of successful candidates (in order or merit). Among his college honors are: Br. Jann Gold Medal (on the results of the Junior Degree), Cunningham Memorial Prize (on the results of the Bachelor's Degree), University Gold and Ambikacharan Gold Medals (on the results of Master's Degree) and several merit scholarships and prizes. His Master's Thesis is entitled "Studies on Synthetic Zeolite." He then worked for about a year in West Bengal State Senior Educational Service as a lecturer in Inorganic Chemistry.

He joined M.I.T. Graduate School in the fall of 1961 as a candidate for the Doctor's Degree in Ceramics.

His professional affiliations include Sigma Xi, the American Ceramic Society and the Indian Ceramic Society.